For Reference

NOT TO BE TAKEN FROM THIS ROOM

Ex libris
universitatis
albertaensis



Digitized by the Internet Archive
in 2023 with funding from
University of Alberta Library

https://archive.org/details/Stovel1983

THE UNIVERSITY OF ALBERTA

A TWO-DIMENSIONAL NUMERICAL MODEL OF AIRFLOW WITHIN A SMALL URBAN VALLEY

by

LESLIE DOROTHY STOVEL

A THESIS

SUBMITTED TO THE FACULTY OF GRADUATE STUDIES AND RESEARCH

IN PARTIAL FULFILMENT OF THE REQUIREMENTS FOR THE DEGREE

OF MASTER OF SCIENCE

IN

METEOROLOGY

DEPARTMENT OF GEOGRAPHY

EDMONTON, ALBERTA

SPRING, 1983

DEDICATION

To Mom,
who has always told me there's no such word as "can't",
and to my sister, Margaret -
thanks for all the letters and encouragement.

ABSTRACT

A two-dimensional numerical model is developed to predict the temperature and wind fields within a small axially symmetric valley cross-section. The thermodynamic equation, coupled with the vorticity equation, is solved using finite-differences subject to either a surface cooling rate which is constant or else dependent on radiative transfer processes, following Brunt (1934). The cooling rates were obtained from experiments performed in 1977 - 1978 within the North Saskatchewan River valley in Edmonton, Alberta, during clear sky and light wind inversion conditions in which downslope winds developed. Advection, turbulent diffusion and radiation processes are incorporated into the heat transfer equation ; K-theory is used to approximate the latter two. Integrations are performed using the Dufort-Frankel formulation for the diffusion terms but, due to inherent numerical problems, a forward-time, centered-space method is proved superior in this application. A forward-time, upstream-space formulation is used to estimate the advection terms. Liebmann sequential relaxation is used to determine the streamfunction field.

The model predicts attainment of quasi-steady-state conditions within about 20 minutes of integration time with the development of downslope wind speeds of $\simeq 0.8$ m s^{-1}. The relative contributions which advective, diffusive, and radiative processes make are illustrated in different conditions and various valley locations. In the early stages

(after 200 seconds), radiative transfer dominates at low levels. As the slope winds develop, advection processes become increasingly important and, after 1600 seconds, cooling rates due to advection of -4×10^{-4} C° s^{-1} are predicted 4 m above the slope, about twice those due to diffusion or radiation. However, when only radiative transfer is permitted, which is simulated in this study as a diffusive process, it is able to account for most of the observed temperature changes alone at low levels. The predicted low-level temperature variations with height and the maximum slope winds agree extremely well with the observations. Sensitivity of the results to the location of the upper boundary of the model and to the presence or absence of a flat valley bottom is small close to the slope.

ACKNOWLEDGEMENTS

I wish to express my sincerest gratitude to my departmental supervisor, Dr. K.D. Hage, for his patient guidance, expert advice, and endless enthusiastic encouragement, all of which have contributed greatly to the completion of this project. As well, I would like to thank Dr. R.B. Charlton of the Division of Meteorology and Dr. U.M. Maydell of the Department of Computing Science for serving on the examining committee along with Dr. Hage.

I would also like to thank all my past and present classmates who have furthered my understanding through interesting discussion. Especially valuable were enlightening talks with Mr. Doug S. Phillips, who gave freely of his time and offered much useful advice. His contribution to this work, although not explicitly referenced, should not go unrecognized. The encouragement and support of a personal friend, Mr. Bryan R. Crofts, is also much appreciated.

In addition, I would like to thank the Natural Sciences and Engineering Research Council (NSERC) for providing the majority of the computing funds, and the Department of Geography for the balance. Financial support for the experimental aspects of this project was provided by the Research Secretariat of Alberta Environment.

Finally, I would like to express my appreciation to the Department of Geography which provided financial support during the first year of my graduate work in the form of a

Teaching Assistantship. A post-graduate fellowship from NSERC, obtained during my second year of study, was greatly valued as well.

Table of Contents

Chapter Page

DEDICATION....iv

ABSTRACT....v

ACKNOWLEDGEMENTS....vii

LIST OF TABLES....xii

LIST OF FIGURES....xiv

LIST OF SYMBOLS....xvii

1. INTRODUCTION....1

1.1 Mountain and Valley Winds....1

1.2 Micrometeorology of the N. Saskatchewan River Valley....4

1.3 Objectives of the Study....7

2. THE THEORETICAL MODEL....9

2.1 Introduction....9

2.2 The Governing Equations....11

2.3 The Assumption of Incompressibility....16

2.4 The Vorticity Equation....17

2.5 Use of Streamfunctions and Related Boundary Conditions....29

2.6 Potential Temperature Boundary Conditions at the Ground....30

2.7 Initial Conditions....33

2.8 Summary - Prognostic and Diagnostic Equations....35

3. NUMERICAL ASPECTS OF THE COMPUTER MODEL....36

3.1 Introduction....36

3.2 The Grid....38

3.3 Initial and Boundary Conditions in Terms of Finite Differences....41

3.3.1 Initial Conditions.....41

3.3.2 Lateral Boundary Conditions.....44

3.3.3 Lower Boundary Conditions 46

3.3.4 Upper Boundary Conditions 47

3.4 Finite Difference Formulation of Prediction Equations 49

3.4.1 General 49

3.4.2 Advection Terms (a) 51

3.4.3 Diffusion Terms 53

3.4.4 Other Term (c) 57

3.5 One-dimensional Heat Conduction Equation 58

3.5.1 Analytical Solution 59

3.5.2 Comparison with Numerical Solution 62

3.6 Liebmann Sequential Relaxation Technique 70

3.7 Summary of Method of Solution 73

4. RESULTS 77

4.1 Introduction 77

4.2 The Standard Run - Run 1 78

4.2.1 General 78

4.2.2 Circulation Development 83

4.2.3 Evolution of Thermodynamic Fields 89

4.3 Effect of Location of Upper Boundary - Run 2 ...102

4.4 Effect of Absence of Horizontal Valley Floor - Run 3 103

4.5 Effect of Steeper Slope - Run 4 106

4.6 Effect of Smaller Vertical Diffusion Coefficient - Run 5 110

4.7 Effect of Stability 113

4.7.1 General.....113

4.7.2 Neutral Case Initially - Run 6.....115

4.7.3 More Stable Case Initially - Run 7 119

4.8 Comparison with Observations - Run 8 and others 120

5. SUMMARY AND CONCLUSIONS 131

5.1 Summary 131

5.2 Conclusions 135

5.3 Suggestions for Future Work 137

REFERENCES 140

APPENDIX A : STABILITY ANALYSIS FOR ADVECTION EQUATION ..143

APPENDIX B - STABILITY ANALYSIS FOR DIFFUSION EQUATION ..146

APPENDIX C - ANALYTICAL SOLUTION TO ONE-DIMENSIONAL DIFFUSION EQUATION 149

APPENDIX D - SOURCE CODE FOR COMPUTER PROGRAM 153

List of Tables

Table — Page

2.1 Estimates of magnitudes of term A ($g/\theta\ \partial\theta/\partial y$) and term C ($\partial p/\partial y\ R/p\ g/C_p\ (1-\gamma/\gamma_d)$) comprising the solenoid term.....28

3.1 Properties of some numerical schemes applied to an advection equation.....52

3.2 Properties of some numerical schemes applied to a diffusion equation.....54

3.3 Comparison of analytical solution to one-dimensional diffusion equation with numerical solutions obtained using Dufort-Frankel and forward-time, centered-space schemes after 2000 seconds.....63

3.4 Comparison of amounts of cooling after 200 seconds obtained from analytical solution to the one-dimensional diffusion equation and valley model solutions obtained using Dufort-Frankel and forward-time, centered-space schemes.....65

3.5 Vorticity changes predicted by various terms in the valley model out to 20 seconds using the DuFort-Frankel scheme.....66

3.6 Vorticity changes predicted by various terms in the valley model out to 20 seconds using the forward-time, centered-space scheme.....67

3.7 Vorticity values (s^{-1}) predicted above mid-slope region after 200 seconds using the Dufort-Frankel and forward-time, centered-space schemes and various time steps.....69

4.1 Parameter values for valley model in the standard run (Run 1).....79

4.2 Summary of parameter values for Runs 2 - 8.....79

4.3 Contributions to $\partial\theta/\partial t$ from advection and diffusion just above mid-slope (J=8,K=7) for Run 1 at 200 second intervals.....91

4.4 Maximum vertical velocities above valley trough for Run 1 (J=3) and for Run 3 (J=1).....105

Table Page

4.5 Contributions to $\partial\theta/\partial t$ from advection and diffusion just above mid-slope (J=8,K=7) for Run 5 at 200 second intervals.....112

4.6 Contributions to $\partial\theta/\partial t$ from advection and diffusion just above mid-slope (J=8,K=7) for Run 6 at 200 second intervals.....118

4.7 Vertical potential temperature gradients (based on surface temperatures and that 32 m above) under different lapse conditions for various locations in the valley.....121

List of Figures

Figure		Page
1.1	Schematic illustration of the diurnal variation of the circulation within a valley (after Defant, 1951)	2
1.2	Topography of Edmonton (height contours in meters)	5
2.1	Relation between isobars and isosteres in a baroclinic fluid	20
2.2	Location of instruments used to estimate horizontal temperature differences within the North Saskatchewan River valley	24
2.3	Assumed temperatures and lapse rates used to estimate hydrostatic pressures at (A) and (B)	25
3.1	Actual and model approximation (dashed) of valley cross-section in Edmonton	39
3.2	Grid configuration for valley model	42
3.3	Schematic illustration of axial symmetry and boundary conditions	45
3.4	Schematic illustration of lower boundary condition	48
3.5	Summary of boundary conditions on velocity components, v and w, vorticity, ξ, and streamfunction, ψ	50
3.6	Potential temperature deviation from initial state versus height for one-dimensional diffusion equation ($K = 1.0\ m^2\ s^{-1}$) out to 1200 seconds	60
3.7	Potential temperature deviation from initial state versus height for one-dimensional diffusion equation ($K = 1.0\ m^2\ s^{-1}$) out to 20000 seconds	61
3.8	Flowchart of finite-difference schemes used in valley model	74
3.9	Example of time differencing used in the valley model	75

Figure Page

4.1 Minimum streamfunction versus time for Run 1 using various diffusion schemes and several time steps.....81

4.2 Cooling predicted by valley model versus height using forward-time, centered-space diffusion scheme and a 4 second time step.....82

4.3 Streamfunction contours ($\Delta\psi$= 2.0 m^2 s^{-1}) at t=600, 1200, and 1400 seconds for the standard run (Run 1).....84

4.4 Trajectory of streamline center for the standard run (Run 1) obtained from available grid point values and interpolation.....86

4.5 Circulation predicted after 400 seconds for the standard run (Run 1) (a.) streamfunction and velocity contours, (b.) horizontal velocity component contours, (c.) vertical velocity component contours.....87

4.6 Relative contributions to $\partial\theta/\partial t$ from advection and diffusion for the standard run (Run 1) in various parts of the valley after 400 seconds and 1200 seconds.....93

4.7 Potential temperature field at t=0, 400, 800, and 1200 seconds for the standard run (Run 1).....94

4.8 Potential temperature deviation from initial state versus height above trough boundary (J=1) for the standard run (Run 1).....97

4.9 Potential temperature deviation from initial state versus height above mid-slope region (J=8) for the standard run (Run 1).....98

4.10 Potential temperature deviation from initial state versus height above ridge boundary (J=16) for the standard run (Run 1).....99

4.11 Difference in cooling predicted by valley model in Run 1 and by one-dimensional vertical diffusion equation (K = 1.0 m^2 s^{-1}) as a function of height.....100

Figure Page

4.12 Schematic illustration of modelled region in Run 4 (hatched), along with that of Run 1.....107

4.13 Minimum streamfunction and maximum downslope wind speed versus time for the standard run (Run 1) and for Run 4.....109

4.14 Minimum streamfunction and maximum downslope wind speed versus time for the standard run (Run 1) and for Runs 6 and 7.....116

4.15 Observed evolution of screen temperatures (1.2 m above ground) for three experiments in 1978 at the Dawson Bridge site.....123

4.16 Observed cooling amounts versus height in 1200 seconds (mean values) and that predicted by the valley model in Run 8.....126

4.17 Horizontal velocity component versus height predicted by valley model in Run 8 out to 1200 seconds.....128

4.18 Observed wind shear and that predicted by valley model in Run 8 at 400 and 1200 seconds.....128

4.19 Two boundary conditions used to specify the surface temperature fields.....130

A.1 Amplification factor versus μ using forward-time, centered-space scheme applied to advection equation.....145

LIST OF SYMBOLS

c	speed of sound
c	general advection speed
C	circulation
C_p	specific heat of air at constant pressure
C_v	specific heat of air at constant volume
f	thermal flux
f_o	thermal flux at z=0
g	gravitational acceleration
H	scale height of the atmosphere
H	height of model upper boundary
J	horizontal grid index ($y=(J-1)\Delta y$)
K	vertical grid index ($z=(K-1)\Delta z$)
K	general diffusivity
$(K_m)_y$, K_y	horizontal momentum diffusivity
$(K_m)_z$, K_z	vertical momentum diffusivity
K_R	radiative diffusivity
$(K_T)_y$	horizontal thermal diffusivity
$(K_T)_z$	vertical thermal diffusivity
L	typical length scale
n	frequency of oscillations in flow
n	time index ($t=n\Delta t$)
n	iteration index in relaxation procedure
p	atmospheric pressure
p_h	hydrostatic pressure
p_{nh}	non-hydrostatic pressure
p_o	reference pressure

R	gas constant for dry air
R_f	flux Richardson number
R_N	net loss of heat by radiation
$R^n(J,K)$	residual at grid point (J,K) after nth iteration
t	time
T	atmospheric temperature
u	horizontal wind speed
U	typical wind speed scale
v	horizontal wind speed
$\vec{V}$	wind velocity
w	vertical wind speed
w'	vertical wind speed deviation
α	inclination of slope
γ	C_p/C_v
γ	ambient lapse rate
γ_d	dry adiabatic lapse rate
δ_{ij}	Kronecker delta
Δy	horizontal grid size
Δz_1	vertical grid size in lower region
Δz_2	vertical grid size in upper region
Δt	time step
ϵ	tolerance level used to stop relaxation procedure
ξ	vorticity component along down-valley axis
θ	potential temperature
θ_o	reference potential temperature
θ'	potential temperature deviation from θ_o
λ	amplification factor

ρ	atmospheric density
ψ	streamfunction
$\psi^n(J,K)$	streamfunction at grid point (J,K) after nth iteration
$\vec{\Omega}$	Earth's angular velocity

Chapter 1

INTRODUCTION

1.1 Mountain and Valley Winds

The phenomenon of mountain and valley winds has been investigated by many authors in the past. Wagner, during the 1930's, published a number of papers giving fairly extensive explanations of the theory of such local circulations. Based on observations conducted within the valleys of the Alps, he concluded that a pressure gradient was created between air over the inclined mountain slope and air at the same height over the center of the valley as a result of differences in the temperature regimes at these two locations. He postulated the existence of a double vortex type of circulation, with weak downslope or drainage winds, ascent above the valley floor, and a generally downvalley wind close to the valley floor. This latter component was fed partly from the side slopes, and also resulted partly from the pressure difference between the mountain and the plain.

Defant (1951) schematically illustrated the successive stages in the diurnal cycle of the mountain-valley wind system. This is reproduced in Figure 1.1. In (a), at sunrise, upslope winds begin, but the valley is still colder than the plains above, and the downvalley winds are still blowing, fed by the return circulation from the slopes. It soon dies out with further heating. In (b), the forenoon, slope winds are strong, and a transition from downvalley to

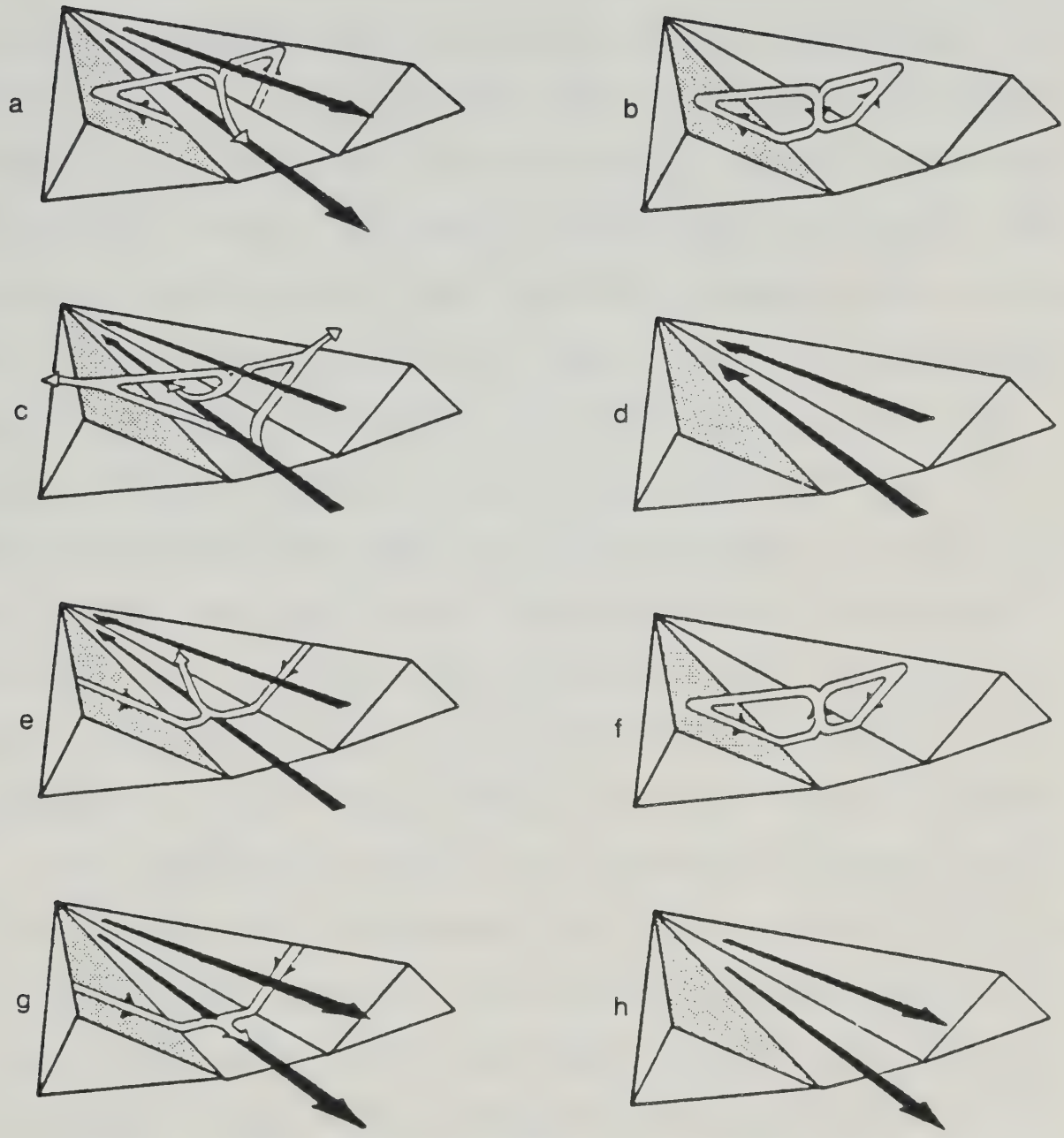


Figure 1.1 Schematic illustration of the diurnal variation of the circulation within a valley (after Defant, 1951).

upvalley wind is occurring with the valley and plains temperature approximately equal. In (c), at noon or early afternoon, the slope winds are diminishing, the upvalley wind is fully developed, and the valley becomes warmer than the plains. By (d), late afternoon, the slope winds cease, the upvalley wind continues, and the valley remains warmer than the plains. During (e), evening, downslope winds begin, the upvalley winds diminish, and the valley remains only slightly warmer than the plains. By (f), early night, the downslope winds become fully developed, with the valley at the same temperature as the plains. During (g), the middle of the night, the downvalley wind is fully developed, with the valley being colder than the plains. The downslope valley wind continues. In (h), late night, the downslope wind has ceased, with the downvalley wind filling the valley completely, and the valley remaining colder than the plains.

This progression can be interrupted or altered under various conditions. Development of cloud cover tends to slow the cooling experienced at the ground and greatly weakens the valley inversion. This can then result in very low or non-existent slope winds. Interaction between the large-scale prevailing flow and the thermally induced slope wind circulation has been investigated by Tang (1976). He showed that a separated cell would form on the lee slope during the day, and that one would form on the windward side at nighttime. Very strong synoptic scale circulation is able to mask the local mountain and valley wind system completely.

1.2 Micrometeorology of the N. Saskatchewan River Valley

The North Saskatchewan River valley bisects the city of Edmonton, Alberta (located at 53° 33′ latitude, 113° 30′ W longitude). Typically, it is 50 m in depth and varies from 1 - 1.5 km across. Along its meandering course (see Figure 1.2) are both steep-sided valley walls as well as more gentle flood plains. Within the city limits, the valley is fairly well covered by wooded areas.

The earliest micrometeorological observations within the North Saskatchewan River valley were made in 1958 - 1959. Klassen (1962) found distinct regimes to exist on the plain, in the ravines, and in the main river valley, which resembled those suggested by Defant (see Section 1.1). Lower surface temperatures and stronger inversions were found to occur within the valley at night. Under clear skies and light winds (less than 5 m s^{-1}), downslope and downvalley winds were generally observed. The speed and depth of the wind down the ravines usually increased to their maximum values (1.8 m s^{-1} and the ravine depth, respectively) within less than two hours after sundown. Trajectories of fog and smoke showed ascending motions above the river and a return flow to the valley slopes, in a helical fashion.

In 1977 and 1978, thirteen field experiments were carried out by Hage (1979) in order to study the influence of a small urban valley on air pollutant concentrations. As part of the program, air temperatures, winds (and some vertical profiles of each) were obtained at various valley

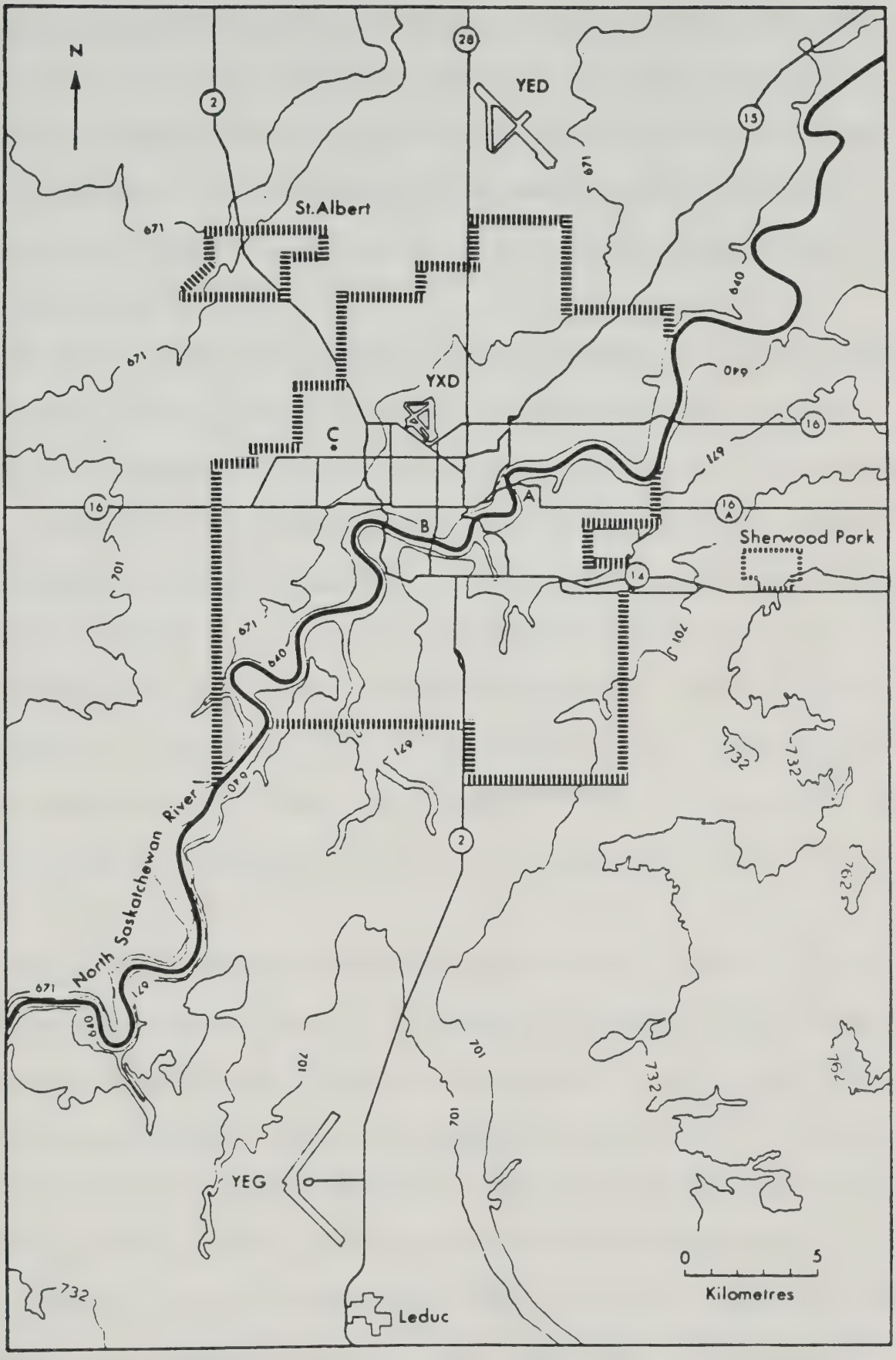


Figure 1.2 Topography of Edmonton (height contours in meters)

locations, as well as measurements of carbon monoxide. These were supplemented by data from the various rural and urban airports in the vicinity. Analyses of the observations, especially under conditions of clear skies and light winds, clearly suggest the existence of a valley micro-climate distinct from that of the city. The general characteristics are summarized below.

In early evening, shortly before sunset, cooling began as the radiation received at the ground dropped. Usually, the valley became isothermal earlier than the air over the city. Inversions developed over both valley slopes and were usually more intense than above the urban plains. That slope which was shaded first (north- or east-facing slope) developed an earlier and stronger inversion (from 8 to 18 K° $(100\ m)^{-1}$). Differences in temperature of 4 to 6 K° were common between the ridge and trough of the valley, with the latter location being similar to the rural airport (Hage ,1972).

Downslope winds with typical speeds of 0.4 to 0.6 m s^{-1} commenced shortly after the inversion formed. Slope wind speed was found to be highly correlated with the vertical temperature gradient (and corresponding horizontal temperature gradient) and must be associated with large pressure gradient forces. The slope wind maximum was observed to occur about 2 to 4 m above the slope, and, as the inversion deepened, it dropped below 0.7 m, the lowest measurement level. Above the ridge, a normal increase in wind speed with

height was observed.

A second evening maximum in pollutant (CO) concentration was observed over the city and especially within the valley. This is due to the development of the surface-based inversion. The increased stability produces much decreased vertical dilution and can overcompensate for the lower pollutant emission rates beyond the rush hour traffic peak. Recirculation of air in organized cells may also contribute to the high evening concentration within the valley.

1.3 Objectives of the Study

Almost all previous numerical work in this area has been aimed at the description of local mountain-valley wind circulations of a physical scale which greatly exceeded the dimensions of the valley under consideration. It was therfore deemed desirable to investigate the valley circulation induced by cooling along a relatively shallow slope (0.1 - 0.2) of a small urban valley (with a depth of about 50 m) by the use of a numerical model. The observational data already available would be useful not only in model verification but also as hints to model development.

This thesis contributes to a three-part study of the micrometeorology of the North Saskatchewan River valley. A one-dimensional radiative-conductive model has been developed by di Cenzo (1979) to describe the evolution of temperature profiles in different parts of the valley. He

concluded that the inclusion of advective processes would produce a major improvement in the results. This leads naturally into the need for prediction of wind fields consistent with the surface temperature changes which occur as the evening progresses. The thermodynamic variables and the corresponding circulation are intimately related and only limited success is to be expected if treated independently. However, the use of simplified variations in the thermal characteristics of the valley can provide some insight into these inter-relationships. Rudolph (1980) developed a pollutant transport model with an assumed double-vortex wind field within a 'V-shaped' valley and dispersion of pollutants by turbulent diffusion. Again, in order for such a model to predict concentrations accurately, the spatial and temporal variations in the thermodynamic and wind fields must be incorporated. This thesis describes the development of a model capable of predicting such fields within a two-dimensional axially symmetric valley cross-section. The thermodynamic equation, coupled with the vorticity equation, is solved using finite differences subject to either a constant surface cooling rate or one which is dependent on radiative transfer processes.

Chapter 2

THE THEORETICAL MODEL

2.1 Introduction

This Chapter gives details of the valley wind model developed. Assumptions, initial and boundary conditions required by the model are outlined. Numerical aspects are considered in Chapter 3.

Ideally, a valley wind model should provide the three velocity components and the temperature, pressure and density fields within the valley, over it, and above the adjacent plains, all as functions of space and time. The initial conditions of geographical location, topography, type of ground surface, the radiation away from it as a function of position and time (or insolation onto the surface in the case of daytime heating), and the prevailing atmospheric conditions such as the synoptic-scale flow, stability, humidity and cloud presence all influence the development of the slope wind in a very complex manner. Given this situation, it is desirable to concentrate on the most fundamental features of the phenomenon. To this end, the model does not possess a detailed boundary layer, nor the inclusion of moist processes (other than assumptions involving rates of heat loss at the surface given cloud-free skies).

Although computers impose much less of a restriction on modelling efforts than at one time, significant increases in

running costs and storage amounts would be expected in going from two to three space dimensions, or in going from simple to real terrain. Checks on the basic method of calculation can be made at this simple stage prior to extension into more complex regions. As well, the interpretation of results generally increases in difficulty as the model complexity increases. The likelihood of encountering new numerical errors, which are also difficult to identify and interpret, increases with complexity.

With the above simplifications, it is hoped that the flow patterns obtained can provide some understanding of the transfer processes involved. This understanding can then serve as a basis for analyzing data already available and those from future field experiments, as well as for understanding more sophisticated models.

Advection processes are of great importance in the circulation being studied and, therefore, the complications induced by the non-linearity of the equations governing temperature and velocity changes are necessary. Thus, a numerical approach to the problem is required. A finite-difference grid model was developed in order to predict the flow and thermodynamic fields as a function of space and time.

The model is initiated with the atmosphere at rest, under a variety of stability regimes. A disturbance is introduced by cooling the air at the surface and the governing equations are solved numerically.

2.2 The Governing Equations

The basic equations used were the equations of motion, the thermodynamic equation, and the continuity equation, along with the equation of state and Poisson's equation. These equations can be expressed, respectively, as

$$\frac{\partial \vec{V}}{\partial t} + (\vec{V}\cdot\vec{\nabla})\,\vec{V} = -\frac{1}{\rho}\vec{\nabla}p - g\hat{k} - 2\,\vec{\Omega}\times\vec{V} + \delta_{ij}\frac{\partial}{\partial x_j}\left[(K_m)_j\frac{\partial \vec{V}}{\partial x_i}\right] \qquad (2.2.1)$$

$$\frac{\partial \theta}{\partial t} + (\vec{V}\cdot\vec{\nabla})\,\theta = \delta_{ij}\frac{\partial}{\partial x_j}\left[(K_T)_j\frac{\partial \theta}{\partial x_i}\right] \qquad (2.2.2)$$

$$-\vec{\nabla}\cdot\vec{V} = \frac{1}{\rho}\frac{\partial \rho}{\partial t} + \frac{1}{\rho}(\vec{V}\cdot\vec{\nabla})\rho \qquad (2.2.3)$$

$$p = \rho R T \qquad (2.2.4)$$

$$\frac{T}{\theta} = \left(\frac{p}{p_0}\right)^{R/C_p} \qquad (2.2.5)$$

where the last term in (2.2.1) represents the turbulent flux of momentum using K-theory in which turbulent transfer of momentum is considered in the same manner as molecular diffusion (which is neglected here). Repeated indices imply a summation with respect to that index. Note $\delta_{i,j}=0$ if $i\neq j$ and $\delta_{i,j}=1$ if $i=j$. All other symbols have their usual meteorological meanings.

Two-dimensional flow fields were treated in this study (in the vertical (z) and cross-valley (y) directions), with

the down-valley flow (u) equal to zero. As a result, the u-component of (2.2.1) is eliminated. As the velocities to be considered are small, the coriolis accelerations were negligible compared to other terms in the equations of motion. Therefore, axial symmetry was assumed and only the fields of one-half the valley cross-section were computed. However, differences in topography, slope aspect, etc. must be taken into account when comparing the south-facing and north-facing slopes and their respective circulation regimes.

As in early treatments of the planetary boundary layer, the turbulent flux of momentum was considered to be analagous to molecular diffusion, using an eddy viscosity coefficient, K_m. Just as random motion of molecules over some mean free path leads to a transport of momentum on a small scale, irregular turbulent motions over some mixing length will also cause such a transport. The essential difference, however, is that the molecular coefficients are known functions of state whereas the corresponding turbulent exchange coefficients depend not only on the characteristics of the fluid but especially on the characteristics of the flow. Except in a millimeter thin layer at the ground, the exchange processes at the molecular level can be effectively disregarded.

In magnitude, the eddy momentum and heat diffusivities are much larger than the corresponding molecular values. The exact nature of the appropriate eddy values is typically a

complicated function of height above the ground, and the velocity and temperature profiles. The height above ground is important in the definition of an eddy mixing length. Close to the ground, the eddy size is physically limited by its distance from the ground. Further aloft, a free atmosphere eddy mixing length can be used which is no longer constrained by surface friction effects. Mechanical turbulence or forced convection is increased when the vertical wind profile indicates large amounts of shear. As the shear increases, a flow which may have been laminar initially will become unstable and develop large eddies which can transport heat and momentum quickly. However, when the atmosphere is stable, any vertical displacements will be suppressed, and the mechanical turbulence weakened. On the other hand, an unstable boundary layer acts to enhance the thermal turbulence through buoyancy forces.

From the turbulent kinetic energy equation, the terms describing production of kinetic energy through buoyancy and shear can be written as $g\overline{\theta' w'}/\theta_0$ and $-\overline{u' w'}\ \partial\bar{u}/\partial z$, respectively. All terms have their usual meteorological meanings with θ_0 representing the potential temperature of some reference atmosphere. The flux Richardson number, R_f, is defined as the ratio of the buoyancy and shear production terms, and is given by

$$R_f = \frac{g\ \overline{\theta' w'}}{\theta_0\ \overline{u' w'}\ \partial\bar{u}/\partial z} \qquad (2.2.6)$$

If the heat transfer is upward ($\overline{\theta' w'} > 0$), R_f is negative because $\overline{u' w'} < 0$ if $\partial \bar{u}/\partial z > 0$. This implies an increase in the turbulent kinetic energy. Upward heat flux usually corresponds to $\partial \bar{\theta}/\partial z < 0$, as in an unstable atmosphere. If the heat transfer is downward ($\overline{\theta' w'} < 0$), then R_f is positive and the buoyant production is negative, indicating that kinetic energy is lost. Negative values of $\overline{\theta' w'}$ typically correspond to positive values of $\partial \bar{\theta}/\partial z$, as in a stable atmosphere. If a positive value of R_f becomes very large, all turbulence becomes suppressed.

The diurnal changes in solar radiation create different wind and temperature regimes during various parts of the day. Just after sunrise, the heat received at the ground is transferred upwards in many ways. In a very thin layer above the ground, heat is transferred by molecular conduction along a very large temperature gradient. Above this, heat is transported almost entirely by forced convection. At even larger distances, a free-convection layer begins to form in which buoyancy production dominates. In order for the temperature of the air to rise, the heat flux (which is directed upwards so that $\overline{\theta' w'} > 0$) must decrease with height. According to Businger (1973), the heat flux at the surface and the height at which the flux is zero generally increase until midday, ultimately resulting in a constant flux layer up to 100 m or so. Much later in the day, as the ground begins to cool through radiational losses, a downward heat flux exists and a stable layer forms close to the

ground. This represents the time of interest in this study. Near the ground, the flux Richardson number is usually small due to the large shear in the wind, and increases from the surface up to some maximum. In the upper part of the boundary layer, instability persists, resulting in a small or negative R_f. The critical R_f is reached first at the height of the maximum, and there a laminar layer forms, effectively preventing further exchange of heat or momentum across this layer. Temperatures near the ground decrease even faster as the downward heat flux is eliminated. Friction with the ground acts to slow down the air below the laminar layer and the associated reduction in shear causes R_f to exceed its critical value, suppressing turbulence everywhere. Vertical transfer drops to near zero as a result.

The time of interest in this study is after sunset, when the inversion is present throughout the valley and slope winds are beginning to develop. For the reasons outlined previously, the vertical fluxes of heat and momentum are quite small during this period. As a result, the vertical transfer coefficients were set to zero in model integrations attempting to simulate realistic valley conditions. On occasion, the model is executed using neutral stability conditions initially, and, in this case, the vertical transfer should be non-zero. However, definition of a vertical transfer coefficient which is a function of stability was precluded in this study due to lack of time and lack of proper knowledge of its variation within small

valleys. This is left for a later study.

2.3 The Assumption of Incompressibility

The assumption of incompressibility of the flow is made ($d\rho/dt = 0$), resulting in simplification of the equation of continuity, (2.2.3). According to Batchelor (1967), the following three conditions are necessary in order for air to behave as if incompressible:

$$U^2/c^2 << 1 \quad , \qquad (2.3.1)$$

$$n^2L^2/c^2 << 1 \quad , \qquad (2.3.2)$$

$$\rho gL/\gamma p << 1 \quad , \qquad (2.3.3)$$

where c = speed of sound, n = measure of the dominant frequency of oscillations in the flow field, $\gamma = C_p/C_v$. Spatial variations of V are characterized by some length scale L and variations in the magnitude of V with respect to position and time have the magnitude, U.

The first equation, (2.3.1), states that the flow velocity must be small compared to the speed of sound. For air at 15 °C and 1 atmosphere pressure, c = 340.6 m s^{-1}, and therefore (2.3.1) was satisfied for all flows considered in this study (where U is about 1 m s^{-1}). The second equation, (2.3.2), states that the frequency of any oscillatory motion in the air must be small compared to the frequency of sound. The highest frequency resolvable in a finite-difference grid model is $n = 1/2\Delta t$ and, in the cases considered, Δt was of the order of 1 second. Thus, (2.3.2) was always satisfied.

Equation (2.3.3) restricts vertical scales of motion of the air to much less than the 'scale height', H, of the atmosphere, which is the vertical distance over which pressure and density diminish by a factor of 1/e, and is equal to $p/\rho g$. For air at 0 °C, H = 8.0 km. Even when the temperature is not uniform, it is evident that this condition will be satisfied for all motions occurring in layers of the atmosphere not exceeding a few hundred meters in depth. From the application of Batchelor's criteria, it can be seen that the assumption of incompressibility is reasonable. Equation (2.2.3) can now be rewritten as

$$\vec{\nabla}\cdot\vec{V} = 0 \quad . \tag{2.3.4}$$

2.4 The Vorticity Equation

As is customary, the vector equation of motion is replaced by a scalar equation, known as the vorticity equation, by taking the curl of (2.2.1), or equivalently by taking appropriate spatial derivatives of the two scalar component equations of motion. The latter derivation is presented here. The component equations of motion for v (cross-valley wind component in y-direction) and w (vertical wind component in z-direction) can be written as the following, after the previously mentioned assumptions have been made to (2.2.1) :

$$\frac{\partial v}{\partial t} + v\frac{\partial v}{\partial y} + w\frac{\partial v}{\partial z} = -\frac{1}{\rho}\frac{\partial p}{\partial y} + K_y\left(\frac{\partial^2 v}{\partial y^2} + \frac{\partial^2 v}{\partial z^2}\right) \tag{2.4.1}$$

$$\frac{\partial w}{\partial t} + v\frac{\partial w}{\partial y} + w\frac{\partial w}{\partial z} = -\frac{1}{\rho}\frac{\partial p}{\partial z} - g + K_z\left[\frac{\partial^2 w}{\partial y^2} + \frac{\partial^2 w}{\partial z^2}\right] \qquad (2.4.2)$$

where K_y = horizontal diffusion coefficient, and K_z = vertical diffusion coefficient. Differentiating (2.4.2) with respect to y, and (2.4.1) with respect to z, and subtracting yields

$$\frac{\partial \xi}{\partial t} + v\frac{\partial \xi}{\partial y} + w\frac{\partial \xi}{\partial z} + \xi\left[\frac{\partial v}{\partial y} + \frac{\partial w}{\partial z}\right] = \frac{1}{\rho^2}\left[\frac{\partial \rho}{\partial y}\frac{\partial p}{\partial z} + \frac{\partial \rho}{\partial z}\frac{\partial p}{\partial y}\right] + K_y\frac{\partial^2 \xi}{\partial y^2} + K_z\frac{\partial^2 \xi}{\partial z^2}$$

where

$$\xi = \frac{\partial w}{\partial y} - \frac{\partial v}{\partial z} \qquad (2.4.3)$$

ξ being the vorticity component along the down-valley axis ($\xi < 0$ for clockwise flow and vice versa). Using the continuity equation approximation for an incompressible fluid, (2.3.4), one obtains

$$\frac{\partial \xi}{\partial t} + v\frac{\partial \xi}{\partial y} + w\frac{\partial \xi}{\partial z} = \frac{1}{\rho^2}\left[\frac{\partial \rho}{\partial y}\frac{\partial p}{\partial z} + \frac{\partial \rho}{\partial z}\frac{\partial p}{\partial y}\right] + K_y\frac{\partial^2 \xi}{\partial y^2} + K_z\frac{\partial^2 \xi}{\partial z^2} \qquad (2.4.4)$$

Therefore, in this model, the local change in vorticity, must be a balance between advective changes in vorticity, the so-called 'solenoid term' given by $1/\rho^2(\partial\rho/\partial y\ \partial p/\partial z - \partial\rho/\partial z\ \partial p/\partial y)$, and diffusion of vorticity.

At this point, the solenoid term will be discussed in terms of how it is able to alter the vorticity values. Such a consideration may shed some light on the kinds of airflow or circulation expected to occur within the valley. In a barotropic atmosphere, $\rho = \rho$(p only), and there will be no contribution to (2.4.4) through this term. This can be seen by considering the definition of circulation, C, in a fluid

as given below

$$C = \oint v\,dy + w\,dz$$

where ξ = C per unit area. It then follows that

$$\frac{dC}{dt} = \oint \frac{dv}{dt}\,dy + \frac{dw}{dt}\,dz$$

If only the terms involving pressure gradients are retained in the expressions for dv/dt and dw/dt, one obtains

$$\frac{dC}{dt} = -\oint \frac{1}{\rho}\left(\frac{\partial p}{\partial y}\,dy - \frac{\partial p}{\partial z}\,dz\right) = -\oint \frac{1}{\rho}\,dp \qquad (2.4.5)$$

With $\rho = \rho(p)$, this becomes the closed line integral of an exact differential and as such is zero.

In general, density is not determined simply from the pressure (in which case the atmosphere is called baroclinic) and the isobaric surfaces (dp = 0) and the isosteric surfaces ($d\rho = 0$) intersect each other. Consider the baroclinic fluid shown in Figure 2.1. Evaluating (2.4.5) around the path indicated results in

$$\frac{dC}{dt} = \frac{-2\,\Delta p}{\rho_{1\to 2}} + 0 + \frac{2\,\Delta p}{\rho_{3\to 4}} + 0$$

This results in growth in circulation in the negative (clockwise) sense about the curve, i.e. in such a direction as to let denser fluid sink while lighter fluid rises.

The direction of the circulation which grows from a state of rest as a result of baroclinicity turns the isosteres more nearly parallel to the isobars by moving the dense fluid towards high pressure and the lighter fluid towards low pressure. This process acts to convert potential

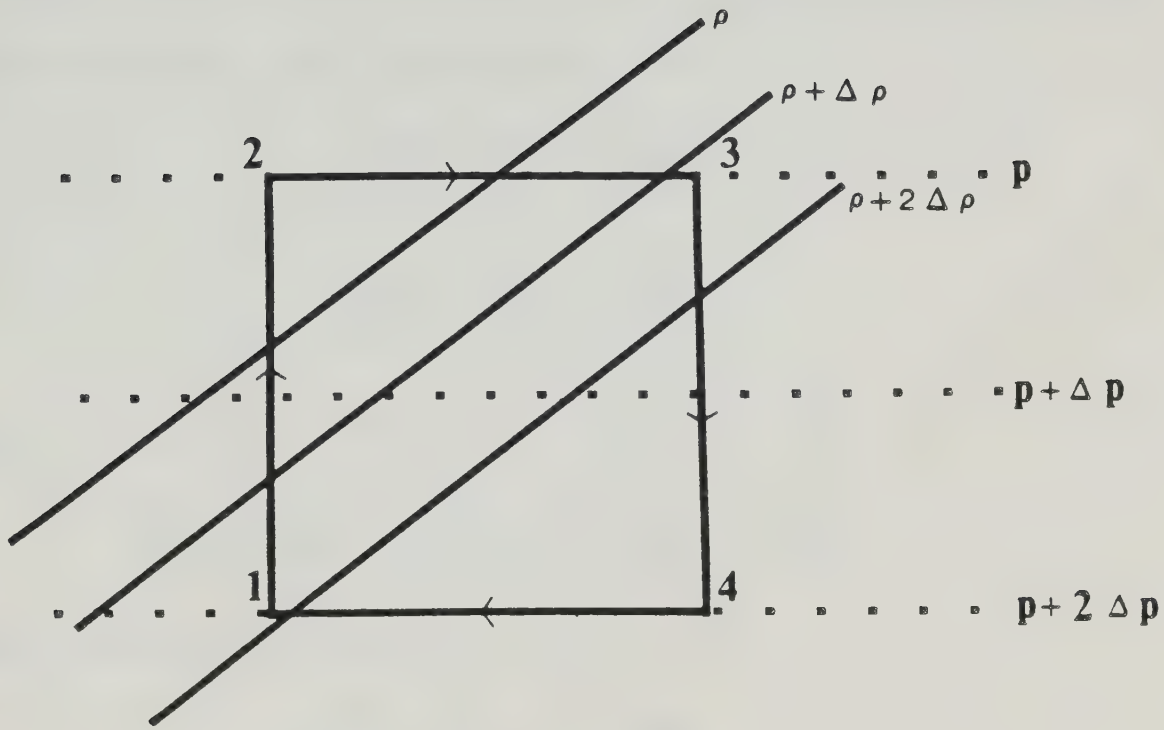


Figure 2.1 Relation between isobars and isosteres in a baroclinic fluid

energy of the mass distribution of the fluid into kinetic energy of circulation, thereby minimizing the potential energy.

In this model of the boundary layer, as in many others, e.g. Malkus and Witt (1959), Thyer (1966), and Orville (1964), the solenoid term was approximated to be $(g/\theta\ \partial\theta/\partial y)$ The equation of state, (2.2.4), by taking logarithms and differentiating, can be rewritten as

$$\frac{1}{\rho}\frac{\partial \rho}{\partial y} = \frac{1}{p}\frac{\partial p}{\partial y} - \frac{1}{T}\frac{\partial T}{\partial y}$$

and

$$\frac{1}{\rho}\frac{\partial \rho}{\partial z} = \frac{1}{p}\frac{\partial p}{\partial z} - \frac{1}{T}\frac{\partial T}{\partial z}$$

These are used to rewrite the solenoid term as

$$\frac{1}{\rho}\frac{\partial p}{\partial z}\left(\frac{1}{p}\frac{\partial p}{\partial y} - \frac{1}{T}\frac{\partial T}{\partial y}\right) - \frac{1}{\rho}\frac{\partial p}{\partial y}\left(\frac{1}{p}\frac{\partial p}{\partial z} - \frac{1}{T}\frac{\partial T}{\partial z}\right)$$

Adding and subtracting $g/\theta\ \partial\theta/\partial y$ with

$$\frac{1}{\theta}\frac{\partial \theta}{\partial y} = \frac{1}{T}\frac{\partial T}{\partial y} - \frac{R}{C_p}\frac{1}{p}\frac{\partial p}{\partial y}$$

from the Poisson equation, (2.2.5), and simplifying, results in

$$\frac{-1}{\rho T}\frac{\partial p}{\partial z}\frac{\partial T}{\partial y} + \frac{1}{\rho T}\frac{\partial p}{\partial y}\frac{\partial T}{\partial z} + \frac{g}{\theta}\frac{\partial \theta}{\partial y} - g\left(\frac{1}{T}\frac{\partial T}{\partial y} - \frac{R}{C_p}\frac{1}{p}\frac{\partial p}{\partial y}\right)$$

Letting $$\gamma = -\frac{\partial T}{\partial z} = \text{ambient lapse rate} \qquad (2.4.6)$$

and $$\gamma_d = \frac{g}{C_p} = \text{dry adiabatic lapse rate} \qquad (2.4.7)$$

one obtains, after combining terms, that the solenoid term can be expressed as

$$\underset{(A)}{\frac{g}{\theta}\frac{\partial\theta}{\partial y}} + \frac{\partial T}{\partial y}\underbrace{\left(-\frac{R}{p}\frac{\partial p}{\partial z} - \frac{g}{T}\right)}_{(B)} + \frac{\partial p}{\partial y}\frac{R}{p}\underbrace{\frac{g}{C_p}\left(1 - \frac{\gamma}{\gamma_d}\right)}_{(C)} \qquad (2.4.8)$$

Rough estimates of the magnitudes of the terms in (2.4.8) can be made by considering the horizontal and vertical pressure gradients which exist within a river valley such as the one being considered in this study. Up to this point, no mention has been made of the hydrostatic assumption,

$$\frac{\partial p_h}{\partial z} = -\rho g = -\frac{p}{RT}g \qquad (2.4.9)$$

obtained from the third equation of motion, (2.4.2), when vertical accelerations and diffusion are neglected. The question of validity of this approximation can be found in comparing the magnitudes of typical hydrostatic and non-hydrostatic pressures.

First, hydrostatic pressures are computed at two points within the valley where differences are expected to be largest. The hydrostatic equation above, (2.4.9), can be used to integrate downwards to estimate the pressures resulting from various temperature regimes in different parts of the valley using

$$\int_{p}^{p'} \frac{dp_h}{p_h} = -\frac{g}{R}\int_{z}^{z'} \frac{dz}{T} \qquad (2.4.10)$$

The assumption is made that at $z = z'$, the temperature, T', and pressure, p', are constant.

Based on observations within the North Saskatchewan River valley on 21-22 October, 1977, horizontal temperature differences between the slope and the free air of close to 1 C° were recorded over a distance of 185 m (Paterson (1978)). These values were obtained from a thermograph located on the slope 26 m above the valley floor (station #2) and from averages of thermocouple readings obtained in the free air at heights of about 30 m (station #4b) and 22 m (station #4c) above ground. The latter were suspended from a bridge which spans the valley. The locations of the instruments are shown in Figure 2.2. Some assumed temperatures and corresponding lapse rates (which were constant with height) were used to simulate the above observations. The pressure and temperature at the top of the model ($z' = 108$ m) were assumed to be 917.8 mb and 278.632 °K, respectively, as assumed in the standard run - see Chapter 4. The variation in temperature with height is given by $T(z) = T' + \gamma(108 - z(m))$. Figure 2.3 illustrates these assumptions. At location A, (2.4.10) becomes

$$\int_{p_A}^{p'} \frac{dp}{p} = -\frac{g}{R}\int_{26}^{108} \frac{dz}{T} = -\frac{g}{R}\int_{26}^{108} \frac{dz}{T' + \gamma\,(108-z)}$$

or

$$\ln \frac{p'}{p_A} = \ln \left(\frac{T'}{T' + \gamma\,(82)}\right)^{g/R\gamma_A}$$

where the integration on the right hand side has been performed using a change of variable technique. Evaluating the above, using a horizontal temperature gradient of 1 C° per 200 m, one obtains p_A = 927.097 mb and p_B = 927.079 mb.

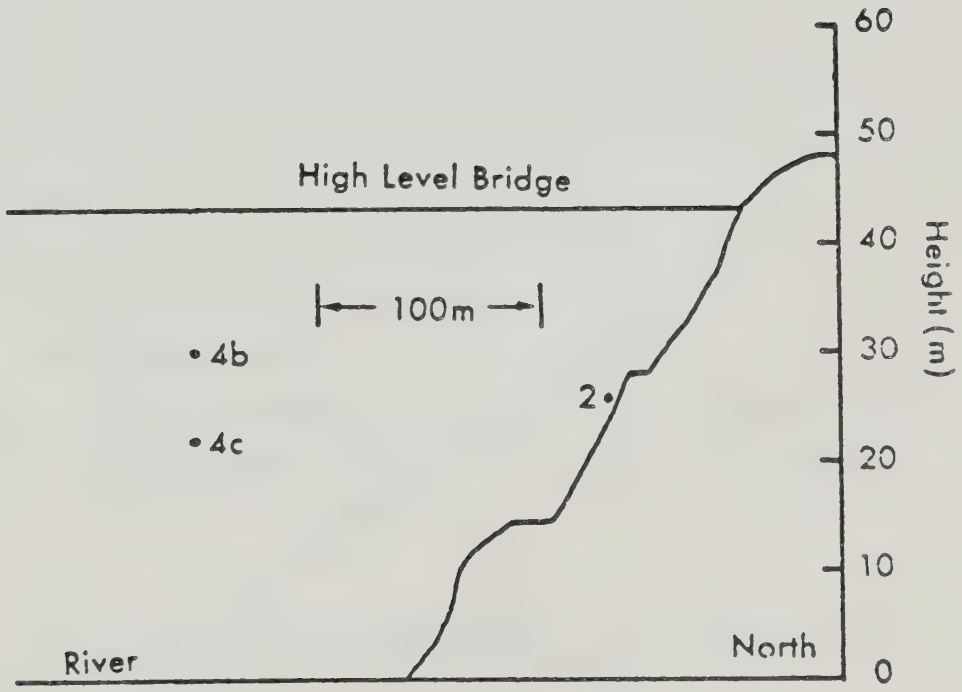


Figure 2.2 Location of instruments used to estimate horizontal temperature differences within the North Saskatchewan River valley

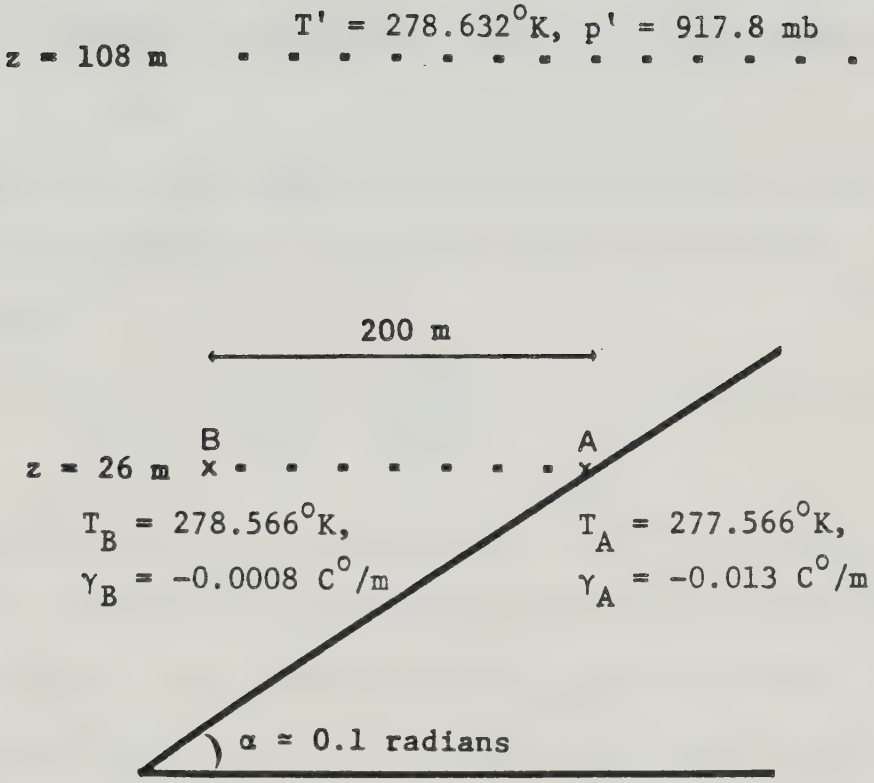


Figure 2.3 Assumed temperatures and lapse rates used to estimate hydrostatic pressures at A and B

This results in a horizontal hydrostatic pressure gradient of 9×10^{-5} mb m^{-1} or 9×10^{-3} Pa m^{-1}. Repeating this calculation for a horizontal temperature difference of 10 C°, where T_A = 267.992 °K, and T_B = 277.972 °K, γ_A = -0.130 C° m^{-1} and γ_B = -0.008 C° m^{-1} results in a horizontal hydrostatic pressure gradient of 6×10^{-2} Pa m^{-1}. This is expected to be an overestimate of the real gradients involved.

Secondly, the non-hydrostatic pressures at these same two points are considered. Equation (2.4.2) can be approximated as

$$\frac{dw}{dt} = -\frac{1}{\rho}\frac{\partial p_h}{\partial z} - \frac{1}{\rho}\frac{\partial p_{nh}}{\partial \partial z} - g$$

neglecting diffusion. By consideration of the typical accelerations involved at the positions under consideration, A and B in Figure 2.3, estimates of p_{nh} can be made. Close to the slope, downslope winds up to 0.5 m s^{-1} are typical in the North Saskatchewan River valley. Assuming the angle of the sloping ground to be 0.1 radians, a vertical velocity component of about 0.05 m s^{-1} results. Thus, w undergoes some deceleration from 0.05 m s^{-1} at mid-slope (say, z = 25 m) to 0.0 at the horizontal valley floor. This occurs over a time interval equal to about 500 seconds (the downslope wind, having speeds of 0.5 m s^{-1}, covers 250 m - mid-slope to valley floor - in about 500 seconds). Substituting this estimate of dw/dt, and integrating $dw/dt = -1/\rho\ \partial p_{nh}/\partial z$ from z = 0 to z = 25 m, one obtains

$p_{nh}|_A = -\rho\ dw/dt|_A \Delta z = +3 \times 10^{-5}$ mb. Similar calculations within the free air, assuming w accelerates from 0.0 at the valley floor to about 0.005 m s^{-1} at z = 25 m in 5000 seconds time, result in $p_{nh}|_B = +3 \times 10^{-7}$ mb. These rough calculations reveal that the non-hydrostatic pressures are much smaller than the hydrostatic ones, and, as a result, the pressures involved in the study are clearly principally hydrostatic in nature. The horizontal gradient in non-hydrostatic pressure, which may contribute to horizontal accelerations through equation (2.4.1), are found to be very small as well.

Returning now to the evaluation of the terms comprising the solenoid term, given by (2.4.8), one finds that term B is identically zero if the pressure is assumed hydrostatic. Terms A and C can be estimated based on the rough calculations given above. Term C depends on the horizontal pressure gradient as well as the stability of the air. Table 2.1 indicates the relative magnitudes of these terms for the two cases considered above, assuming $p = p_h$: 1.) a horizontal temperature difference of 1 C° over 200 m, 2.) a horizontal temperature difference of 10 C° over 200 m. Potential temperatures required for term A are computed from the assumed temperatures and hydrostatically derived pressures. From the Table, it is clear that term C is much smaller than term A, and therefore is neglected in the model.

Finally, the vorticity equation, (2.4.4), can be expressed as

Table 2.1 Estimates of magnitudes of term A ($g/\theta\ \partial\theta/\partial y$) and term C ($\partial p/\partial y\ R/p\ g/C_p\ (1-\gamma/\gamma_d)$) comprising the solenoid term

$\partial T/\partial y = 1C^o/200m$		
term A		term C
$-2\times10^{-4}\ s^{-2}$	neutral (γ=+.01 C^o/m)	0
	stable (γ=-.004 C^o/m)	$+4\times10^{-7}\ s^{-2}$
	very stable (γ=-.04 C^o/m)	$+1\times10^{-6}\ s^{-2}$
$\partial T/\partial y = 10C^o/200m$		
term A		term C
$-2\times10^{-3}\ s^{-2}$	neutral (γ=+.01 C^o/m)	0
	stable (γ=-.004 C^o/m)	$+3\times10^{-6}\ s^{-2}$
	very stable (γ=-.04 C^o/m)	$+9\times10^{-6}\ s^{-2}$

$$\frac{\partial \xi}{\partial t} = - v \frac{\partial \xi}{\partial y} - w \frac{\partial \xi}{\partial z} + \frac{g}{\theta} \frac{\partial \theta}{\partial y} + K_y \frac{\partial^2 \xi}{\partial y^2} + K_z \frac{\partial^2 \xi}{\partial z^2} \qquad (2.4.11)$$

2.5 Use of Streamfunctions and Related Boundary Conditions

For two-dimensional incompressible flow fields, the non-divergent velocity field, $\vec{V} = v\,\hat{j} + w\,\hat{k}$, where $\hat{j}$ and $\hat{k}$ are unit vectors in the y and z directions, respectively, can be expressed using a streamfunction, ψ. In this case, the velocity, streamfunction and vorticity fields are related by

$$v = \frac{\partial \psi}{\partial z} \qquad (2.5.1)$$

$$w = - \frac{\partial \psi}{\partial y} \qquad (2.5.2)$$

and

$$\xi = - \nabla^2 \psi = - \left(\frac{\partial^2 \psi}{\partial y^2} + \frac{\partial^2 \psi}{\partial z^2} \right) \qquad (2.5.3)$$

These three diagnostic equations were used to obtain the velocity components, v and w, from the vorticity values predicted by (2.4.11).

In order to satisfy certain velocity boundary conditions, corresponding boundary conditions must be imposed on the streamfunction, ψ. The relationship between velocities and streamfunction may be better understood by writing $\vec{V}$ as $- \hat{i} \times \vec{\nabla}\psi$, where $\hat{i}$ is a unit vector in the x-direction. If $\vec{\nabla}\psi$ happens to be in the y-direction, then $\vec{V}$ is in the z-direction, and vice versa. In other words, $\vec{V}$ is parallel to a surface of constant ψ. As well, if $\vec{\nabla}\psi = 0$, then $\vec{V} = 0$.

Since axial symmetry was assumed (about the vertical lines bordering the valley cross-section briefly described previously), the horizontal velocity component was required to be zero. Equivalently, this disallowed outflow or inflow along these lateral boundaries. Therefore, $\partial\psi/\partial z = 0$ or ψ is constant with height there.

Using similar arguments for the upper and lower boundaries, ψ was required to be a constant everywhere along the cross-section boundary. Since ψ occurred only in the form of derivatives in the equations, this constant was arbitrary and set to zero for simplicity. Flow everywhere parallel to the boundary ('free-slip') was guaranteed through these boundary conditions on the streamfunction.

2.6 Potential Temperature Boundary Conditions at the Ground

The diurnal temperature change at the surface is the driving force for the valley wind development. Cooling along the valley slopes creates a non-zero horizontal potential temperature gradient, and this in turn is responsible for the creation of vorticity (through the solenoid term).

Following the approach of Thyer (1966), the surface temperature boundary condition was initially determined through a requirement that the temperature gradient at the ground surface be consistent with the rate of heat flow and the eddy conductivity. Assuming some rate of heat loss per unit area, Q_o, the outgoing energy from the sloping surface is $Q_o \cos(\alpha)$, where α is the angle the sloping ground makes

with the horizontal. In order for this heat loss to be completely balanced by conduction from the air with some eddy conductivity, K_T, a certain vertical temperature gradient must exist which satisfies

$$Q_0 \cos(\alpha) = - K_T \rho C_p \frac{\partial \theta}{\partial z} \qquad (2.6.1)$$

based on the heat conduction equation.

Such constraints, however, provided inappropriate cooling rates at the surface. In reality, surface temperatures are altered through radiation effects, advection, and diffusion processes, and this early approach was soon abandoned in favour of simply prescribing a rate of surface temperature change.

Some observations of surface temperature changes within valleys are available. Orville (1964) chose to model the diurnal trend in temperature in mountainous terrain as reported in Geiger (1957). In his model, a sinusoidal potential temperature change at the surface was used, having a period of 24 hours and an amplitude of 7 C° at the valley bottom and decreasing linearly with height to 3 C° at the top (1 km above).

Rao and Snodgrass (1981) attempted to determine a steady-state drainage flow, and they used a constant cooling rate of 2 C° per hour for the first hour. Subsequently, the surface temperature was unchanging. Steady drainage flow was attained "in a few hours". The specified cooling rate was rather arbitrary, and the time scale of the evolution of the

flow was interpreted simply as an indicator of the corresponding surface temperature deficit.

In most valley model integrations in this study, which lasted well under an hour, a constant surface cooling rate of 2 C° per hour was used. All the sensitivity analyses were performed under these conditions. A radiative approach to the problem of heat transfer in the lower layers of the atmosphere was used by Brunt (1934). He showed that radiative transfer of heat could be approximated as a diffusion process, with a constant exchange coefficient, K_R, called the radiative diffusivity, i.e.

$$\frac{\partial T}{\partial t} = K_R \frac{\partial^2 T}{\partial z^2} \qquad (2.6.2)$$

This is based on the absorption spectrum of water vapour ; long-wave radiation emitted by the surface of the earth is partly absorbed by the water vapour in the atmosphere and reradiated. The numerical value of K_R was a function of temperature, the distribution of vapour pressure with height, etc. but by using typical values, Brunt suggested that $K_R = 0.13\ m^2\ s^{-1}$. Anfossi et al. (1976) experimentally determined a value of $0.3\ m^2\ s^{-1}$ under conditions favourable for radiative inversions. The use of a diffusion process to model the radiative heat transfer near the ground was attractive and easily implemented into the model under development simply by modifying $(K_T)_z$ in (2.2.2). Differentiating (2.6.2) once with respect to z, and replacing $\partial T/\partial z$ by the thermal flux, f, one obtains

$$\frac{\partial f}{\partial t} = K_R \frac{\partial^2 f}{\partial z^2} \qquad (2.6.3)$$

The solution to this differential equation was obtained by Brunt in order to predict nighttime minimum temperatures, resulting from radiative cooling at the ground alone with a constant heat flux, $f_o = \partial T/\partial z|_{z=o}$. In other words, it was assumed that the net loss of heat by radiation from the ground to the atmosphere, R_N, was constant. From (2.6.2), R_N can be expressed as $K_R \rho C_p \partial T/\partial z|_{z=o}$. By integrating the solution to (2.6.3), f(z,t), the original variable, T(z,t), was determined to be

$$T(z,t)=T(0,0)-\frac{2 R_N}{\pi^{\frac{1}{2}}\rho C_p K_R}\left[(K_R t)^{\frac{1}{2}}\exp(-z^2/4K_R t) - \frac{z}{2}\int_{\frac{z}{2(K_R t)^{\frac{1}{2}}}}^{\infty} \exp(-u^2)\, du\right] \qquad (2.6.4)$$

Therefore, the surface temperature, T(0,t), is expressed simply as

$$T(0,t) = T(0,0) - \frac{2 R_N t^{\frac{1}{2}}}{(\pi K_R)^{\frac{1}{2}}\rho C_p} \qquad (2.6.5)$$

In Chapter 4, the results of an integration using (2.6.3) as the surface temperature boundary condition are given.

2.7 Initial Conditions

For the initial conditions of a state of complete rest, the vorticity, velocity components, and streamfunction were all set to zero. The only other quantity which required initialization was the potential temperature. Given an initial lapse rate and the temperature and pressure at the lowest

level, the potential temperature field everywhere in the valley cross-section was computed using Poisson's equation, (2.2.5), the hydrostatic equation, (2.4.9), and the equation of state, (2.2.4). Poisson's equation can be written in logarithmic form as

$$d \ln\theta = d \ln T - \frac{R}{C_p} d \ln p$$

Substituting (2.2.4) and simplifying results in

$$d \ln\theta = \frac{dz}{T}\left\{\frac{dT}{dz} + \frac{g}{C_p}\right\}$$

Using the lapse rates defined by (2.4.6) and (2.4.7), one obtains

$$d \ln\theta = \frac{dz}{T}\{\gamma_d - \gamma\} \qquad (2.7.1)$$

The potential temperature at the valley trough can be computed using (2.2.5) given the trough temperature and pressure. A surface pressure of 930 mb was used for Edmonton. The potential temperature at any height z above the valley floor is computed using (2.7.1) and by integrating upwards from the ground surface. The actual temperature, T, is required for this computation but it can be found from the known constant lapse rate. The isentropic (constant potential temperature) surfaces are assumed constant with height initially everywhere within the valley.

2.8 Summary - Prognostic and Diagnostic Equations

The simplified prediction equations which describe the thermodynamics and circulation are

$$\frac{\partial \theta}{\partial t} = - v \frac{\partial \theta}{\partial y} - w \frac{\partial \theta}{\partial z} + K_y \frac{\partial^2 \theta}{\partial y^2} + K_z \frac{\partial^2 \theta}{\partial z^2} \qquad (2.2.2)$$

$$\frac{\partial \xi}{\partial t} = - v \frac{\partial \xi}{\partial y} - w \frac{\partial \xi}{\partial z} + \frac{g}{\theta} \frac{\partial \theta}{\partial y} + K_y \frac{\partial^2 \xi}{\partial y^2} + K_z \frac{\partial^2 \xi}{\partial z^2} \qquad (2.4.11)$$

Given initial and boundary conditions, these equations were solved numerically. From the ξ field so derived, the following diagnostic equations were used to solve for the corresponding velocity components :

$$v = \frac{\partial \psi}{\partial z} \qquad (2.5.3)$$

$$w = - \frac{\partial \psi}{\partial y} \qquad (2.5.1)$$

$$\xi = - \nabla^2 \psi \qquad (2.5.2)$$

Chapter 3

NUMERICAL ASPECTS OF THE COMPUTER MODEL

3.1 Introduction

As previously indicated, the non-linear character of the system of equations to be solved necessitates the use of numerical methods, since general analytical solutions are not available. To this end, the relevant equations were set up in finite-difference representations in time and space. The numerical method described is, in principle, applicable to three space dimensions as well as to two. However, the actual computations are two-dimensional in order to make computer storage and run-time costs feasible. According to the Eulerian system of equations, time (t) and two space co-ordinates (y and z) were chosen as independent variables. Boundary conditions appropriate to the chosen finite-difference formulation of the equations are required. Approximate finite-difference formulae to the equations under consideration may be obtained by various methods. However, each formulation possesses certain levels of accuracy, consistency, stability, convergence and efficiency.

The accuracy of a given finite-difference formulation is determined by estimating the truncation error involved in estimating a derivative, say, by some grid point approximation. For such an approximation to be considered consistent, it should approach the derivative as the grid

interval approaches zero. Given that the true solution is bounded, a finite-difference formulation is termed stable if the difference between the numerical solution and the true solution remains bounded with time. Typically, some constraint on the time step, Δt, is required, in order for the method to remain stable. If the error approaches zero as both the grid size and time step are decreased, then the solution is called convergent. For properly posed initial boundary value problems described by partial differential equations with consistent finite-difference formulations, stability is the necessary and sufficient condition for convergence. Finally, computer storage and costs must be considered in the selection of a numerical scheme. For a simple problem with a small number of variables, little computer time is required and a sophisticated scheme of high-order accuracy may be used, whereas for a system of many variables, accuracy must be compromised in the interests of efficiency. Whether a given scheme is explicit or implicit comes into consideration in this regard. For an excellent discussion of numerical methods for atmospheric studies, see Mesinger and Arakawa (1976) or for a more mathematical discussion see Potter (1973).

In order to compare the numerical solutions obtained from various finite-difference formulations for diffusion type terms, a simple equation for which the analytical solution was available, was used. This was the one-dimensional heat conduction equation, subject to certain relevant

initial and boundary conditions. In this chapter, various numerical solutions to this equation are presented along with the analytical ones derived. In the early stages of the valley model integration, vertical diffusion processes dominate, and, as a result, the solutions obtained from the one-dimensional diffusion equation with the same initial and boundary conditions are very similar to those of the valley model equations. This provides a check on the early stages of the evolution of the thermodynamic fields. Finally, in this chapter, a technique for solving an elliptic Poisson equation is outlined. It was used to obtain the streamfunction field, given vorticity values, through equation (2.5.3) and is termed Liebmann sequential relaxation.

3.2 The Grid

In order to study the circulation within a small urban river valley, it is necessary to define a physical boundary which is realistic but also fairly simple. A nearly 'V-shaped' valley was used with physical dimensions resembling those of the North Saskatchewan River valley. Due to the meandering nature of the river, asymmetries in the topography of the valley are evident. Figure 3.1 indicates a typical vertical cross-section through the valley, close to the city center, at a point where the river is aligned east-west. The north-facing, or south, slope was modelled in this study, using a much simplified lower boundary indicated by the dashed line.

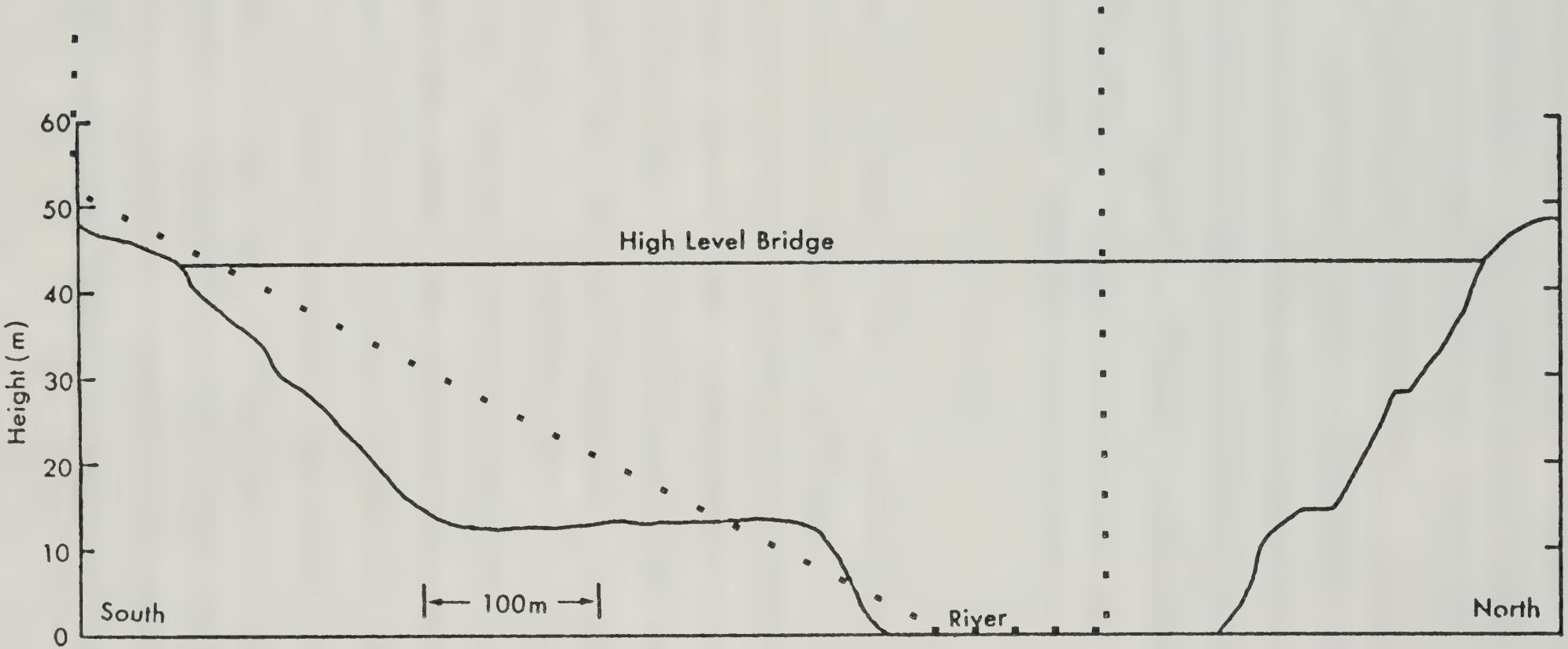


Figure 3.1 Actual and model approximation (dashed) of valley cross-section in Edmonton

Most simulations, therefore, occupied a two-dimensional region bounded by a lower surface consisting of a ridge 52 m high, and a horizontal valley floor 80 m wide. The slope of the ground surface was approximated to be 0.1, forming an angle, α, of about 5.7° with the horizontal valley floor. Some results are also presented in Chapter 4 for a slope of 0.2. In order to associate grid points at the boundary with the surface of the earth, constraints are placed upon the horizontal and vertical grid spacings permissible in that region, Δy and Δz, respectively such that

$$\tan(\alpha) = \frac{\Delta z}{\Delta y} \qquad (3.2.1)$$

Close to the ground surface, gradients in most variables are large and higher resolution in terms of the grid spacing is needed. A logarithmic grid was felt difficult to implement due to the geometry of the area being considered. A finite element approach, which can incorporate variable grid spacings and is generally well suited for complex terrain, is now becoming useful in meteorological applications. However, it was not considered at the time when model development was begun. Use of terrain-following co-ordinates has much to offer in terms of reducing complex geometry to a simple rectangular region but introduces many other complications once the equations have been transformed. As indicated earlier, a finite-difference technique was selected to integrate the equations numerically. The grid length finally chosen was constant in the

lower part of the valley cross-section (Δz_1) and larger, but still constant in the upper region (Δz_2) where the variables are expected to change more smoothly. A constant grid length (Δy) was used in the horizontal, or north-south, direction.

According to Thyer (1966), the height of the horizontal upper boundary should be at least twice the ridge height, if it is to include the entire region which such a circulation is likely to occupy. In most runs, the height of the upper boundary was chosen as 108 m but sensitivity to this value is considered in Chapter 4. A schematic diagram of the grid point lattice is given in Figure 3.2.

At any time t, any point in the region can be referred to by a set of indices (J,K,n), the points being numbered horizontally by J from the valley axis (J = 1) to the ridge line (J = JMAX), vertically by K from the valley trough (K = 1) upward to K = KMAX, and a time index n where $t = n \Delta t$. This notation will be used in subsequent sections which deal with the finite-difference formulations and boundary conditions.

3.3 Initial and Boundary Conditions in Terms of Finite Differences

3.3.1 Initial Conditions

Since the atmosphere is assumed to be at rest initially, all grid point values of vorticity, ξ, streamfunction, ψ, and velocity components, v and w, are set to zero :

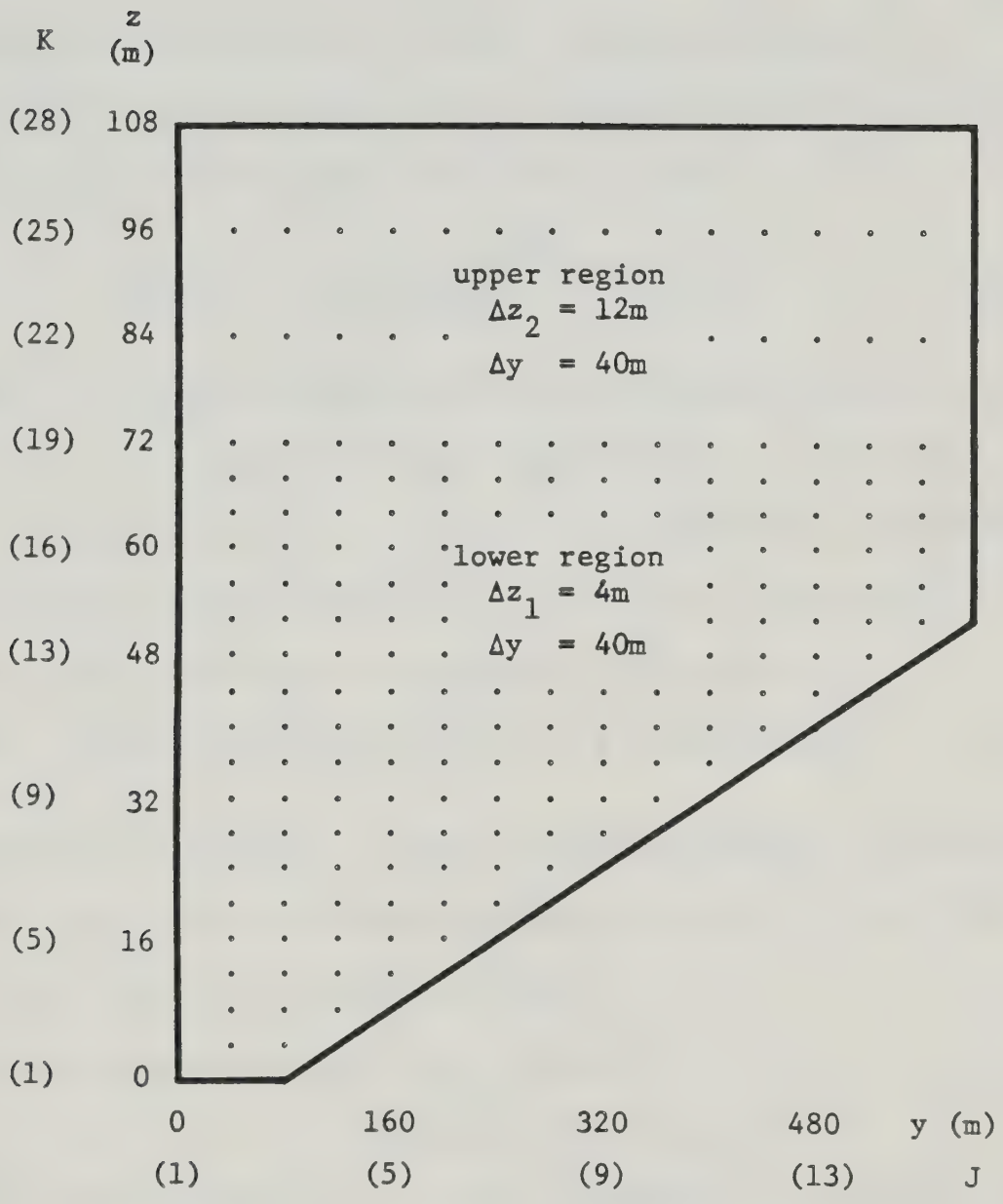


Figure 3.2 Grid configuration for valley model

$$\left.\begin{aligned} \xi(J,K,0) &= 0 \\ \psi(J,K,0) &= 0 \\ v(J,K,0) &= 0 \\ w(J,K,0) &= 0 \end{aligned}\right\} \begin{aligned} &1 \leq J \leq JMAX, \\ &1 \leq K \leq KMAX. \end{aligned} \qquad (3.3.1)$$

The potential temperature at the valley trough, $\theta(1,1,0)$, is easily obtained from the initial temperature, T(1,1,0), and pressure, p(1,1,0), using (2.2.5), to be

$$\theta(1,1,0) = \left(\frac{P_0}{P(1,1,0)} \right)^{R/C_p} T(1,1,0) \quad . \qquad (3.3.2)$$

Remember T(1,K,0) is specified by the valley trough temperature, T(1,1,0), and the known lapse rate, γ, through (2.4.6). Using (2.7.1) to obtain the potential temperature field directly above the valley trough by integrating upwards using centered differences, one obtains

$$\theta(1,K,0) = \exp\{\ln \theta(1,K-2,0) + (\gamma_d - \gamma)\, 2\, \Delta z/T(1,K-1,0)\} \quad . \qquad (3.3.3)$$

For the first interval, a one-sided difference formulation must be used, using the mean temperature for that layer, (T(1,1,0) + T(1,2,0))/2, as below,

$$\theta(1,2,0) = \exp\{\ln \theta(1,1,0) + (\gamma_d - \gamma)\, \Delta z/ (T(1,1,0) + T(1,2,0))/2\} \quad . \qquad (3.3.4)$$

The isentropic surfaces are all horizontal initially, and, therefore,

$$\theta(J,K,0) = \theta(J-1,K,0), \quad 1 < J \leq JMAX \quad , \qquad (3.3.5)$$

and the entire potential temperature field is now specified.

3.3.2 Lateral Boundary Conditions

According to arguments outlined in Section 5 of Chapter 2, the flow must be purely vertical at the lateral boundaries, J = 1 and J = JMAX. Therefore,

$$\left.\begin{aligned} v(1,K,n) &= 0 \\ v(JMAX,K,n) &= 0 \end{aligned}\right\} \begin{aligned} &1 \leqslant K \leqslant KMAX, \\ &n \geqslant 0. \end{aligned} \qquad (3.3.6)$$

As well, these boundaries form lines of symmetry, and the circulation on either side is assumed to be a mirror image of that computed within the valley cross-section being considered. Thus, the streamfunction values on one side of a lateral boundary are equal in magnitude but opposite in sign to those on the other. See Figure 3.3. The vertical velocity along these boundaries, e.g. at the grid location denoted by A on Figure 3.3, can be computed from (2.5.2), assuming $\psi(B) = -\psi(C)$, to be

$$w(A) = -(\psi(C) - \psi(B))/2\Delta y = -\psi(C)/\Delta y$$

In general, then,

$$\left.\begin{aligned} w(1,K,n) &= -\psi(2,K,n)/\Delta y \\ w(JMAX,K,n) &= \psi(JMAX-1,K,n)/\Delta y \end{aligned}\right\} \begin{aligned} &1 \leqslant K \leqslant KMAX, \\ &n \geqslant 0. \end{aligned} \qquad (3.3.7)$$

Since $\partial w/\partial y = 0$ through symmetry and $v = 0$ as before, the vorticity along the lateral boundaries must also be zero, through (2.4.3). Thus,

$$\left.\begin{aligned} \xi(1,K,n) &= 0 \\ \xi(JMAX,K,n) &= 0 \end{aligned}\right\} \begin{aligned} &1 \leqslant K \leqslant KMAX, \\ &n \geqslant 0. \end{aligned} \qquad (3.3.8)$$

The streamfunction is constant and arbitrarily set to zero.

$$\left.\begin{aligned} \psi(1,K,n) &= 0 \\ \psi(JMAX,K,n) &= 0 \end{aligned}\right\} \begin{aligned} &1 \leqslant K \leqslant KMAX, \\ &n \geqslant 0. \end{aligned} \qquad (3.3.9)$$

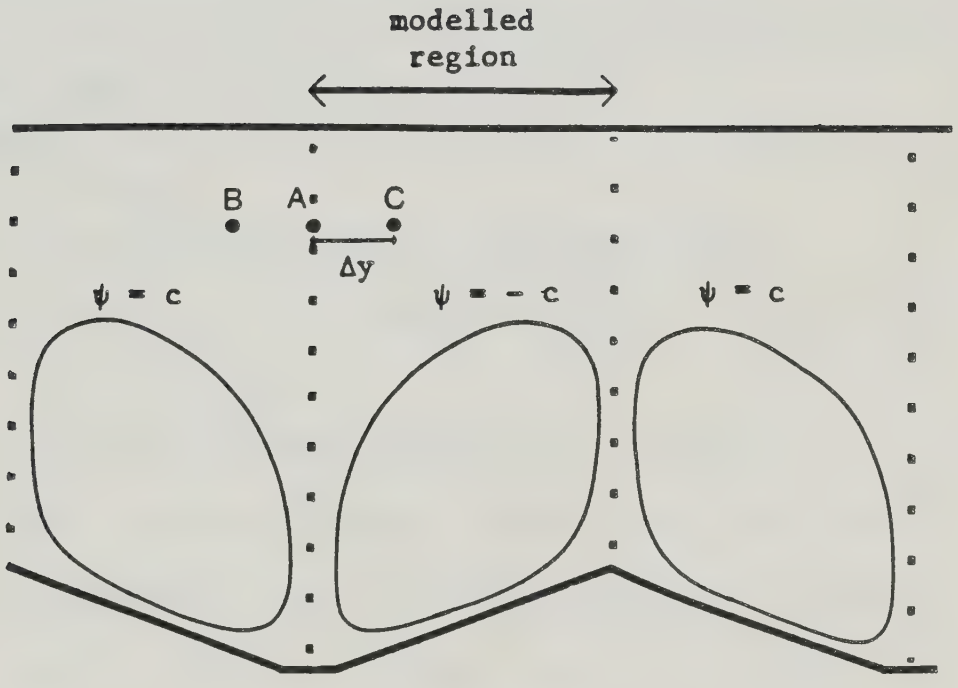


Figure 3.3 Schematic illustration of axial symmetry and boundary conditions

Horizontal temperature gradients across the lateral boundaries vanish through symmetry.

3.3.3 Lower Boundary Conditions

As free-slip boundary conditions are applied at the ground, velocities must be parallel to the lower surface. Along the horizontal part, therefore, $w(J,K,n) = 0$, and v is determined from the vertical streamfunction gradient using one-sided differences, since streamfunctions below the ground are not available. A one-sided formula, using two points above the surface, is given by

$$v(J,K,n) = \left.\frac{\partial \psi}{\partial z}\right|_{(J,K,n)} \qquad (3.3.10)$$
$$= \{-3/2\psi(J,K,n)+2\psi(J,K+1,n)-1/2\psi(J,K+2,n)\}/\Delta z \quad .$$

This approximation is also used to obtain the vorticity, since $\xi = -\partial v/\partial z$ there, or

$$\xi(J,K,n) = -\{-3/2v(J,K,n)+2v(J,K+1,n)-1/2v(J,K+2,n)\}/\Delta z \quad . \qquad (3.3.11)$$

Along the sloping ground surface, the magnitude of the velocity is computed from the streamfunction gradients above the slope (again, in a one-sided fashion) since from (2.5.4)

$$|\vec{V}| = |\vec{\nabla}\psi| = \{(\partial\psi/\partial y)^2 + (\partial\psi/\partial z)^2\}^{\frac{1}{2}} \quad . \qquad (3.3.12)$$

The individual velocity components are then determined using $\vec{V} = v\,\hat{j} + w\,\hat{k} = -(|\vec{V}|\cos(\alpha)\,\hat{j} + |\vec{V}|\sin(\alpha)\,\hat{k})$, where α = angle of the sloping terrain. The minus sign appears in order to ensure downslope flow. In finite-difference form, then,

$$\left.\frac{\partial\psi}{\partial y}\right|_{(J,K,n)} = \{-3/2\psi(J,K,n)+2\psi(J-1,K,n)-1/2\psi(J-2,K,n)\}/\Delta y \quad ,$$

$$\left.\frac{\partial\psi}{\partial z}\right|_{(J,K,n)} = \{-3/2\psi(J,K,n)+2\psi(J,K+1,n)-1/2\psi(J,K+2,n)\}/\Delta z \quad ,$$

$$v(J,K,n) = -\{(\partial\psi/\partial y|_{(J,K,n)})^2 + (\partial\psi/\partial z|_{(J,K,n)})^2\}^{\frac{1}{2}} \cos(\alpha) \quad , \tag{3.3.13}$$

$$w(J,K,n) = -\{(\partial\psi/\partial y|_{(J,K,n)})^2 + (\partial\psi/\partial z|_{(J,K,n)})^2\}^{\frac{1}{2}} \sin(\alpha) \quad .$$

See Figure 3.4. The velocity components, at grid points which intersect the sloping surface, must satisfy

$$\frac{w(J,K,n)}{v(J,K,n)} = \tan(\alpha) = \text{slope of ground} \tag{3.3.14}$$

and flow parallel to the material surface is thereby guaranteed. Having obtained the surface velocity components, the surface vorticity is evaluated using (2.4.3), from one-sided differences of the velocity components, as usual :

$$\begin{aligned}\xi(J,K,n) = {} & \{-3/2w(J,K,n)+2w(J-1,K,n)-1/2w(J-2,K,n)\}/\Delta y \\ & - \{-3/2v(J,K,n)+2v(J,K+1,n)-1/2v(J,K+2,n)\}/\Delta z\end{aligned} \tag{3.3.15}$$

The streamfunction is set to zero on grid points intersecting the lower boundary. The potential temperature is simply prescribed as some function of time, as alluded to earlier.

3.3.4 Upper Boundary Conditions

Consistent with the upper boundary being located above the valley circulation, both velocity components vanish

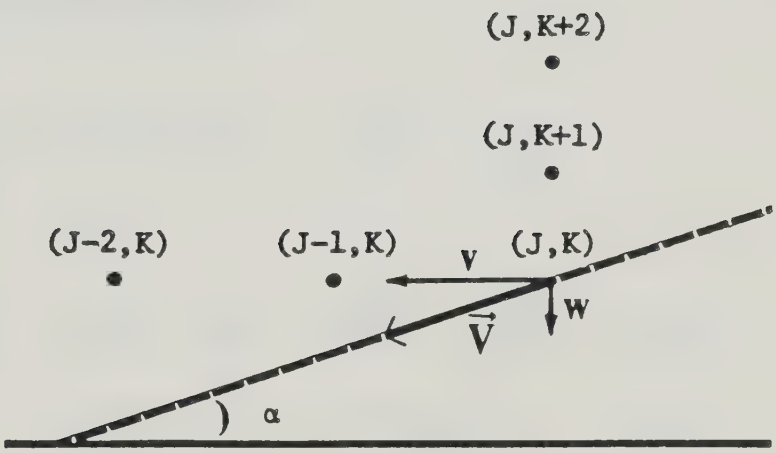


Figure 3.4 Schematic illustration of lower boundary condition

along K = KMAX. In addition, the vorticity and streamfunction values are set to zero. The boundary conditions on the flow are summarized in Figure 3.5. The potential temperature at the top of the region is assumed constant, being far enough away from the cooling surface.

3.4 Finite Difference Formulation of Prediction Equations

3.4.1 General

The simplified prediction equations to be formulated using finite-differences are

$$\frac{\partial \theta}{\partial t} = -v \frac{\partial \theta}{\partial y} - w \frac{\partial \theta}{\partial z} + K_y \frac{\partial^2 \theta}{\partial y^2} + K_z \frac{\partial^2 \theta}{\partial z^2} \quad , \qquad (2.2.2)$$

$$\frac{\partial \xi}{\partial t} = -v \frac{\partial \xi}{\partial y} - w \frac{\partial \xi}{\partial z} + K_y \frac{\partial^2 \xi}{\partial y^2} + K_z \frac{\partial^2 \xi}{\partial z^2} + \frac{g}{\theta} \frac{\partial \theta}{\partial y} \qquad (2.4.11)$$

advection (a) diffusion (b) other (c)

Typically, it is possible to examine the stability properties of a given numerical scheme only when it is applied to simple types of differential equations. This is because it is only with simple equations that the mathematics involved become tractable. When an equation involves more than one type of term (e.g. advection and diffusion, as in (2.2.2) and (2.4.11)), Mesinger and Arakawa (1976) recommended the use of "different schemes for the different types of terms". For this reason, terms (a), (b), and (c) were considered separately and the most appropriate

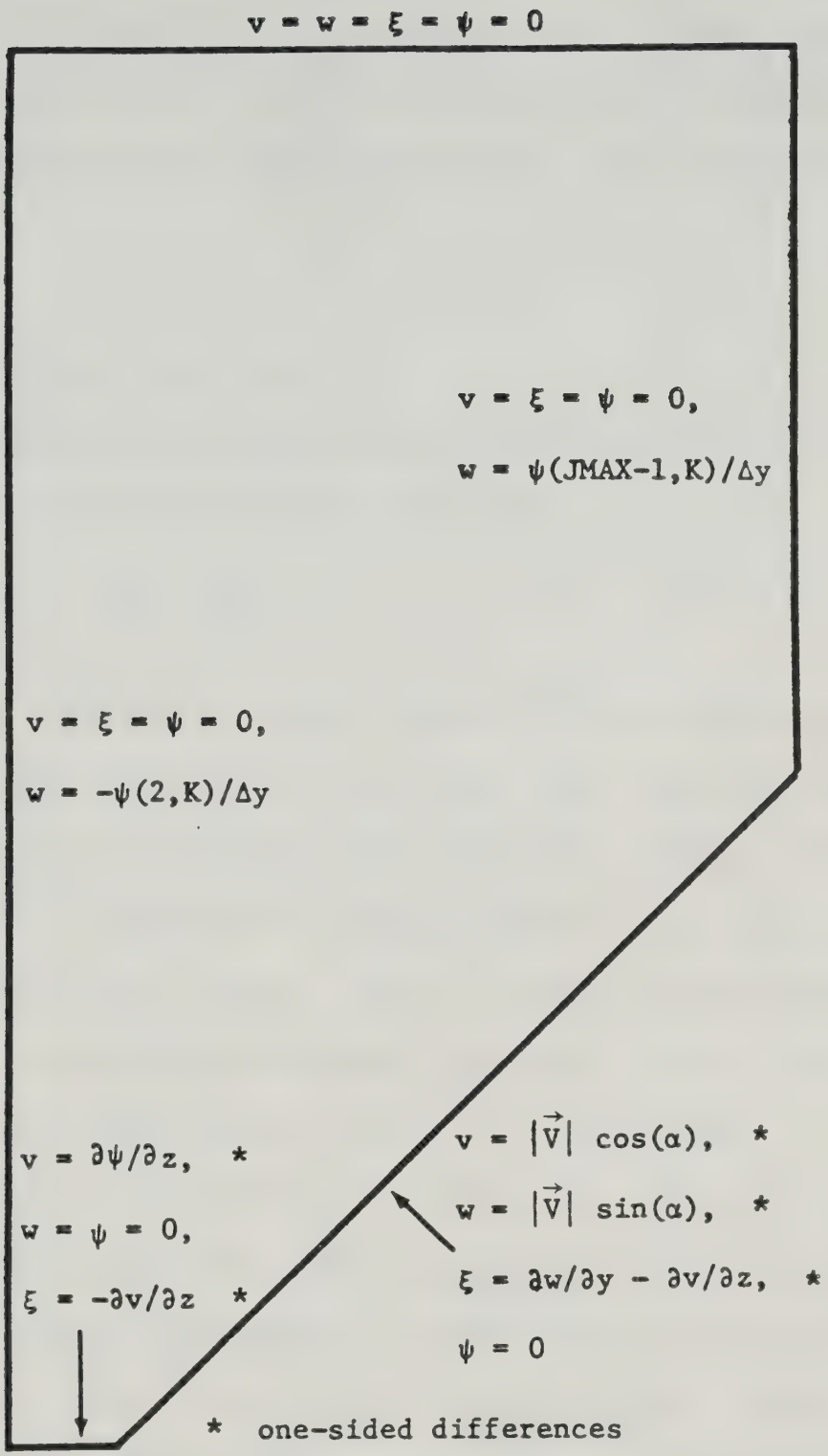


Figure 3.5 Summary of boundary conditions on velocity components, v and w, vorticity, ξ, and streamfunction, ψ

numerical scheme chosen for each. As it is difficult to determine the stability criteria for non-linear equations, it was assumed that linear stability criteria would provide a close approximation when applied to the prediction equations.

3.4.2 Advection Terms (a)

A comparison of numerical schemes available for solving a one-dimensional advection equation,

$$\frac{\partial S}{\partial t} + c \frac{\partial S}{\partial y} = 0, \quad c > 0 \quad , \tag{3.4.1}$$

is given in Table 3.1. After examining the advantages and disadvantages of each, the forward-time, upstream-space formulation was chosen to determine the changes in vorticity and potential temperature through advection. Aside from its explicit two-level nature, this scheme was recognized to be reasonable in a physical sense, at least intuitively. Gradients in S upstream of the grid point under consideration are advected towards that grid point whereas those downstream do not enter into the computation. This method has been recommended by many authors such as Orville (1964, 1965, 1968), Molenkamp (1968), Pielke (1974), and Mesinger and Arakawa (1976). According to stability considerations, the solution will remain stable if

$$\frac{|c|\ \Delta t}{\Delta y} \leq 1 \quad . \tag{3.4.2}$$

However, damping proportional to wavelength can occur and is

Numerical Scheme	Accuracy	Efficiency	Stability	Comments
fwd-time, upstream-space	$O(\Delta t+\Delta y)$	2-level, explicit	$\frac{\lvert c\rvert \Delta t}{\Delta y} \leq 1$	damping depends on wavelength
fwd-time, cnt-space	$O(\Delta t+\Delta y^2)$	2-level,exp.	unstable	unadvised - no stability
Euler-backward (Matsuno)	$O(\Delta t+\Delta y^2)$	2-level,exp.	$\frac{\lvert c\rvert \Delta t}{\Delta y} \leq 1$	damping depends on wavelength, increased computing time
cnt-time, cnt-space	$O(\Delta t^2+\Delta y^2)$	3-level,exp.	$\frac{\lvert c\rvert \Delta t}{\Delta y} \leq 1$	2 modes in solution (comp.-large)
Lax-Wendroff	$O(\Delta t^2+\Delta y^2)$	2-level,exp.	$\frac{\lvert c\rvert \Delta t}{\Delta y} \leq 1$	extreme damping at 2 Δx
trapezoidal	$O(\Delta t^2+\Delta y^2)$	2-level,imp.	stable	solution to simult. eqns.
cnt-time, 4^{th} order space	$O(\Delta t^2+\Delta y^4)$	3-level,exp.	$\frac{\lvert c\rvert \Delta t}{\Delta y} \leq .73$	increased computer time (more terms)
Roberts-Weiss *	$O(\Delta t^2+\Delta y^4)$	2-level,exp.	$\frac{\lvert c\rvert \Delta t}{\Delta y} \leq 2$	increased computer time (4 times as many grid points)
Reference : Haltiner and Williams (1980), except * which is Molenkamp (1968)				

Table 3.1 Properties of some numerical schemes applied to an advection equation

most pronounced for wavelengths of 2 Δy when $|c|\ \Delta t/\Delta y \simeq 1/2$. Further details can be found in Appendix A. The forward-time, upstream-space formulation, applied to a non-linear advection equation, such as

$$\frac{\partial \xi}{\partial t} = -v \frac{\partial \xi}{\partial y} - w \frac{\partial \xi}{\partial z} \quad , \tag{3.4.3}$$

can be expressed as

$$\xi(J,K,n+1) = \xi(J,K,n) + \Delta t \{A(J,K,n) + B(J,K,n)\}$$

where

$$A(J,K,n) = \begin{cases} -v(J,K,n) \dfrac{\{S(J,K,n) - S(J-1,K,n)\}}{\Delta y} & v(J,K,n) > 0 \\ -v(J,K,n) \dfrac{\{S(J+1,K,n) - S(J,K,n)\}}{\Delta y} & v(J,K,n) < 0 \end{cases}$$

$$B(J,K,n) = \begin{cases} -w(J,K,n) \dfrac{\{S(J,K,n) - S(J,K-1,n)\}}{\Delta z} & w(J,K,n) > 0 \\ -w(J,K,n) \dfrac{\{S(J,K+1,n) - S(J,K,n)\}}{\Delta z} & w(J,K,n) < 0 \end{cases}$$

3.4.3 Diffusion Terms

A comparison of numerical schemes available for solving a one-dimensional parabolic diffusion equation such as

$$\frac{\partial S}{\partial t} - K \frac{\partial^2 S}{\partial y^2} = 0, \tag{3.4.4}$$

is given in Table 3.2. Initially, the Dufort-Frankel scheme was chosen to evaluate the changes in θ and ξ due to horizontal and vertical diffusion. Even though this scheme requires computer storage of the vorticity and potential temperature matrices at three time levels, the extremely

Numerical Scheme	Accuracy	Efficiency	Stability	Comments
fwd-time, cnt-space	$O(\Delta t+\Delta y^2)$	2-level, exp.	$\frac{K\Delta t}{\Delta y^2} \leqslant \frac{1}{2}$	
cnt-time, cnt-space	$O(\Delta t^2+\Delta y^2)$	3-level, exp.	unstable	unadvised - no stability
DuFort-Frankel	$O(\Delta t^2+\Delta y^2+(\Delta t/\Delta y)^2)$	3-level, semi-implicit	stable	increased computer time, consistent with $\frac{\partial S}{\partial t}+K\frac{\partial^2 S}{\partial y^2}+\left\|\frac{\Delta t}{\Delta y}\right\|^2\frac{\partial^2}{\partial t^2} = 0$
fwd-time, 4^{th} order space	$O(\Delta t^2+\Delta t\Delta y^2+\Delta y^4)$	2-level, exp.	$\frac{K\Delta t}{\Delta y^2} \leqslant \frac{2}{3}$	not applicable near boundary
Crank-Nicholson	$O(\Delta t^3+\Delta t\Delta y^2)$	2-level, imp.	stable	solution to simult. eqns.
Reference : Ames (1969)				

Table 3.2 Properties of some numerical schemes applied to a diffusion equation

stable nature of the solution warranted its use. Further details can be found in Appendix B. The Dufort-Frankel scheme has been widely used in numerical modelling of the boundary layer (e.g. Estoque (1963) and most recently Kozo (1982)), and is favourably promoted in mathematical discussions of numerical techniques for solving parabolic partial differential equations (e.g. Richtmeyer and Morton (1957), Ames (1969), and Mitchell and Griffiths (1980)).

If a centered-time, centered-space formulation was applied to a one-dimensional diffusion equation, such as (3.4.4), it would be expressed as

$$\frac{S(J,n+2) - S(J,n)}{2\Delta t} = K \frac{S(J+1,n+1) - 2S(J,n+1) + S(J-1,n+1)}{\Delta y^2}, \quad (3.4.5)$$

where S(J,n) denotes the value of S at the Jth grid point at time $t = n\Delta t$. This scheme would lead to numerically unstable solutions, as noted in Table 3.2. However, replacing S(J,n+1) on the right hand side of (3.4.5) by (S(J,n) + S(J,n+2))/2 results in the greater stability of the Dufort-Frankel scheme. Even though terms involving S at time $t + 2\Delta t$ appear on both sides of the equation, implying an implicit system, the term on the right may be transposed to the left - such schemes are called semi-implicit or pseudo-implicit as they may be rewritten in an explicit form. In this case, (3.4.5) becomes

$$S(J,n+2)\{1+2r\} = \{1-2r\}S(J,n) + 2r\{S(J-1,n+1) + S(J+1,n+1)\} \quad (3.4.6)$$

where $r = K\Delta t/\Delta y^2$.

Numerous difficulties arose when this method was applied to the diffusion terms (b) in (2.4.11). As the time step was reduced, various parameters of the circulation (e.g. the extremum of the streamfunction field) were noted to behave as if the truncation error associated with the scheme was very large. Note that the Dufort-Frankel scheme has truncation error of $O(\Delta t^2 + \Delta y^2 + (\Delta t/\Delta y)^2)$.

To examine this more closely, another formulation was applied which is only first order in time. This scheme uses a forward-time, centered-space finite-difference technique and was applied to the prediction equations. In terms of (3.4.4), it can be expressed as

$$\frac{S(J,n+1) - S(J,n)}{\Delta t} = K \frac{S(J+1,n) - 2S(J,n) + S(J-1,n)}{\Delta y^2} \quad . \qquad (3.4.7)$$

Again, with $r = K \Delta t/\Delta y^2$, this becomes

$$S(J,n+1) = r\, S(J-1,n) + \{1-2r\}\, S(J,n) + r\, S(J+1,n) \quad . \qquad (3.4.8)$$

The stability criterion for this representation, as noted in Table 3.2, is

$$\frac{K \Delta t}{\Delta y^2} \leq \frac{1}{2} \quad . \qquad (3.4.9)$$

As the time step was reduced using (3.4.8), more consistent results were obtained than with (3.4.6), even though the latter was second order in time. This revealed the existence of a numerical problem when the Dufort-Frankel scheme was implemented and incited further exploration. For this purpose, a simple one-dimensional heat diffusion (or conduction) equation was considered, for which analytical

solutions were available. Initial and boundary conditions similar to those of the valley model under consideration were applied and numerical results using both the Dufort-Frankel and the forward-time, centered-space schemes are presented in Section 3.5 for comparison. Further discussion at that time is made regarding the proper choice of a diffusion scheme for the prediction equations.

3.4.4 Other Term (c)

The solenoid term, denoted by (c) at the beginning of this section, expresses the non-linear dependence of ξ and θ. The relationship is such that a theoretical investigation of the behavior of the various possible numerical schemes is precluded. Accordingly, through accuracy considerations alone, the centered-time, centered-space formulation was selected. The truncation error for this scheme is $O(\Delta t^2 + \Delta y^2)$. This formulation was used by Thyer (1966) and Orville (1964, 1965, 1968) in their models of flow above sloping terrain and is recommended by Mesinger and Arakawa (1976).

An example of the finite-difference representation applied to

$$\frac{\partial \xi}{\partial t} = \frac{g}{\theta} \frac{\partial \theta}{\partial y} \tag{3.4.10}$$

is

$$\frac{\xi(J,K,n+2) - \xi(J,K,n)}{2\Delta t} = \frac{g}{\theta(J,K,n+1)} \frac{\{\theta(J+1,K,n+1) - \theta(J-1,K,n+1)\}}{2\Delta y} \tag{3.4.11}$$

Using this scheme, changes in ξ over the time period from t to $t + 2\Delta t$ are evaluated at the middle of the interval and,

for this reason, it is often called the mid-point rule.

3.5 One-dimensional Heat Conduction Equation

As indicated in Section 3.4.3, analytical and numerical solutions to the one-dimensional heat conduction equation were obtained in order to examine the accuracy of the numerical solutions. This is the classical partial differential equation of mathematical physics used to describe the conduction of heat in a solid body. Here, it is applied to predict the potential temperature, $\theta(z,t)$, determined by diffusion away from a steadily cooling surface located at $z = 0$. The top of the atmosphere is assumed to be at a height $z = H$. The partial differential equation governing this transfer process can be written

$$\frac{\partial \theta}{\partial t} = K \frac{\partial^2 \theta}{\partial z^2} \quad , \quad 0 \leq z \leq H, \; t > 0 \qquad (3.5.1)$$

It is assumed that the temperature at the top of the atmosphere remains constant, whereas that at the surface is a linearly decreasing function of time. Therefore, the boundary conditions are

$$\theta(H,t) = T, \quad t > 0 \quad , \qquad (3.5.2)$$

$$\theta(0,t) = \theta(0,0) - \alpha t, \quad t > 0, \qquad (3.5.3)$$

where α = constant surface cooling rate. Initially, some vertical distribution of temperature is assumed so that

$$\theta(z,0) = f(z), \quad 0 \leq z \leq H. \qquad (3.5.4)$$

3.5.1 Analytical Solution

An analytical solution to (3.5.1), subject to the non-homogeneous boundary conditions, (3.5.2) and (3.5.3), and initial conditions

$$\theta(z,0) = f(z) = (T - \theta(0,0))z/H + \theta(0,0), \quad 0 \leq z \leq H \quad , \tag{3.5.5}$$

is derived in Appendix C to be

$$\theta(z,t) = \sum_{n=1}^{\infty} \{(-2H^2\alpha/(n\pi)^3K) \exp(-n^2\pi^2Kt/H^2) \sin(n\pi z/H\} + \frac{\alpha}{K} (z^3/6H - z^2/2 - zH/3) + (\theta(0,0) - \alpha t) (1 - z/H) + zT/H, \quad 0 \leq z \leq H, \; t > 0 \quad . \tag{3.5.6}$$

Attempts at solution with $\theta(z,0)$ satisfying the Poisson equation, (2.2.5), as in the valley model, failed and a simple linear temperature profile was assumed as an approximation. The two initial fields differed at most by 0.0008 C°.

The potential temperature fields given by (3.5.6) are plotted for various times in Figures 3.6 and 3.7. The abscissa gives the total cooling relative to t = 0 seconds. Here, the infinite series in (3.5.6) was truncated at 500 terms. After 20,000 seconds or ≃ 333 minutes, the temperature profile varied almost linearly from the cooled surface temperature, $\theta(0,t) = \theta(0,0) - \alpha t$, to the constant temperature at the upper boundary, $\theta(H,t) = T$. At earlier times,

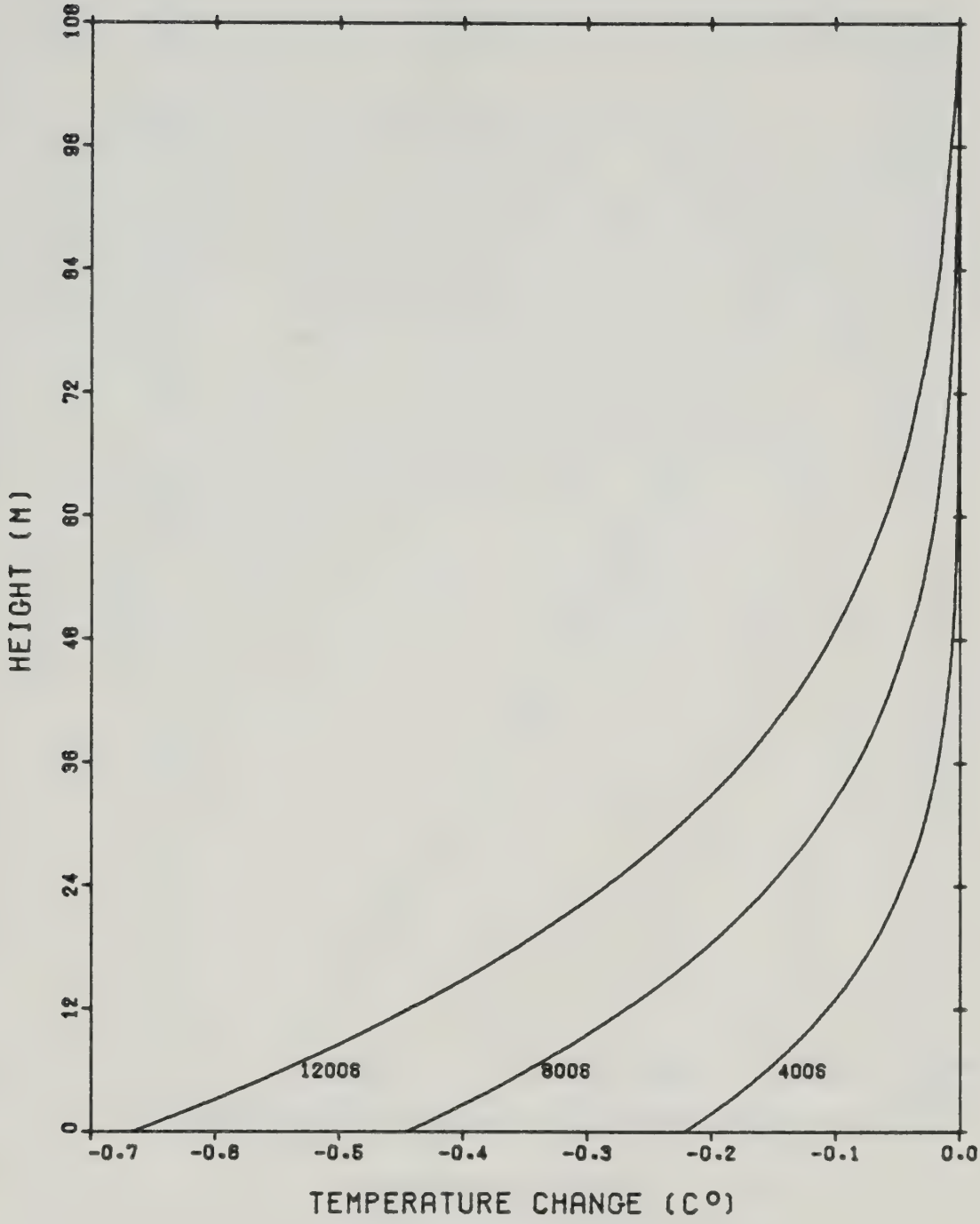


Figure 3.6 Potential temperature deviation from initial state versus height for one-dimensional diffusion equation ($K = 1.0\ m^2\ s^{-1}$) out to 1200 seconds

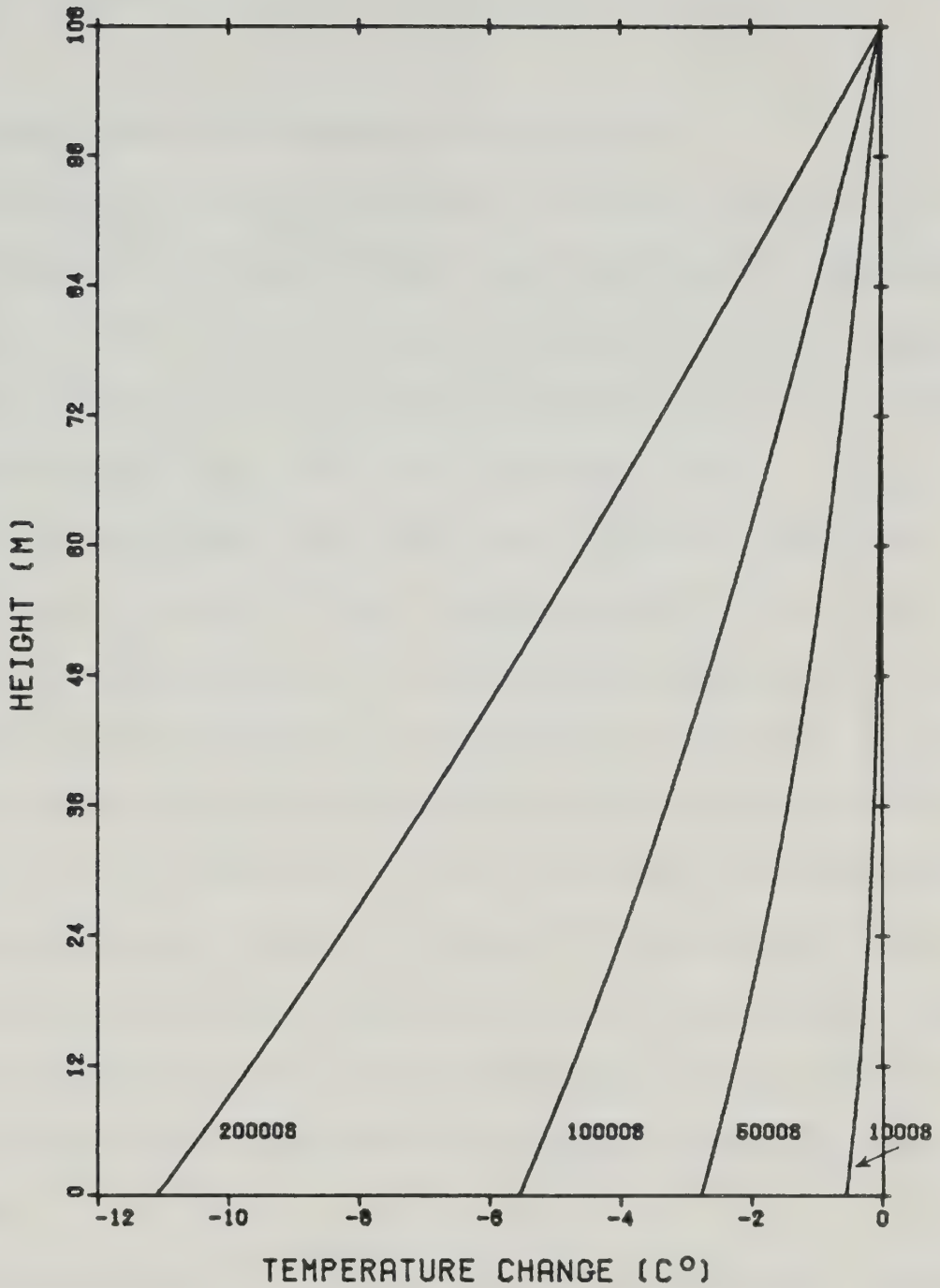


Figure 3.7 Potential temperature deviation from initial state versus height for one-dimensional diffusion equation ($K = 1.0\ m^2\ s^{-1}$) out to 20000 seconds

e.g. Figure 3.6, the non-linear variation with height is very evident. Gradually the cooling specified at the surface diffuses upwards to greater and greater heights.

3.5.2 Comparison with Numerical Solution

Generally, the two numerical schemes examined (Du-fort-Frankel and forward-time, centered-space) compared favourably with the analytical results. A sample computation is given in Table 3.3, up to 20 m height at t = 2000 seconds, using Δz = 2 m, Δt = 0.5 seconds, and K = 1.0 $m^2 s^{-1}$. These values satisfy the stability criterion for the forward-time, centered-space formulation, (3.4.9). At z = 0, the numerical solutions are exactly the analytical ones, as specified by the boundary condition, (3.5.3). For a constant grid size, the numerical solutions tended to overshoot the analytical ones, as much of the inaccuracy is involved in Δz, the grid size. However, as both Δt and Δz are reduced, both numerical methods approach the true analytical one. Thus, it appeared that either numerical scheme would behave satisfactorily when applied to a simple purely diffusional problem.

At this point, the numerical and analytical results were compared with the two-dimensional valley model results. Initially, temperature changes are brought about, according to (2.2.2), virtually as a result of vertical diffusion from the cooling ground surface alone, since both horizontal diffusion and advection are small. The valley model predicted

Table 3.3 Comparison of analytical solution to one-dimensional diffusion equation with numerical solutions obtained using Dufort-Frankel and forward-time, centered-space schemes after 2000 seconds

Height (m)	Analytical Solution	Numerical Solution (DuFort-Frankel)	Numerical Solution (fwd-time,cnt-spc)
0	282.8738034	282.8738034	282.8738034
4	283.0376210	283.0376174	283.0376198
8	283.1930005	283.1929934	283.1929983
12	283.3403911	283.3403806	283.3403878
16	283.4802385	283.4802247	283.4802342
20	283.6129835	283.6129667	283.6129783

temperature profile above the valley trough (J = 1) was selected for comparison since this column is most remote from the sloping surface and would, thus, have the smallest contribution from horizontal diffusion. Table 3.4 compares the total cooling predicted (relative to t = 0 seconds) out as far as 200 seconds from the various numerical diffusion schemes applied to the valley model with the analytical one-dimensional solution. The valley model results shown are for an integration with Δy = 40 m, Δz = 4 m, and Δt = 2 seconds.

These results are consistent with those previously described, i.e. the various numerical diffusion schemes perform adequately when used on a purely diffusional problem as in the early stages of the evolution of the model when advection processes are quite small. The vorticity equation, (2.4.11), however, is a different matter. As soon as surface cooling commences, the solenoid term ($g/\theta\ \partial\theta/\partial y$) becomes important and the vorticity changes are not solely the result of diffusion of vorticity. When the two different numerical diffusion schemes are applied to (2.4.11), certain discrepancies arise.

In Tables 3.5 and 3.6, the grid point values of ξ, $\partial\xi/\partial t|_{adv}$, $\partial\xi/\partial t|_{dif}$, and $\partial\xi/\partial t|_{sol}$ are given for each of the numerical schemes at grid points located in a vertical line midway up the slope. These are for a valley model integration out to 20 seconds, with input parameters of Δy = 40 m, Δz = 4 m, and Δt = 4 seconds. The pattern of vorticity

Table 3.4 Comparison of amounts of cooling after 200 seconds obtained from analytical solution to the one-dimensional diffusion equation and valley model solutions obtained using Dufort-Frankel and forward-time, centered-space schemes

Height (m)	Analytical Solution	Valley Model (DuFort-Frankel, J=1)	Valley Model (fwd-time, cnt-spc, J=1)
0	-.111	-.111	-.111
4	-.080	-.081	-.080
8	-.056	-.057	-.057
12	-.039	-.040	-.039
16	-.026	-.028	-.027
20	-.017	-.018	-.017
24	-.011	-.012	-.011
28	-.007	-.008	-.007
32	-.004	-.005	-.005
36	-.002	-.004	-.003
40	-.001	-.003	-.002

Table 3.5 Vorticity changes predicted by various terms in the valley model out to 20 seconds using the Dufort-Frankel scheme

t	height	ξ	$\left.\frac{\partial \xi}{\partial t}\right\|_{adv}$	$\left.\frac{\partial \xi}{\partial t}\right\|_{dif}$	$\left.\frac{\partial \xi}{\partial t}\right\|_{sol}$
(s)	(m)	(s^{-1})	(10^7 s^{-2})	(10^7 s^{-2})	(10^7 s^{-2})
0	0	0	-	-	-
	4	0	0	0	0
	8	0	0	0	0
	12	0	0	0	0
4	0	0	-	-	-
	4	0	0	0	-10
	8	0	0	0	0
	12	0	0	0	0
8	0	-91	-	-	-
	4	-77	0	-4	-19
	8	0	0	-3	-3
	12	0	0	0	0
12	0	-211	-	-	-
	4	-184	+0	-5	-28
	8	-52	-0	-8	-6
	12	0	0	-2	-1
16	0	-381	-	-	-
	4	-335	+0	-5	-36
	8	-114	-0	-11	-11
	12	-26	-0	-5	-2
20	0	-576	-	-	-
	4	-516	+0	-6	-44
	8	-225	-0	-15	-15
	12	-56	-0	-8	-4

Table 3.6 Vorticity changes predicted by various terms in the valley model out to 20 seconds using the forward-time, centered-space scheme

t	height	ξ	$\left.\frac{\partial \xi}{\partial t}\right\|_{adv}$	$\left.\frac{\partial \xi}{\partial t}\right\|_{dif}$	$\left.\frac{\partial \xi}{\partial t}\right\|_{sol}$
(s)	(m)	(s^{-1})	(10^7 s^{-2})	(10^7 s^{-2})	(10^7 s^{-2})
0	0	0	-	-	-
	4	0	0	0	0
	8	0	0	0	0
	12	0	0	0	0
4	0	0	-	-	-
	4	0	0	0	-10
	8	0	0	0	0
	12	0	0	0	0
8	0	-91	-	-	-
	4	-77	0	0	-19
	8	0	0	0	0
	12	0	0	0	0
12	0	-185	-	-	-
	4	-153	+0	+4	-29
	8	0	-0	-5	-5
	12	0	0	0	0
16	0	-315	-	-	-
	4	-275	+0	+8	-38
	8	-77	-0	-10	-10
	12	0	0	0	0
20	0	-449	-	-	-
	4	-399	+0	+10	-45
	8	-155	-0	-8	-14
	12	0	-0	-5	-2

changes due to diffusion shows quite a difference between the two schemes. The solenoid terms, which depend only on the temperature fields, are very similar as the two temperature evolutions are not drastically different. However, after only 20 seconds, the vorticity resulting from the Dufort-Frankel formulation is more than 28 percent higher than that resulting from the forward-time, centered-space scheme, and 40 percent higher after only 52 seconds. This discrepancy can be traced mainly to the different techniques involved in diffusing the vorticity values.

The Dufort-Frankel scheme is a three-level scheme in time, and, as a result, the changes at time t depend on values at $t - \Delta t$ and $t - 2\Delta t$. If these values have previously been altered only through diffusive processes, then reasonable results are obtained. With the solenoid term coming into play at every time step, however, the values at the intermediate time, $t - \Delta t$, cause a shock or disturbance in the diffusion computation. The forward-time, centered-space scheme, on the other hand, considers only the field at a single previous time step and results in reasonable diffusion changes over that time interval.

Since the problem is suggested to lie in the magnitude of the time step, the scheme which is most nearly correct is expected to show the least difference when the time step is reduced. This turns out to favour the use of the forward-time, centered-space formulation. Table 3.7 shows the vorticity values predicted above the mid-slope region

Table 3.7 Vorticity values (s^{-1}) predicted above mid-slope region after 200 seconds using the Dufort-Frankel and forward-time, centered-space schemes and various time steps

Height	Δt=30s	Δt=15s	Δt=10s	Δt=5s	Δt=2s	Δt=.5s	Δt=4s	Δt=2s
(m)	D u F o r t - F r a n k e l						fwd-time,	cnt-spc
	*	**						
0	-.0069	-.0048	-.0039	-.0028	-.0022	-.0018	-.0018	-.0018
4	-.0068	-.0048	-.0038	-.0028	-.0022	-.0018	-.0018	-.0017
8	-.0059	-.0043	-.0034	-.0025	-.0019	-.0016	-.0016	-.0016
12	-.0046	-.0035	-.0028	-.0021	-.0016	-.0014	-.0013	-.0013
16	-.0032	-.0027	-.0022	-.0017	-.0013	-.0011	-.0010	-.0010
20	-.0018	-.0020	-.0017	-.0012	-.0010	-.0008	-.0008	-.0008
24	-.0006	-.0014	-.0012	-.0009	-.0007	-.0006	-.0006	-.0006
28	-.0000	-.0009	-.0008	-.0006	-.0005	-.0004	-.0004	-.0004
32	-.0000	-.0005	-.0005	-.0004	-.0003	-.0003	-.0003	-.0003
36	-.0000	-.0003	-.0003	-.0003	-.0002	-.0002	-.0002	-.0002
40	-.0000	-.0001	-.0002	-.0002	-.0001	-.0001	-.0001	-.0001

* based on linear interpolation between 180 and 210 seconds

** based on linear interpolation between 195 and 210 seconds

after 200 seconds using the two numerical schemes and various time steps. Clearly, as the time step is reduced, the results of the Dufort-Frankel scheme seem to approach the results of the forward-time, centered-space scheme, as anticipated. This is also reflected in Figure 4.1, which depicts the evolution of the minimum streamfunction value with time for the two schemes. Based on these results, the latter finite-difference formulation was chosen to approximate the diffusion terms in this model. This scheme was used by Pielke (1974).

3.6 Liebmann Sequential Relaxation Technique

A solution to the equation relating the streamfunction values, $\psi(J,K,t)$, to the vorticity values, $\xi(J,K,t)$, (2.5.3), was obtained numerically using Liebmann sequential relaxation (Haltiner and Williams (1980)). From (2.4.11), the vorticity field was predicted for all grid points. At each time step, the velocity components were required by the model (for use in predicting contributions to $\partial\theta/\partial t$ and $\partial\xi/\partial t$ through advection) and these were obtainable from (2.5.1) and (2.5.2), once the streamfunction field corresponding to the vorticity field was known. Since the streamfunction value everywhere on the boundary was set to zero, the relaxation technique was applied only on the interior of the grid away from the boundary. Details of the technique follow.

Let the nth guess at the streamfunction value at grid point (J,K) be $\psi^n(J,K)$. Then,

$$\xi(J,K) + \nabla^2 \psi^n(J,K) = R^n(J,K) \tag{3.6.1}$$

where $R^n(J,K)$, called the residual, is a measure of the error of the guess. If $\psi^n(J,K)$ satisfies (2.5.3) exactly, then $R^n(J,K)$ will be zero. Since a guess at $\psi(J,K)$ is unlikely to be the correct solution, the residual, $R^n(J,K)$, will not be zero at every point of the grid, if anywhere at all. However, successive estimates of the streamfunction field are made, according to the algorithm below, until all residuals are less than some preassigned tolerance level, ϵ.

Expanding (3.6.1) into its centered finite-difference representation yields

$$\xi(J,K) + \frac{\{\psi^n(J+1,K)-2\psi^n(J,K)+\psi^n(J-1,K)\}}{\Delta y^2} + \frac{\{\psi^n(J,K+1)-2\psi^n(J,K)+\psi^n(J,K-1)\}}{\Delta z^2} = R^n(J,K) \tag{3.6.2}$$

We wish to determine a new guess, $\psi^{n+1}(J,K)$, which will reduce the residual to zero. Therefore,

$$\xi(J,K) + \frac{\{\psi^n(J+1,K)-2\psi^{n+1}(J,K)+\psi^n(J-1,K)\}}{\Delta y^2} + \frac{\{\psi^n(J,K+1)-2\psi^{n+1}(J,K)+\psi^n(J,K-1)\}}{\Delta z^2} = 0 \tag{3.6.3}$$

Subtracting (3.6.3) from (3.6.2), and solving for the new guess, $\psi^{n+1}(J,K)$, results in

$$\psi^{n+1}(J,K) = \psi^n(J,K) + R^n(J,K) \frac{1}{(2/\Delta y^2 + 2/\Delta z^2)} \tag{3.6.4}$$

This shows that the (n+1)th guess of $\psi(J,K)$, which is increased over the previous guess by the quantity

$R^n(J,K)/(2/\Delta y^2 + 2/\Delta z^2)$, will reduce the residual to zero at that particular grid point. However, such a correction at a particular point affects the residuals at adjacent grid points. Nevertheless, each guess made according to (3.6.4) represents overall progress in reducing all the residuals, and the method is guaranteed to converge towards the true streamfunction values.

It has been noted that an overrelaxation technique will result in faster convergence. In this case, a larger correction than that given by (3.6.4) is added to the old guess, using

$$\psi^{n+1}(J,K) = \psi^n(J,K) + \frac{\alpha\, R^n(J,K)}{(2/\Delta y^2 + 2/\Delta z^2)} \quad , \qquad (3.6.5)$$

where α is an overrelaxation factor and usually $1 < \alpha < 2$. Theoretical estimates of α have been made based on the grid size but numerical experiments are sometimes used to determine the optimal overrelaxation factor which produces fastest convergence.

The technique of sequential or Liebmann relaxation was usually found to converge even more rapidly. With this method, each new guess made using (3.6.5) is immediately incorporated into the determination of the next new guess at adjacent grid points. As well, this scheme is more economical with respect to computer storage. It is this scheme, with $\alpha = 1.2$ (determined experimentally), which was used to solve for the streamfunction field in this model.

3.7 Summary of Method of Solution

A summary flowchart which describes the numerical schemes utilized in the valley model is given in Figure 3.8. Certain peculiarities not previously mentioned should be noted. For the first increment in time, forward or Euler differencing must be used as the values at the midpoint of the time interval are unknown. Subsequently, at least for the solenoid term, a three-level scheme is possible.

According to the stability criterion for the forward-time, upstream-space formulation of the advective terms, (3.4.2), the time step used must satisfy

$$\Delta t \leq \frac{\Delta y}{v} \quad \text{and} \quad \Delta t \leq \frac{\Delta z}{w} \tag{3.7.1}$$

As v and w change with time, an estimate of their maximum values is used in (3.7.1) to determine the corresponding maximum time step. As the magnitude of the circulation increases, provisions are made in the computer code to ensure that (3.7.1) remains satisfied. An insurance factor of 0.80 was used so that the time step required oversatisfied the above inequality. If the time step became no longer suitable, it was halved successively until both

$$\Delta t \leq \frac{0.8\ \Delta y}{v} \quad \text{and} \quad \Delta t \leq \frac{0.8\ \Delta z}{w} \tag{3.7.2}$$

were true. The first increment in time after such a reduction would again require forward differencing as in the beginning. This procedure is illustrated in Figure 3.9 for a case with an initial time step of 5 seconds. It is

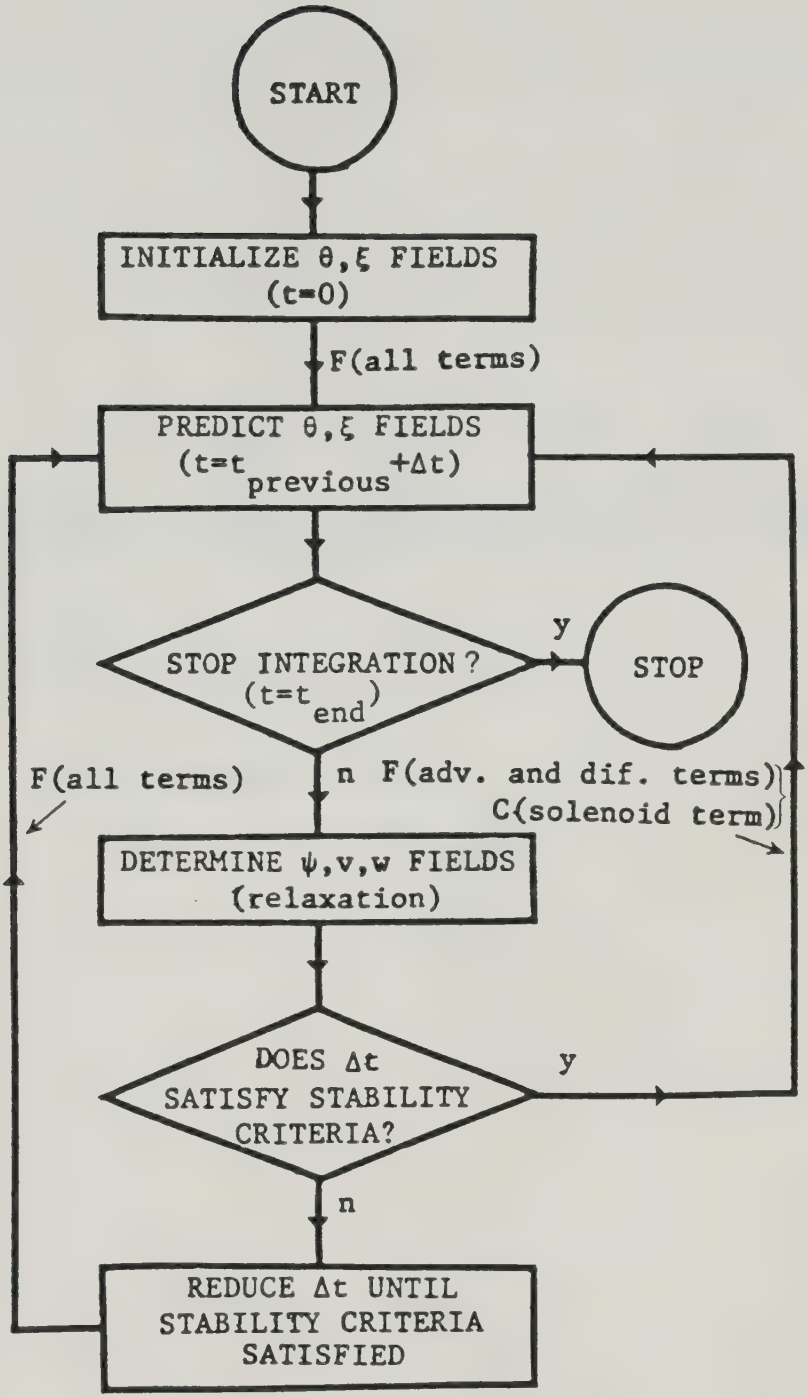


Figure 3.8 Flowchart of finite-difference schemes used in valley model

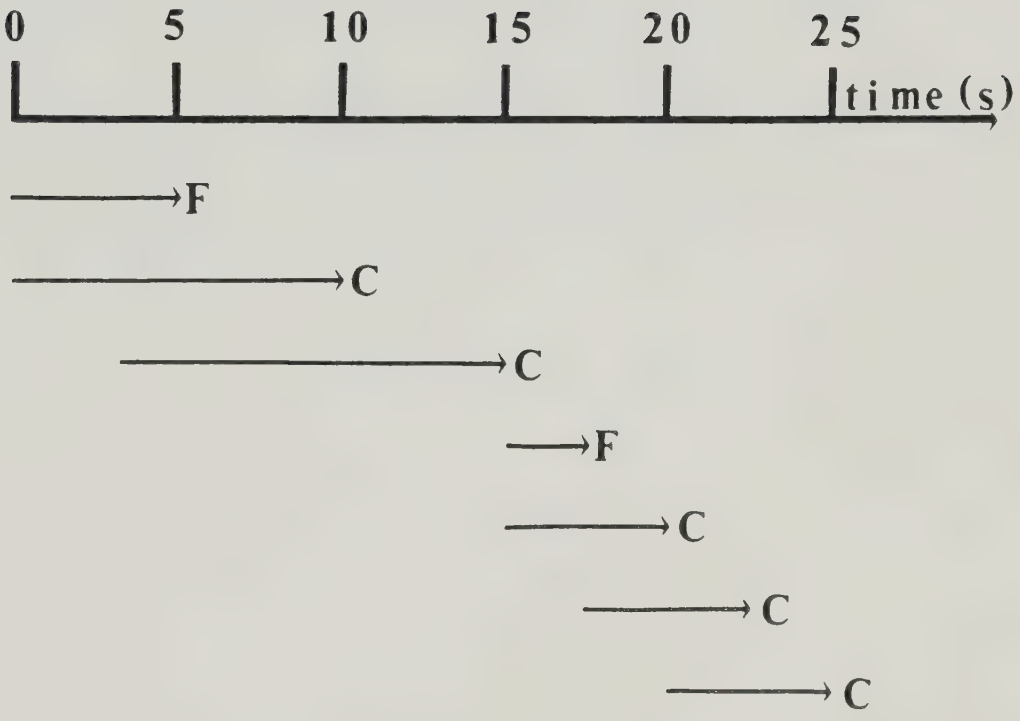


Figure 3.9 Example of time differencing used in the valley model (F = forward, C = centered)

postulated that at t = 15 seconds, the time step must be reduced to 2.5 seconds in order to satisfy (3.7.2) and the appropriate type of differencing (either forward or centered) is indicated.

Chapter 4

RESULTS

4.1 Introduction

In this chapter, the results of numerous valley model integrations are presented. Initially, the input parameter values for a standard run are considered. Sensitivity analyses are presented in which several of these parameters are varied, one at a time, in order to determine the effect of each. Some discussion, of a numerical nature, is given in regard to the choice of time step suitable for a particular run, etc. along with the actual CPU costs.

The results are presented in a variety of manners : two-dimensional streamline plots, time and space evolution of the streamline center, development of slope winds with time, cooling amounts at different heights in different parts of the valley, relative contributions of advection and diffusion, etc. Variations in the geometry of the grid configuration (location of upper boundary, presence of horizontal valley floor versus 'V-shaped' region, angle of slope) are considered. Sensitivity to the vertical diffusion coefficient under an initially stable regime is provided through two integrations with quite different values. Several initial stabilities are implemented, with vertical temperature gradients ranging from -0.04 C°/m up to +0.01 C°/m (the neutral case).

Finally, the results from simulations in which values most appropriate to the microclimatology of the river valley are presented. Limited comparison of the model with observations made within the valley is carried out.

4.2 The Standard Run - Run 1

4.2.1 General

In this section, the results from what was considered a standard run are presented. As Run 1 will be frequently used for comparison with other model integrations, analysis of the results obtained is presented in greater detail than for some subsequent runs. The input parameters used for the standard run are given in Table 4.1. Those variables denoted by an asterisk were allowed to vary as part of the sensitivity analyses and these results are shown in later sections. An initial valley trough temperature, T(1,1,0), of 278.2 °K was used in this set of runs, along with an initial valley trough pressure, P(1,1,0) of 930 mb. Using these values and the various lapse rates, the initial potential temperature profile was computed according to Section 3.3.1. Under stable conditions, isotherms were assumed to be horizontal within the valley cross-section, as shown later in Figure 4.7. Table 4.2 provides a summary of parameter values used in subsequent runs.

Preliminary tests were conducted in order to determine the appropriate time step. As an estimate of what the time step should be, the stability criteria for the various

Table 4.1 Parameter values for valley model in the standard run (Run 1)

	$(K_m)_y = (K_T)_y$	$1.0\ m^2\ s^{-1}$
	$(K_m)_z = (K_T)_z$ *	$1.0\ m^2\ s^{-1}$
PHYSICAL GRID PROPERTIES	vertical grid size (below 72 m)	4 m
	(above 72 m)	12 m
	horizontal grid size	40 m
	height of upper boundary *	108 m
	inclination of slope *	$.0997^R \simeq 5.7^\circ$
INITIAL CONDITIONS	time step *	2 s
	lapse rate *	$-.004\ C^\circ/m$
BOUNDARY CONDITIONS	surface cooling rate *	$2\ C^\circ/hr$
* allowed to vary for sensitivity analysis		

Table 4.2 Summary of parameter values for Runs 2 - 8

Run 2	* except upper boundary at 144 m
Run 3	* except V-shaped valley cross-section
Run 4	* except angle of inclination of slope (α) = 0.2
Run 5	* except $(K_m)_z = (K_T)_z = 0.01\ m^2\ s^{-1}$
Run 6	* except initial lapse rate = $g/C_p = +0.01\ C^\circ/m$
Run 7	* except initial lapse rate = $-0.04\ C^\circ/m$
Run 8	* except initial lapse rate = g/C_p, surface cooling rate = $2.5\ C^\circ/hr$, $(K_m)_z = (K_T)_z = 0.0$
* as in Run 1 (see Table 4.1)	

numerical schemes were examined. For the advective terms, a time step of about 20 seconds or less was needed, based on (3.7.2) and considerations outlined in Section 3.7. The diffusion scheme chosen was more restrictive, however, at least in terms of the vertical grid spacing. Substituting into (3.4.9), and recalling that integration was in a forward sense over two time steps, revealed the requirement of a time step of 4 seconds or less.

The location of the minimum streamfunction value at a given time showed little variation as the time step was reduced. For this reason, the magnitude of the streamfunction minimum, typically located somewhere above the sloping ground, could be compared under the various numerical schemes and time steps implemented. In Figure 4.1, the minimum streamfunction value predicted is plotted versus time for various time steps. The problematic Dufort-Frankel scheme is also presented for comparison.

The forward-time, centered-space diffusion scheme appears to converge consistently to a single value, and, at first glance, a time step of 4 seconds would seem sufficient. However, upon closer examination, an oscillation in sign appeared in the diffusion changes predicted at vertical grid points above the valley trough when a time step of 8 or 4 seconds was used. An example of this instability is shown in Figure 4.2, in which the amount of cooling predicted after various times is plotted versus height above the valley trough using a time step of 4 seconds. A similar

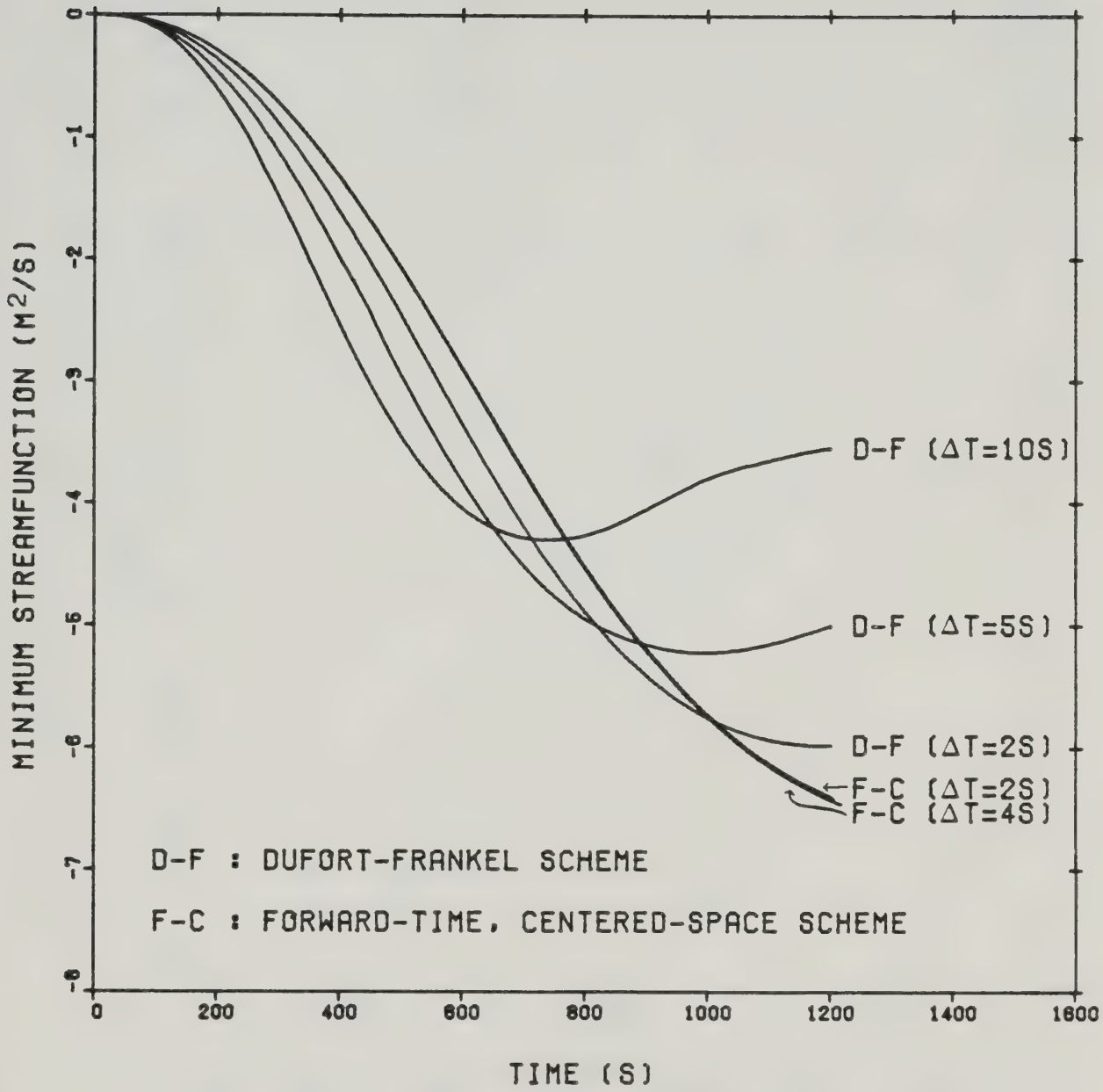


Figure 4.1 Minimum streamfunction versus time for Run 1 using various diffusion schemes and several time steps

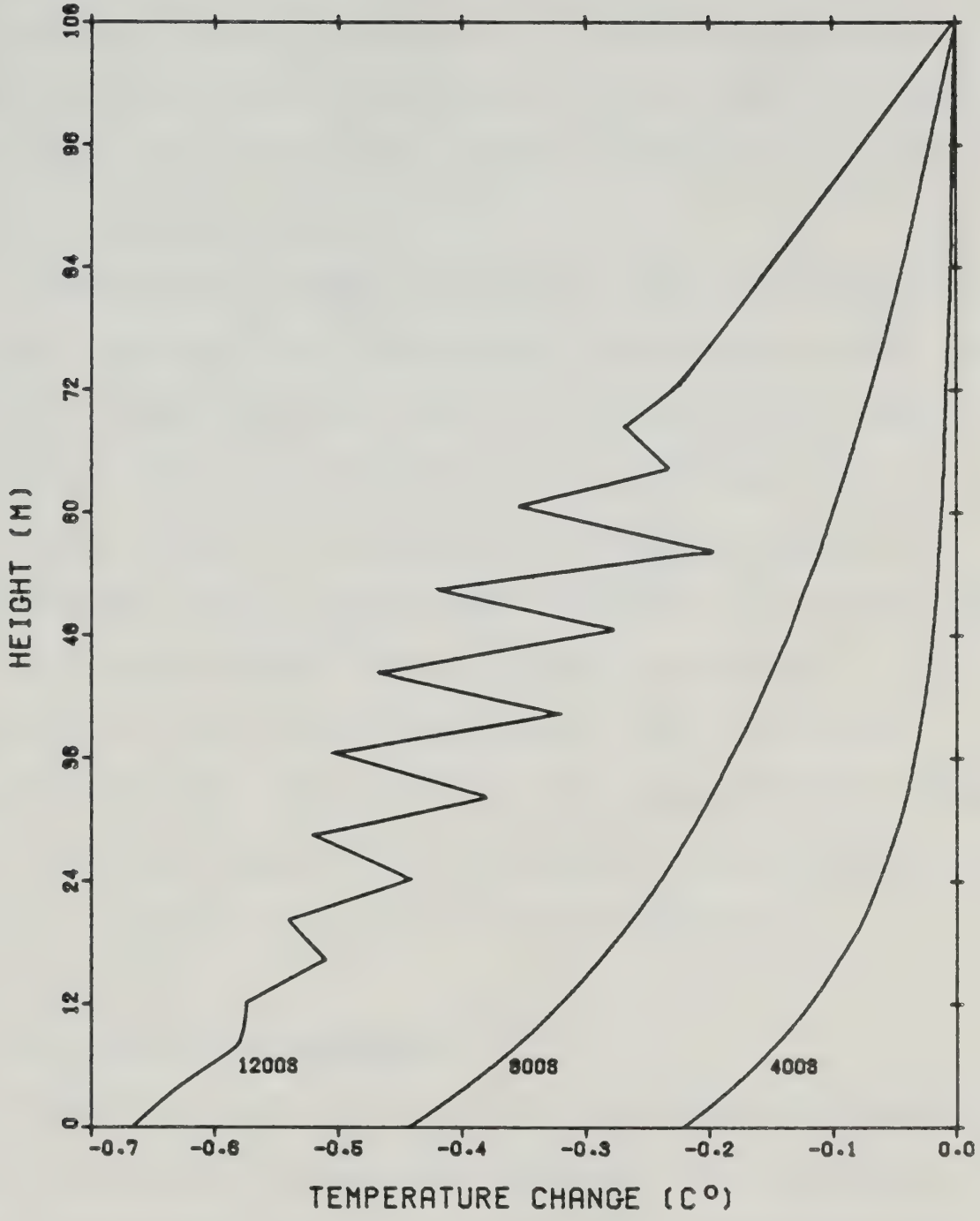


Figure 4.2 Cooling predicted by valley model versus height using forward-time, centered-space diffusion scheme and a 4 second time step

oscillation occurred at an earlier time when a time step of 8 seconds was used, again only above the valley trough. Above the sloping surface, it did not appear and is therefore not evident in Figure 4.1. With a time step of 2 seconds, such an oscillation did not occur, at least out to integration times where other difficulties arose and it was chosen for this reason.

A compromise between the cost of each integration using a certain time step and the results achieved was made. This run, with a time step of 2 seconds, required 1000 seconds of CPU time in order to integrate out to 2000 seconds. A similar run, with a time step of 4 seconds, required 408 seconds of CPU time to reach 1500 seconds, indicating the non-linear relationship between time step and CPU requirements. Most of the CPU time is used up in the relaxation process. With smaller time steps,smaller changes in the vorticity are produced and thus fewer relaxations are required in order to achieve a certain accuracy.

4.2.2 Circulation Development

Initially, negative vorticity was generated close to the ground surface through the solenoid term, according to (2.4.9). This resulted in a corresponding downslope flow close to the sloping surface with a weaker return flow aloft. Figure 4.3 depicts the streamlines predicted after 600, 1200, and 1400 seconds. Minimum streamfunction values and their location are noted. Out to an integration time of

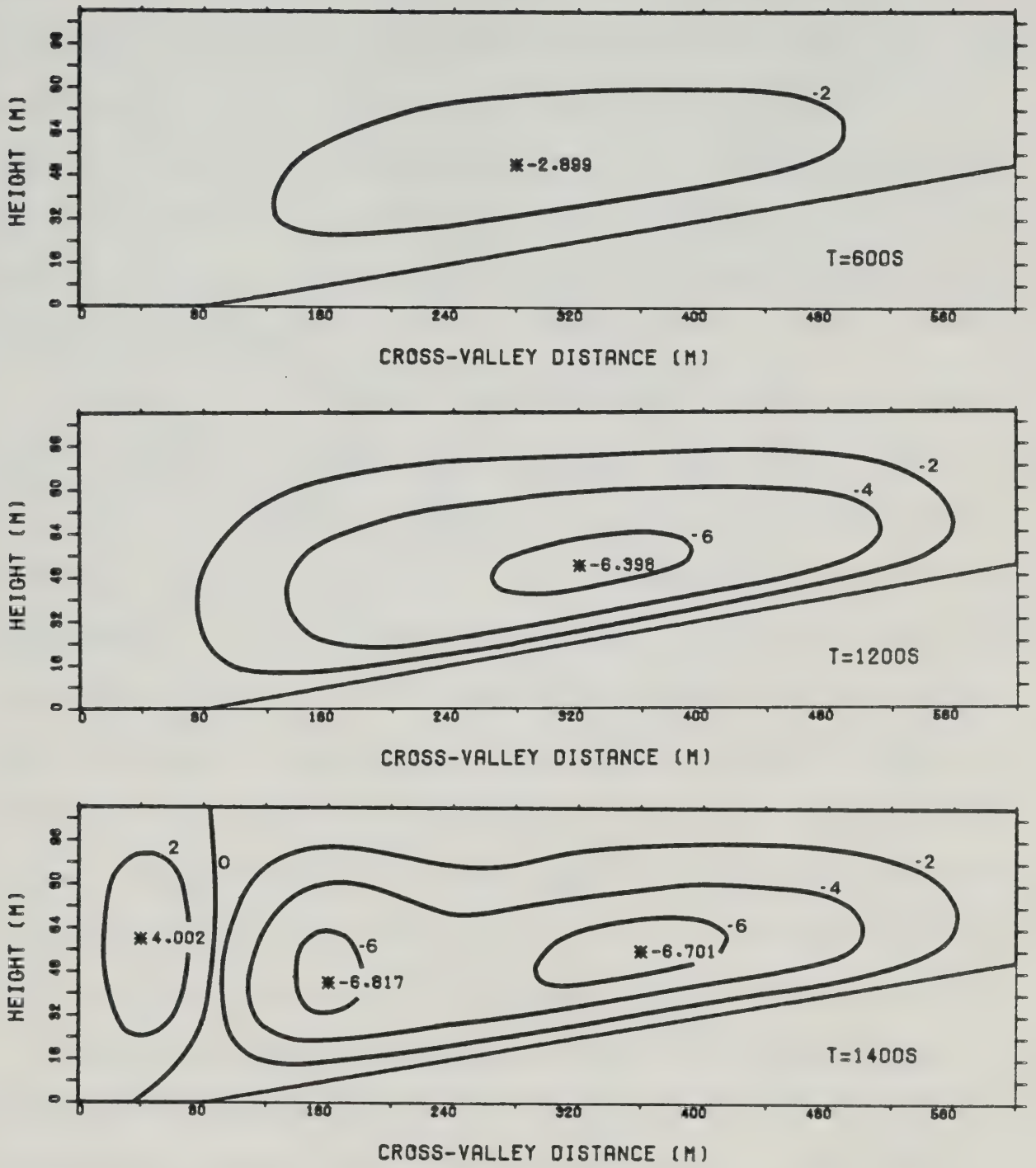


Figure 4.3 Streamfunction contours ($\Delta\psi$ = 2.0 m^2 s^{-1}) at t = 600, 1200, and 1400 seconds for the standard run (Run 1)

about 1250 seconds, the qualitative nature of the flow pattern remained essentially the same. There was a well-developed downslope wind, which was confined to a thin layer near the surface. A weak updraft existed above the valley trough which spread horizontally at some height. In the upper parts of the region, there exists this mainly horizontal flow away from the trough, with weak downward motion towards the ridge.

Figure 4.4 indicates the trajectory of the streamline center obtained a.)from the available grid point values, and b.) from a non-linear interpolation procedure. This method, although somewhat arbitrary, was felt to offer a significant improvement in the estimation of the location of the streamline center. From this Figure, the streamline center was generally seen to move up the sloping surface at some height above it (24 - 28 m). It originated near the middle of the slope, strengthened with time, and eventually moved up and slightly further away from the surface. Little movement of the center occurred once the ridge height was reached.

Along the sloping ground surface, the velocities predicted by the model were quite uniform. The rate of development of the downslope wind appeared to decrease beyond about 1000 seconds of integration time, as it approached a speed of about 50 cm s^{-1}. An illustration of the relationship between the streamfunction field and the velocity components themselves is given in Figure 4.5. Figure 4.5a consists of the isopleth contours of the

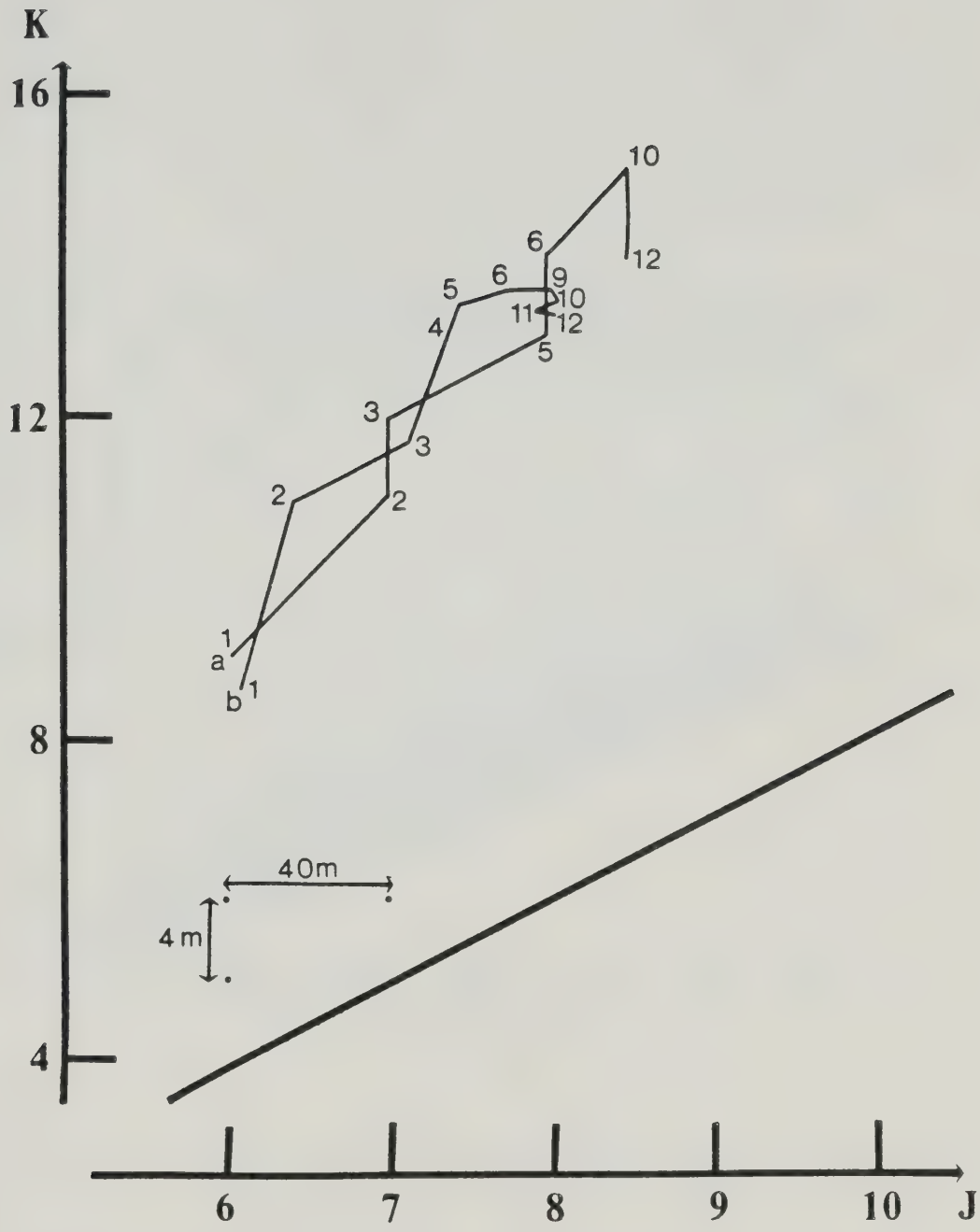


Figure 4.4 Trajectory of streamline center for the standard run (Run 1) obtained from (a.) available grid point values and (b.) interpolation. Numeral indicates time in hundreds of seconds

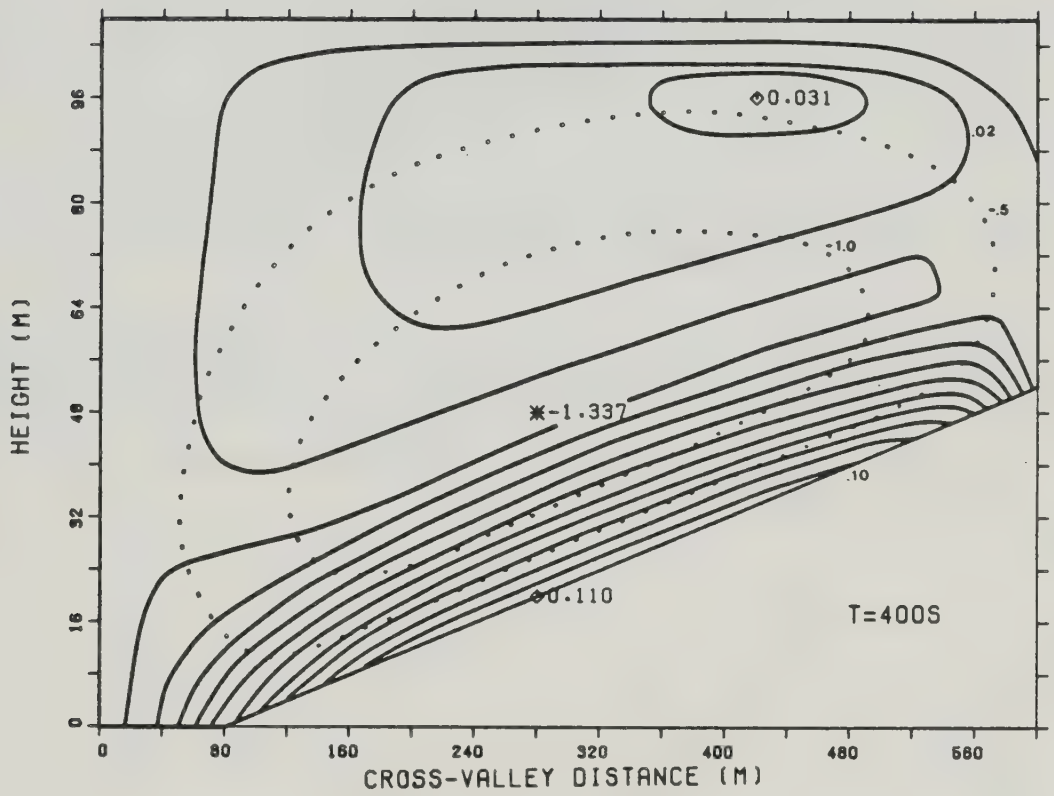


Figure 4.5a Circulation predicted after 400 seconds for the standard run (Run 1) - streamfunction ($\Delta\psi$ = 0.5 m^2 s^{-1}, dotted) and velocity ($\Delta|\vec{V}|$ = 0.01 m s^{-1}, solid) contours

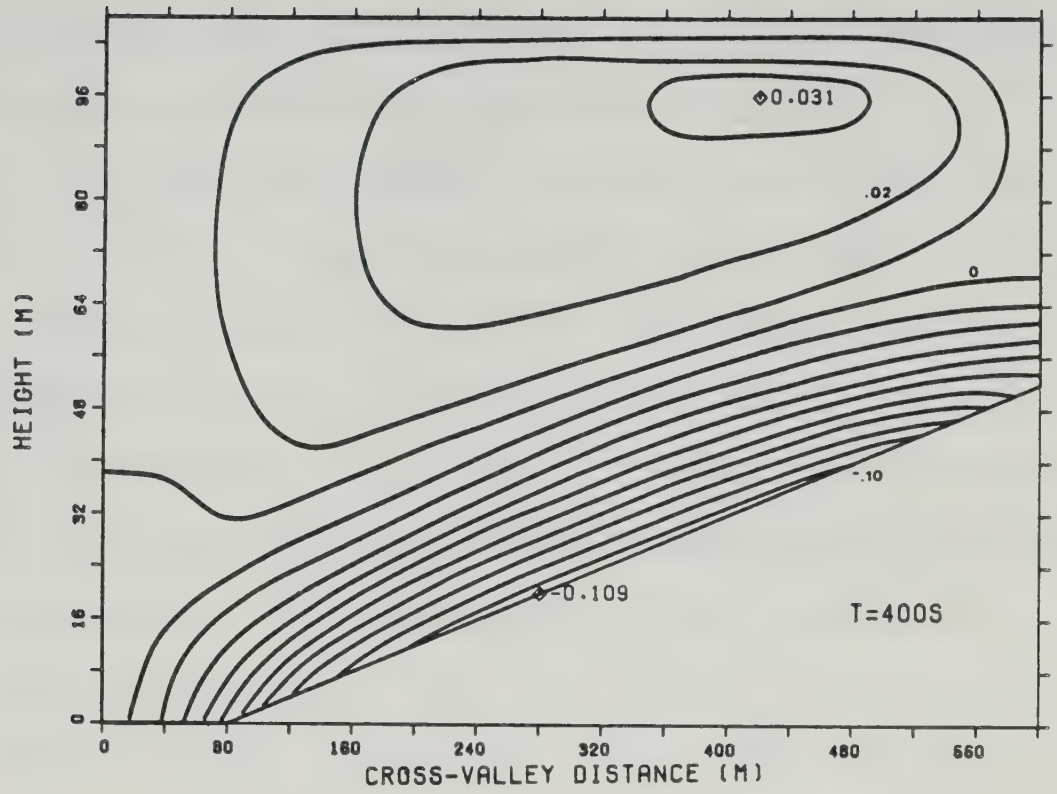


Figure 4.5b Circulation predicted after 400 seconds for the standard run (Run 1) - horizontal velocity component (Δv = 0.01 m s^{-1}) contours

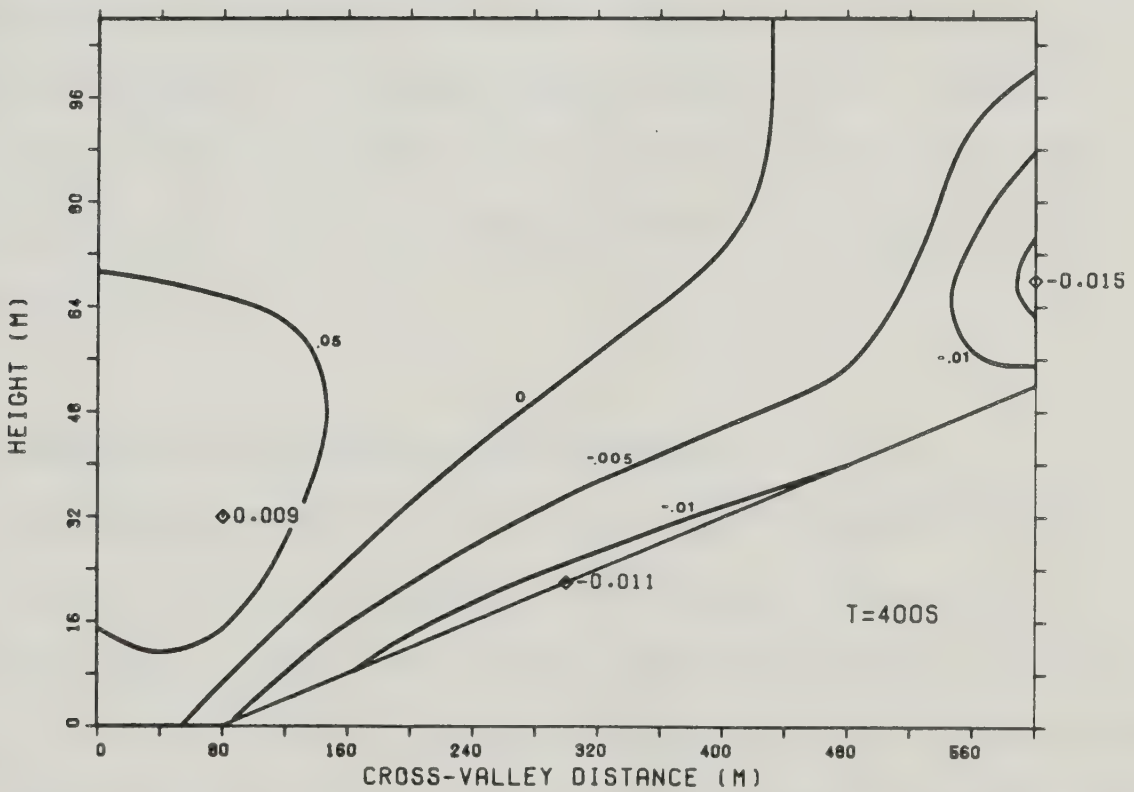


Figure 4.5c Circulation predicted after 400 seconds for the standard run (Run 1) - vertical velocity component (Δw = 0.005 m s^{-1}) contours

streamfunction after 400 seconds, along with contours of the speed of the corresponding flow given by $|\vec{V}| = \{v^2+w^2\}^{0.5}$ Large velocities were present between the surface and the streamline center where the gradients in streamfunction were high. Surface velocities at this time reached 11 cm s^{-1}. Figures 4.5b and 4.5c illustrate the spatial pattern of the two velocity components, v and w, respectively. Figure 4.5b is quite similar to Figure 4.5a as the vertical velocity components were relatively small. Since the gradients in temperature were large under this stable regime, however, these small vertical velocities were able to alter the temperature fields significantly through vertical advection. Initially the maximum upward velocity occurred not along the symmetry axis but rather several grid points to the interior, along J = 3, above where the sloping surface intersected the horizontal valley bottom. Gradually, the maximum vertical velocity moved towards the valley trough boundary.

4.2.3 Evolution of Thermodynamic Fields

The thermodynamic field is altered through both advective and diffusive/radiative processes. The winds generated act to bring warmer air down from above and vice versa. Diffusion acts to mix the cooled air near the surface with the warmer air aloft. The relative magnitudes of these processes change with time and with position in the valley and are given in Table 4.3 for a grid point 4 m above the

middle of the slope (at J = 8, K = 7) at 200 second intervals. Each term in (2.2.2) was evaluated using the various numerical schemes outlined in the previous chapter.

Horizontal advection was found to always act as a cooling process. The horizontal wind component was always negative or directed away from the cooling slope, and therefore acted to transport cooler air away from the surface. The vertical component was also negative and approximately equal to 10 percent of the horizontal component at this grid location. The vertical temperature gradient was large and positive here, resulting in the transport of warmer air from above towards the surface. At all times, the amount of vertical advection exceeded that of horizontal - a layer of warming through advection was the overall result just above the surface.

Referring again to Table 4.3, both horizontal and vertical diffusion terms resulted in cooling at this grid location. Due to the large cooling rates at the surface, the temperature gradient between the surface and this grid point exceeded that between this grid point and the next one away from the surface. Thus, the Laplacian in temperature $(\partial/\partial y\ \partial\theta/\partial y + \partial/\partial z\ \partial\theta/\partial z)$ was clearly negative. Since the horizontal and vertical coefficients of diffusivity were equal and Δz was much smaller than Δy, cooling through vertical diffusion greatly exceeded horizontal diffusion.

Figure 4.6 illustrates the relative contributions of advection and diffusion in various parts of the valley after

Table 4.3 Contributions to $\partial\theta/\partial t$ from advection and diffusion just above mid-slope (J=8,K=7) for Run 1 at 200 second intervals

t	v	w	$-v\frac{\partial\theta}{\partial y}$	$-w\frac{\partial\theta}{\partial z}$	ADV.	$K_y\frac{\partial^2\theta}{\partial y^2}$	$K_z\frac{\partial^2\theta}{\partial z^2}$	DIF.	TOTAL
(s)	(m/s)	(m/s)	($^\circ$K/s)	($^\circ$K/s)	($^\circ$K/s)	($^\circ$K/s)	($^\circ$K/s)	($^\circ$K/s)	($^\circ$K/s)
0	0	0	0	0	0	0	0	0	0
200	-.023	-.002	-2×10^{-5}	$+5\times10^{-5}$	$+3\times10^{-5}$	-5×10^{-6}	-5×10^{-4}	-5×10^{-4}	-5×10^{-4}
400	-.090	-.009	-1×10^{-4}	$+2\times10^{-4}$	$+1\times10^{-4}$	-7×10^{-6}	-6×10^{-4}	-6×10^{-4}	-5×10^{-4}
600	-.181	-.018	-3×10^{-4}	$+5\times10^{-4}$	$+2\times10^{-4}$	-9×10^{-6}	-7×10^{-4}	-7×10^{-4}	-5×10^{-4}
800	-.274	-.026	-5×10^{-4}	$+8\times10^{-4}$	$+3\times10^{-4}$	-1×10^{-5}	-8×10^{-4}	-8×10^{-4}	-5×10^{-4}
1000	-.347	-.032	-7×10^{-4}	$+1\times10^{-3}$	$+3\times10^{-4}$	-2×10^{-5}	-8×10^{-4}	-8×10^{-4}	-5×10^{-4}
1200	-.392	-.036	-9×10^{-4}	$+1\times10^{-3}$	$+3\times10^{-4}$	-2×10^{-5}	-8×10^{-4}	-8×10^{-4}	-5×10^{-4}
1400	-.393	-.035	-9×10^{-4}	$+1\times10^{-3}$	$+3\times10^{-4}$	-1×10^{-5}	-8×10^{-4}	-8×10^{-4}	-5×10^{-4}

400 seconds (Figure 4.6a) and after 1200 seconds (Figure 4.6b). Generally, warming through subsidence occurred along the slope and above the valley ridge. Greater cooling through diffusion occurred at these locations, however, but as the velocities increased with time the difference in the magnitudes of advection and diffusion diminished. Cooling through diffusion was a maximum just above the ridge surface where cooling below and warming above together created large differences in the vertical temperature gradient.

The actual potential temperature fields predicted can be examined in a number of ways. A sequence in time of two-dimensional plots of potential temperature over the valley cross-section are shown in Figure 4.7 at 400 second intervals. Early in the model integration, distortion of the horizontal isotherms through cooling at the surface was very evident. Above the ridge, slight packing of the isotherms appeared as a result of cooling from below and warming through subsidence from above. This acted to strengthen the vertical temperature gradient close to the ground. The vertical temperature gradient was 0.014 $C^{\circ}\ m^{-1}$ at t = 0 seconds. After 1200 seconds, the potential temperature at the ridge surface had dropped to 284.046 °K, whereas that 32 m above had increased to 285.170 °K - a vertical temperature gradient of 0.035 $C^{\circ}\ m^{-1}$ resulted, over twice the initial value. At the trough axis, there was cooling at the surface and somewhat less cooling aloft - a vertical temperature gradient of 0.022 $C^{\circ}\ m^{-1}$ resulted after 1200 seconds. The

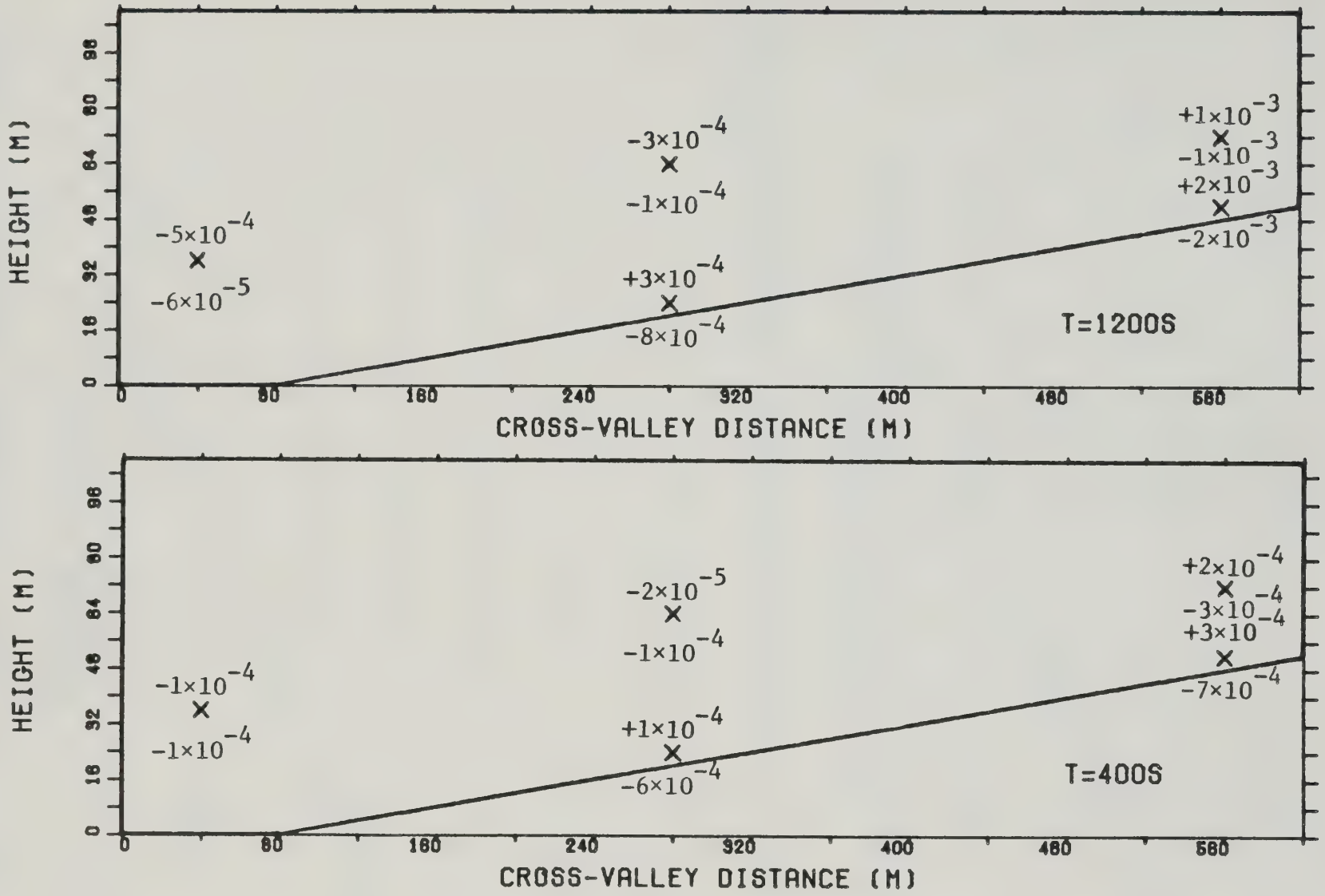


Figure 4.6 Relative contributions to $\partial\theta/\partial t$ from advection (denoted above grid point) and diffusion (denoted below grid point) for the standard run (Run 1) in various parts of the valley after (a.) 400 seconds and (b.) 1200 seconds

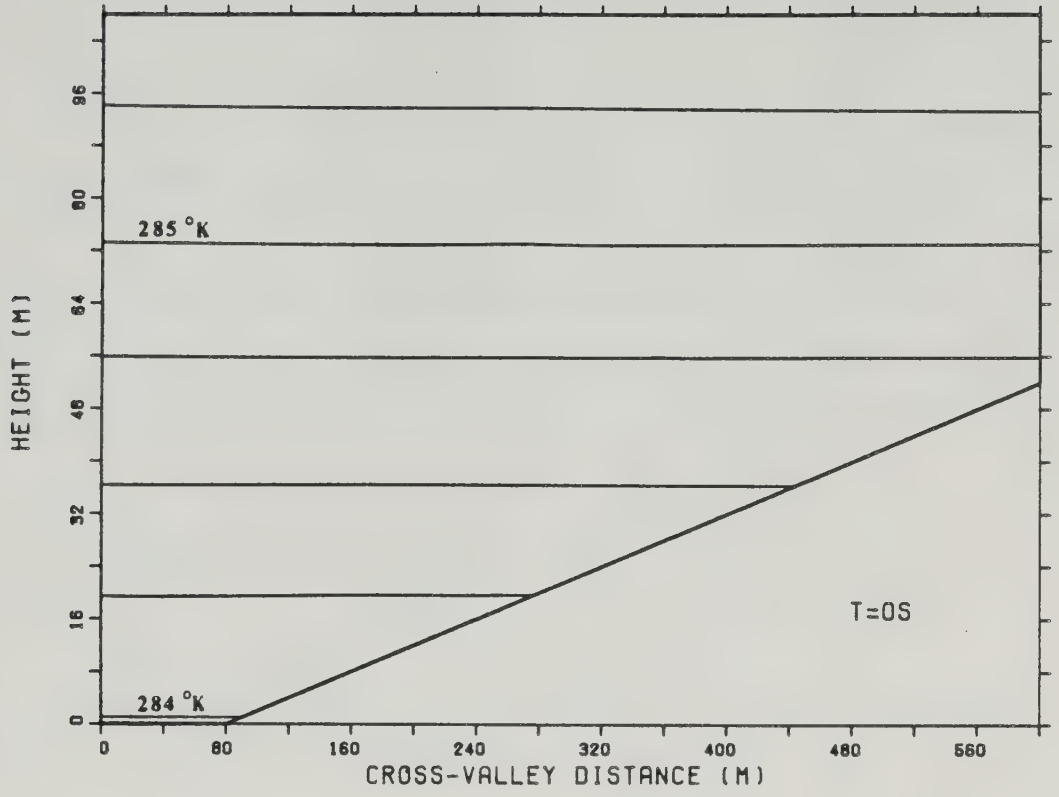


Figure 4.7a Potential temperature field at t = 0 seconds for the standard run (Run 1)

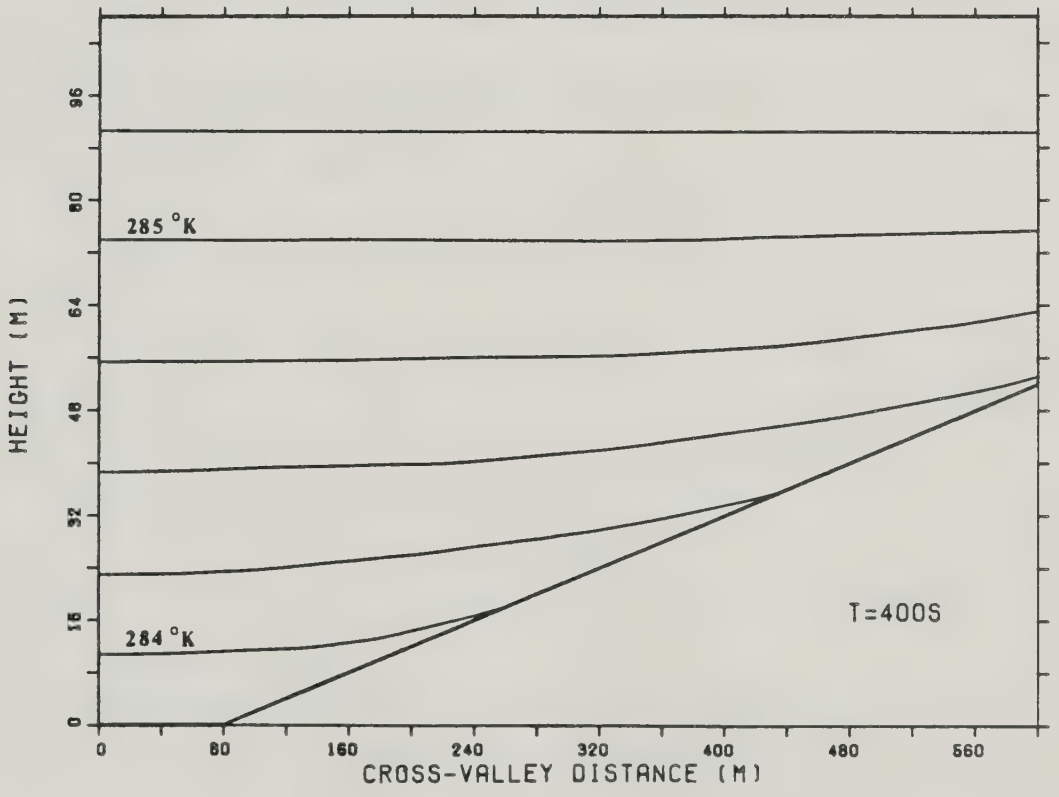


Figure 4.7b Potential temperature field at t = 400 seconds for the standard run (Run 1)

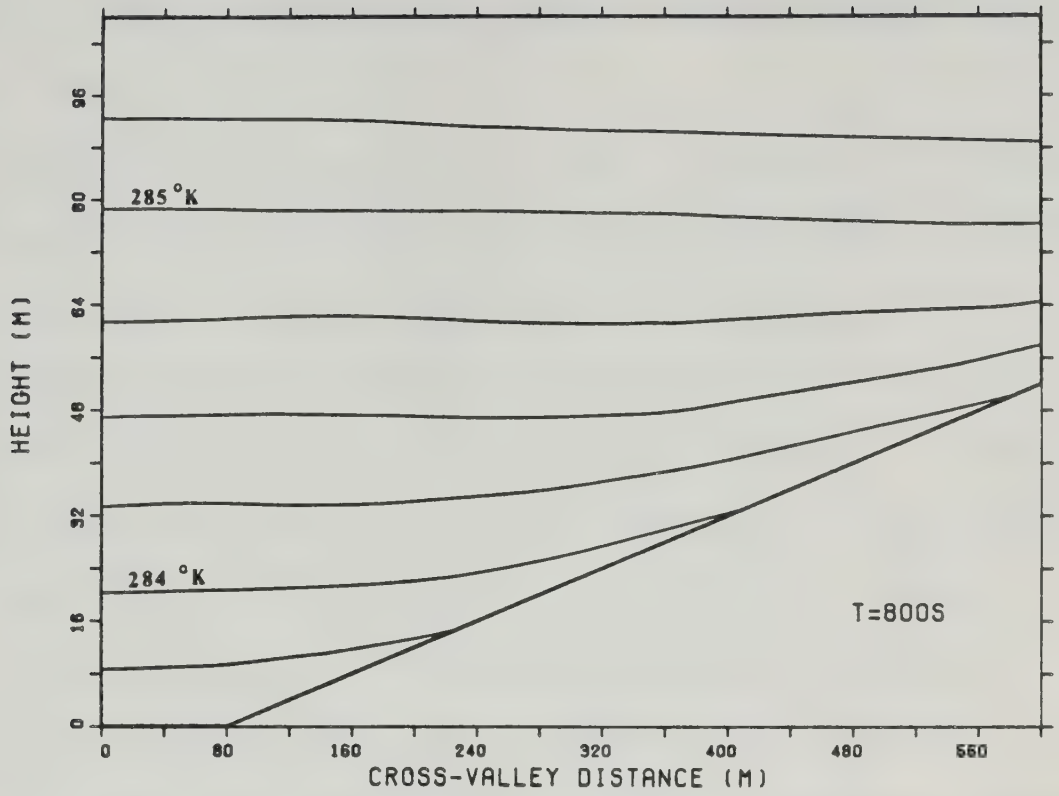


Figure 4.7c Potential temperature field at t = 800 seconds for the standard run (Run 1)

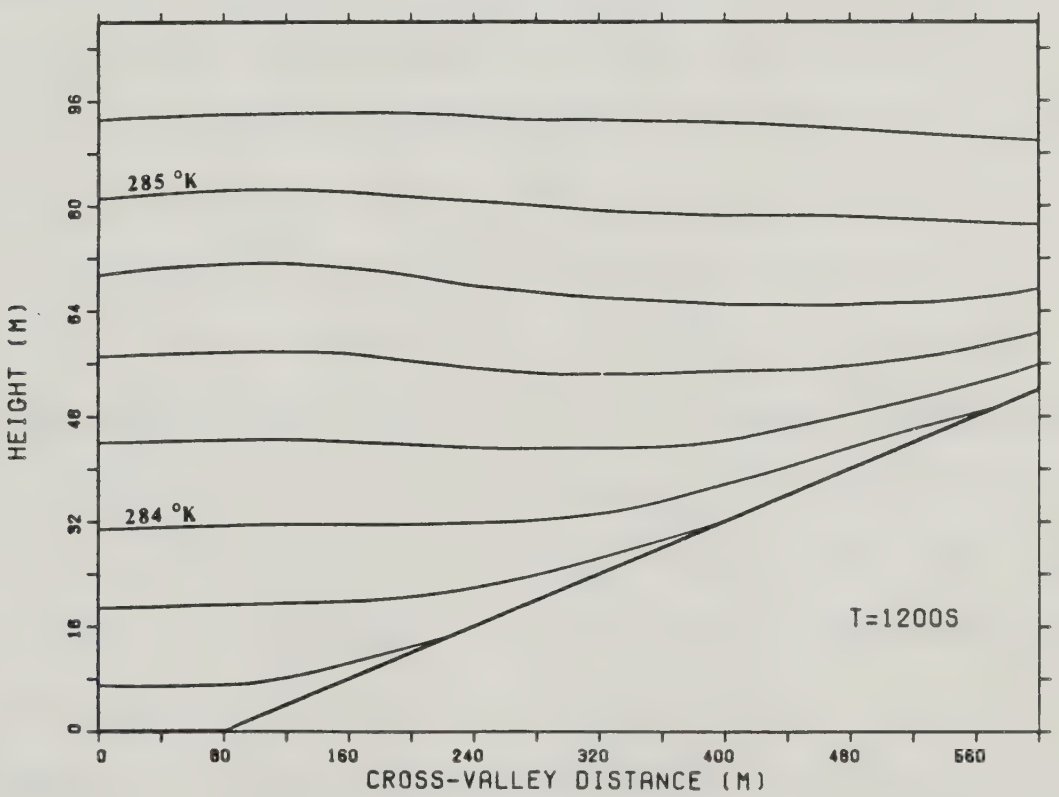


Figure 4.7d Potential temperature field at t = 1200 seconds for the standard run (Run 1)

stability had increased more at the ridge height than at the trough level.

Another useful manner in which to examine the temperature changes as functions of time and position is through plots of the vertical temperature profile in different parts of the valley cross-section for several times. Figures 4.8, 4.9, and 4.10 illustrate vertical profiles of the cooling predicted as a function of height at the trough, mid-slope and ridge positions, respectively. Comparing Figure 4.8 with Figure 3.6, in which the amount of cooling predicted through vertical diffusion alone is given, reveals the contributions which advection and horizontal diffusion make to the temperature deviation. Figure 4.11 provides such a comparison. The difference between the valley model results and the analytically derived one-dimensional solution are given at several times in this set of curves. At early times (up to 200 - 300 seconds of integration time), there was very little difference between the two solutions, indicating that the predicted valley model changes occurred through vertical diffusion, as expected. The difference between the two solutions was zero at the upper and lower boundaries, where exactly the same boundary conditions were specified in both cases. Close to the ground surface, vertical diffusion played a larger role in altering the temperatures than in the atmosphere above, and so the two solutions differed less and less as the surface was approached.

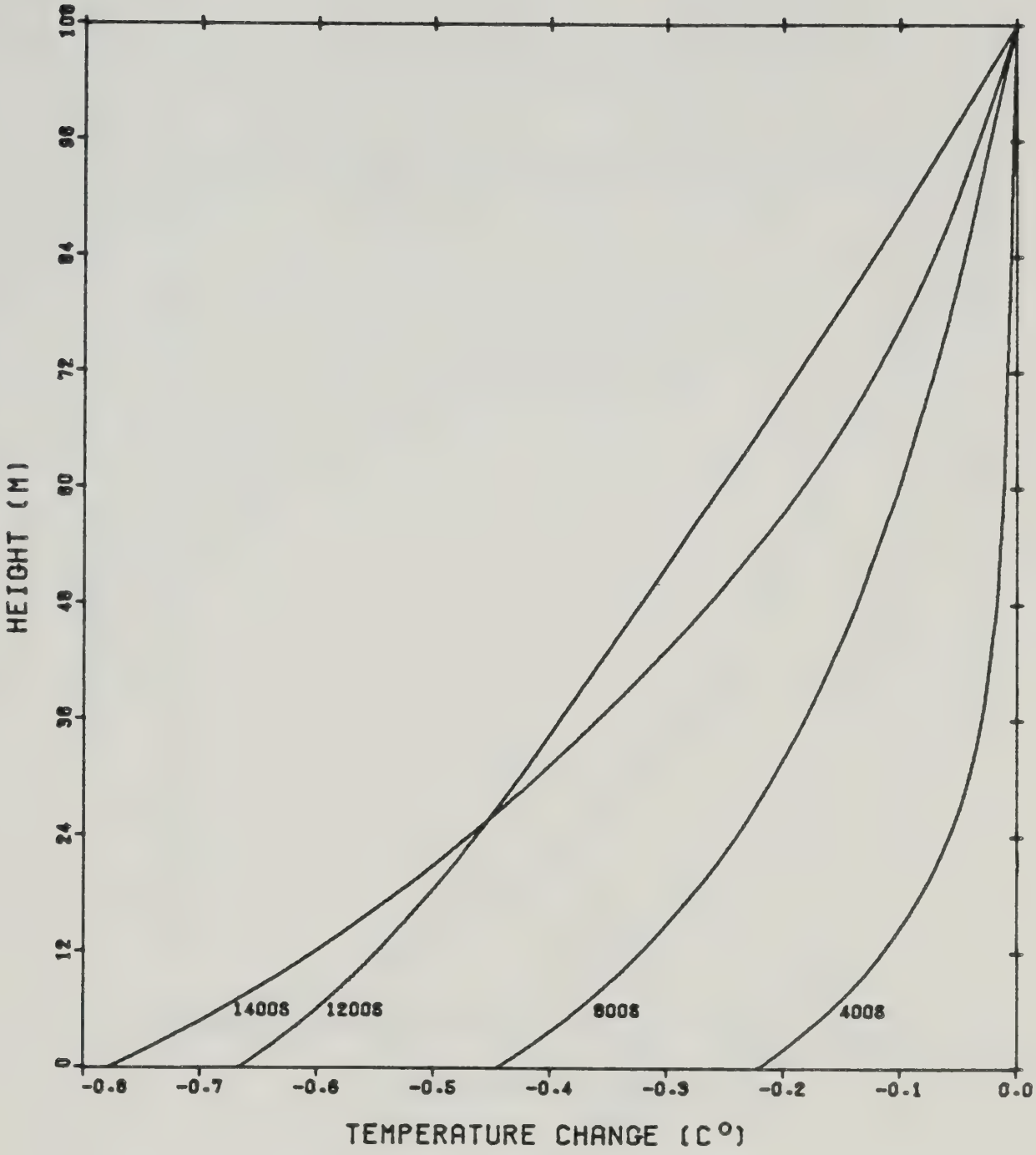


Figure 4.8 Potential temperature deviation from initial state versus height above trough boundary (J=1) for the standard run (Run 1)

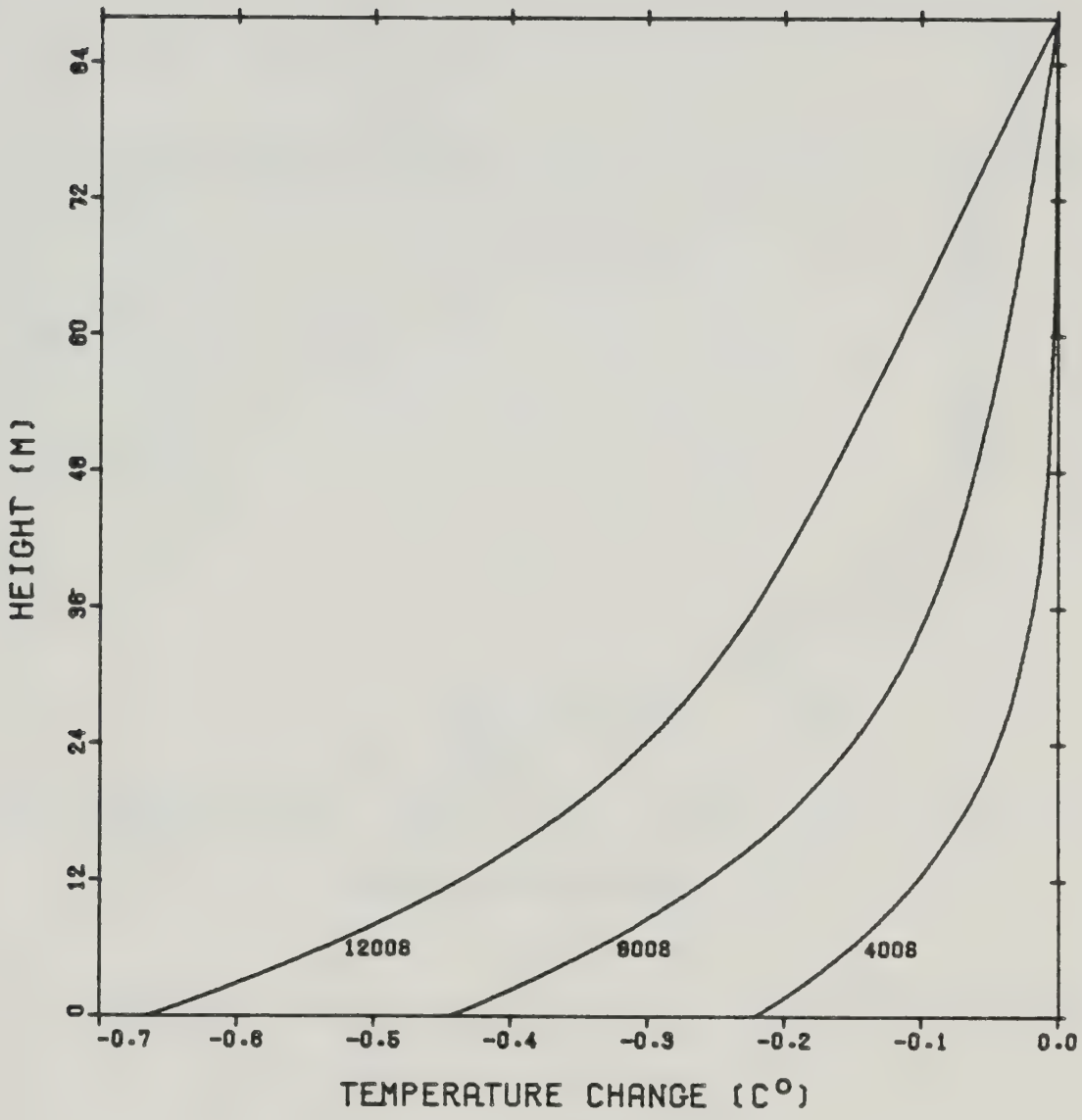


Figure 4.9 Potential temperature deviation from initial state versus height above mid-slope region (J=8) for the standard run (Run 1)

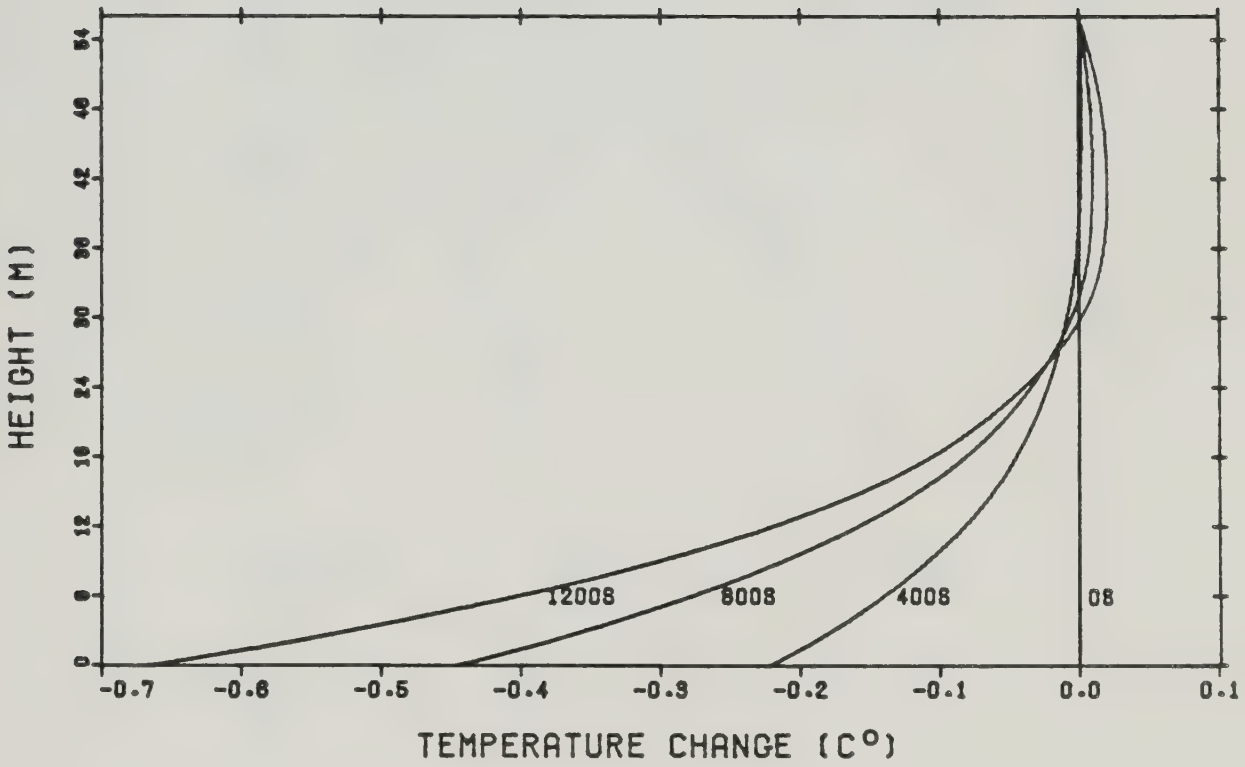


Figure 4.10 Potential temperature deviation from initial state versus height above ridge boundary (J=16) for the standard run (Run 1)

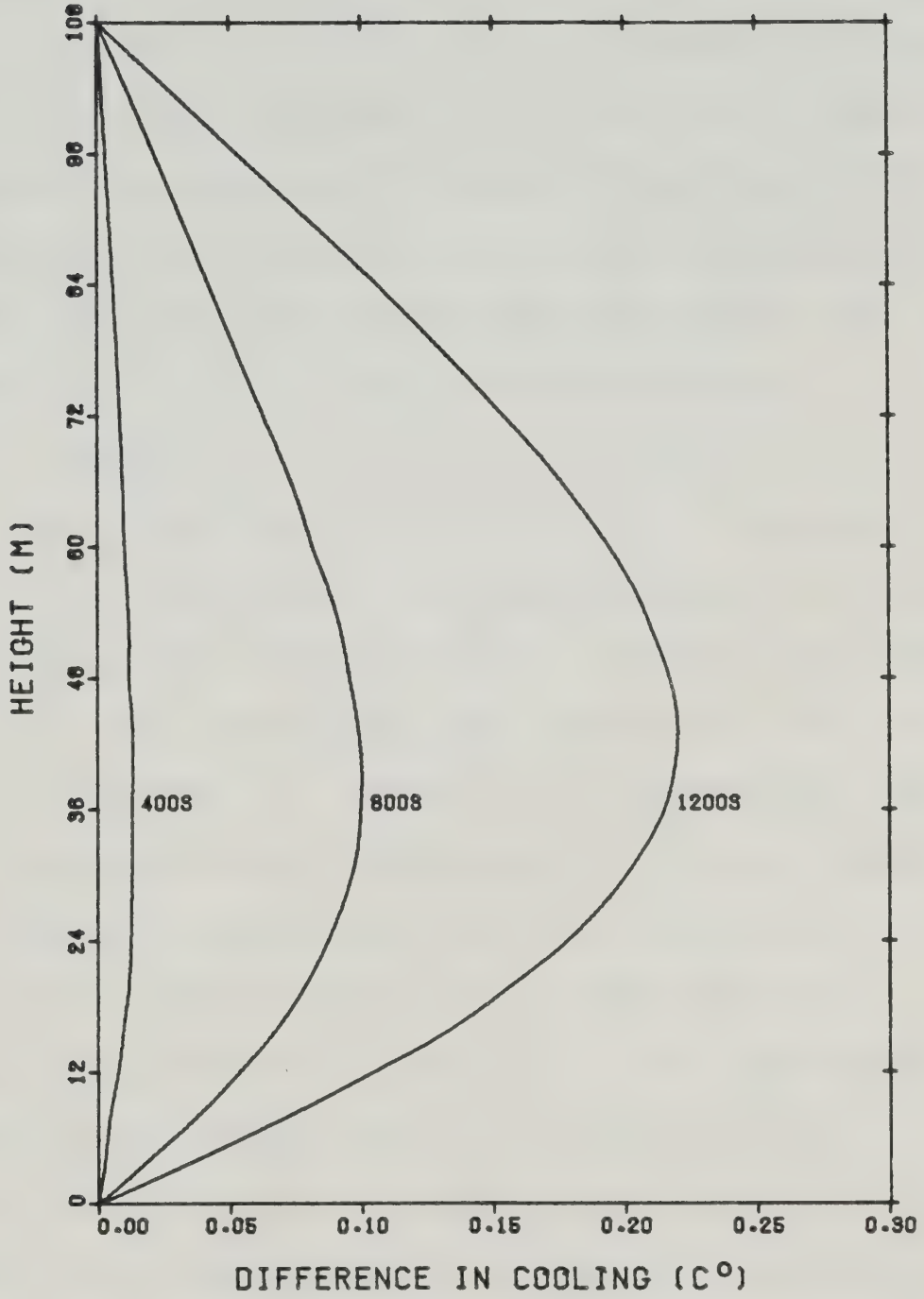


Figure 4.11 Difference in cooling predicted by valley model in Run 1 and by one-dimensional vertical diffusion equation ($K = 1.0\ m^2\ s^{-1}$) as a function of height

Beyond about 1260 seconds, the temperature profile above the trough, shown in Figure 4.8, began to exhibit some unusual features. The source of this extreme warming aloft was revealed upon re-examination of the circulation regimes depicted in Figure 4.3 at this time. A counterclockwise cell had begun to develop well above the valley floor just after 1200 seconds. This resulted in downward motion along the trough boundary, with accompanying warming through subsidence. The origin of this counterclockwise motion was the larger vertical velocities which occurred along J = 3 compared to those along J = 1, as is evident in Figure 4.5c. A maximum upward velocity of about 0.9 cm s^{-1} existed along J = 3 at 400 seconds whereas the maximum along J = 1 (the lateral boundary) was about 0.8 cm s^{-1} at that time. After 1200 seconds, these velocities had increased to 3.5 cm s^{-1} and 1.9 cm s^{-1} along J = 3 and J = 1, respectively. The resulting differential in the amounts of vertical advection created a slightly cooler area at some distance from the boundary. As the magnitude of the vertical velocity increased, the amplitude of the wave in the temperature field close to the trough increased. Through these variations in the horizontal temperature gradient, the vorticity eventually gained positive values well above the valley trough and this corresponded to a counterclockwise flow in this area beyond 1260 seconds.

Figures 4.9 and 4.10 illustrate the vertical temperature profiles above the mid-slope region (J = 8) and ridge

(J = 16), respectively. The general shape of the curves in Figure 4.9 is similar to those in Figure 4.8, especially at early times. Later, warm advection along the slope acted to retard the effect of the cooling ground surface below. In Figure 4.10, the increase in potential temperature at heights of 30 m or more above the ground is clearly shown. This was due to, as mentioned previously, the downward flow above the ridge which created warming through subsidence. At low levels, cooling persists due to mixing of the air near the cooled surface.

4.3 Effect of Location of Upper Boundary - Run 2

A second model integration was performed using the same input parameters as in Run 1 (listed in Table 4.1) except that the upper boundary was located at a height of 144 m rather than 108 m. Thus, a vertical grid spacing of 4 m was used from the surface up to 72 m, and a spacing of 12 m from 72 m up to 144 m. An initial time step of 2 seconds was again used, with integration out to 1400 seconds requiring 706 seconds of CPU time.

The predicted streamfunction fields were found to exhibit very similar properties to those of Run 1, at least qualitatively. The return flow aloft reached to somewhat greater heights but because of weaker vertical gradients between the streamfunction center and the upper boundary, smaller horizontal winds resulted. For example, at 600 seconds, the maximum horizontal wind was about 5.1 mm s^{-1} at a

height of 72 m in Run 1 but was only about 3.6 mm s^{-1} when the flow was permitted to greater heights. Vertical winds near the trough boundary were slightly raised over those of Run 1, with the result that the counterclockwise cell appeared somewhat earlier following the reasoning given in Section 4.2.3. Development of downslope winds near the sloping surface was generally identical. The trajectory of the streamline center appeared to move farther up and away from the slope than in Run 1, especially within the early stages of the integration. Significant movement of the center ceased once the height of the ridge was reached, as in Run 1.

The temperature profiles out to 1000 seconds or so were virtually identical to those for Run 1 for the valley region below ridge height. Further above, the greater height of the upper boundary permitted temperatures there to be altered through both advection and diffusion, although the warming or cooling predicted was quite small. Beyond about 1000 seconds, large differences existed between the two runs, principally due to the cellular nature of the flow in the second run by this time.

4.4 Effect of Absence of Horizontal Valley Floor - Run 3

In order to determine the influence of including a horizontal valley floor, one integration within a 'V-shaped' valley cross-section was performed. All input parameters were the same as in Run 1, except that the two columns of

grid points above the flat valley bottom were eliminated. This effectively moved the lateral trough boundary over to where the sloping ground intersected the previously included valley bottom. Again, a 2 second time step was specified initially, and 506 seconds of CPU time were used in reaching 1600 seconds of model time.

In the earlier stages of this run, out to about 1000 seconds of integration time, the primary difference was found close to the trough boundary, as expected. Maximum vertical velocities above where the sloping ground met the horizontal are given in Table 4.4 for Run 1 (J = 3) and Run 3 (J = 1). This enables the same relative positions with respect to the sloping ground to be compared. The height at which the maximum vertical velocity was found, based on the available grid points, is also provided in this Table. In Run 3, the flow is forced to rise very close to the slope, resulting in larger horizontal gradients in the streamfunction (and therefore larger vertical velocities) in this area.

The potential temperature profile above the valley trough reflected the larger vertical velocities as greater cooling through adiabatic expansion was evident. At a height of 52 m, for example, the results for Run 3 indicated a potential temperature of 284.64 °K after 600 seconds whereas Run 1 predicted 284.66 °K. After 1000 seconds, Run 3 and Run 1 predicted temperatures of 284.46 °K and 284.50 °K, respectively, at 52 m. The mid-slope temperature profiles were

Table 4.4 Maximum vertical velocities above valley trough for Run 1 (J=3) and for Run 3 (J=1). Quantity in parentheses denotes height at which maximum occurred

time	Run 1 (J=3)	Run 3 (J=1)
(s)	w_{mx} (z(m) at w_{mx})	w_{mx} (z(m) at w_{mx})
0 0	0	0
200	0.0025 (30)	0.0041 (28)
400	0.0087 (32)	0.0132 (32)
600	0.0158 (36)	0.0210 (34)
800	0.0224 (36)	0.0271 (36)
1000	0.0275 (38)	0.0312 (38)
1200	0.0357 (40)	0.0425 (42)
1400	0.1064 (48)	0.1692 (52)

quite similar, however, with slightly less warming at low levels, and slightly more cooling at upper levels through advective differences. Above the ridge, little difference, if any, was evident in the temperature profiles.

4.5 Effect of Steeper Slope - Run 4

In order to determine the effect on the evolution of the circulation of a lower boundary which was twice as steep as that of the standard run, a fourth integration was performed. Apart from interest in discovering how the model would behave under such conditions, this run was felt to be useful due to the asymmetric topography of the North Saskatchewan River valley. From Figure 3.1, it is evident that the valley is much steeper on the north bank as the river meanders eastward cutting into the bank on the outside corner. There, a slope angle of about $\tan^{-1}(0.22)$ or 0.21 radians would be more representative. For these reasons, the slope angle for Run 4 was set to $\tan^{-1}(0.20)$ or about 0.20 radians. As the permissible grid spacings are closely related to the slope angle through (3.2.1), the horizontal grid size, Δy, was reduced to 20 m for this run. Both Δz_1 and Δz_2 remained 4 m and 12 m , respectively. The region being modelled here is shaded in Figure 4.12, and is shown relative to the region under consideration in the standard run. A time step of 2 seconds sufficed since the vertical grid spacing, which was the limiting factor in the standard run, remained unchanged. In order to reach 1400 seconds, 772

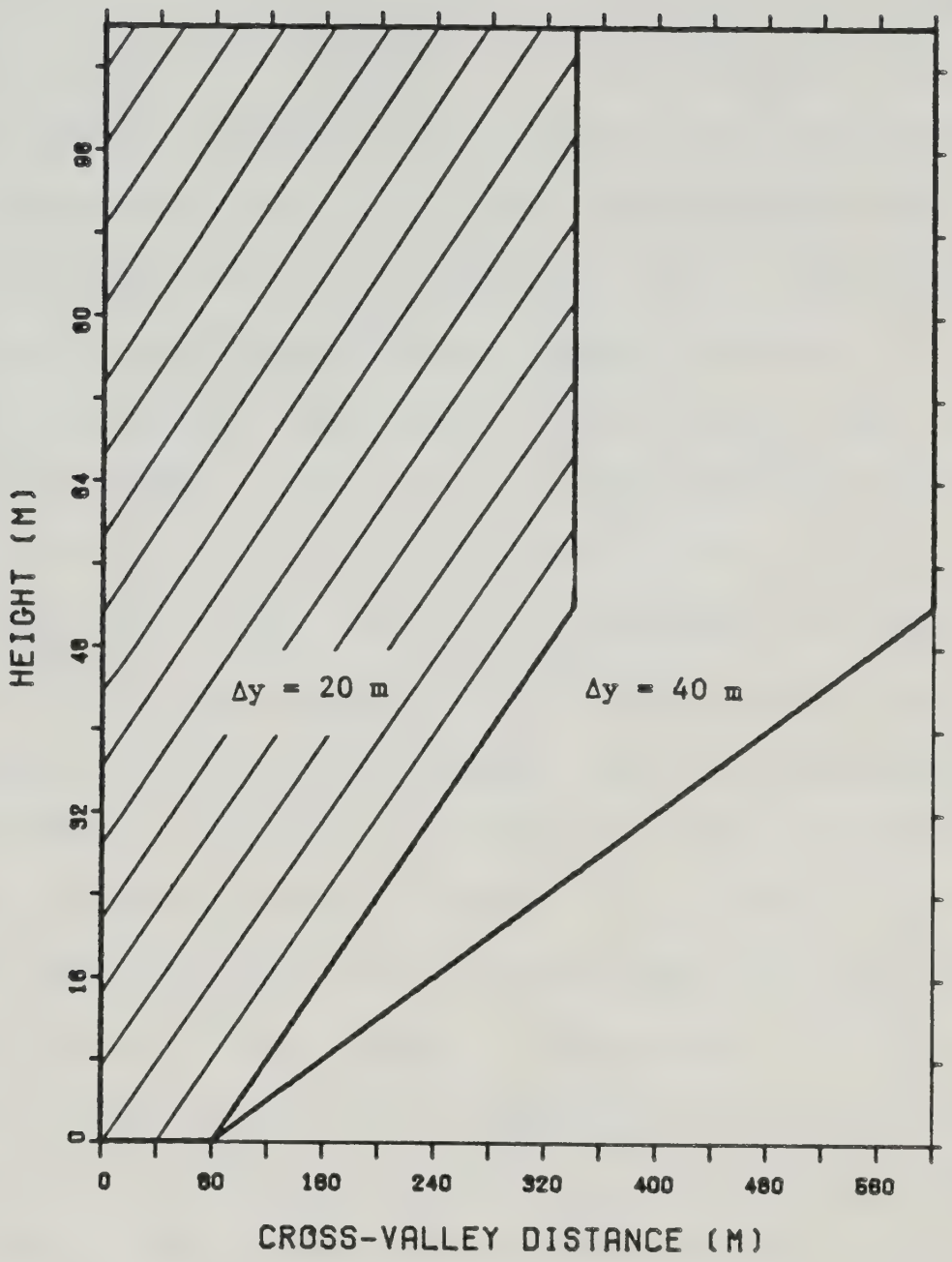


Figure 4.12 Schematic illustration of modelled region in Run 4 (hatched), along with that of Run 1

seconds of CPU time were required.

The intensity of the circulation as development proceeded can be obtained from Figure 4.13, in which the variation of the streamfunction extremum and the maximum downslope wind at the surface with time are given for both the standard run and Run 4. The steeper slope resulted in larger velocities close to the ground, and after about 800 seconds, downslope winds of about 0.40 m s^{-1} were predicted. Thereafter, a quasi-steady-state regime existed in the circulation while cooling proceeded at the ground. The term quasi-steady-state is used here to indicate that the rate of change of vorticity, $\partial\xi/\partial t$, was close to zero at all grid points. This means that the three processes which can act to alter the vorticity (advection, diffusion, and the solenoid term) were in balance. For example, close to 800 seconds, the solenoid term acted to generate negative vorticity just above the mid-slope region. As well, the vorticity gradients were such that transport by the downslope wind acted to decrease the vorticity. However, changes due to diffusion were positive and approximately balanced the two processes above. In the standard run, however, a quasi-steady-state period did not occur prior to the formation of a counter-clockwise cell above the trough as in Run 4.

Increased vertical velocities relative to the standard run resulted in increased cooling above the valley trough. Similarly, above the ridge, increased warming through subsidence was predicted for Run 4 as the downward velocities

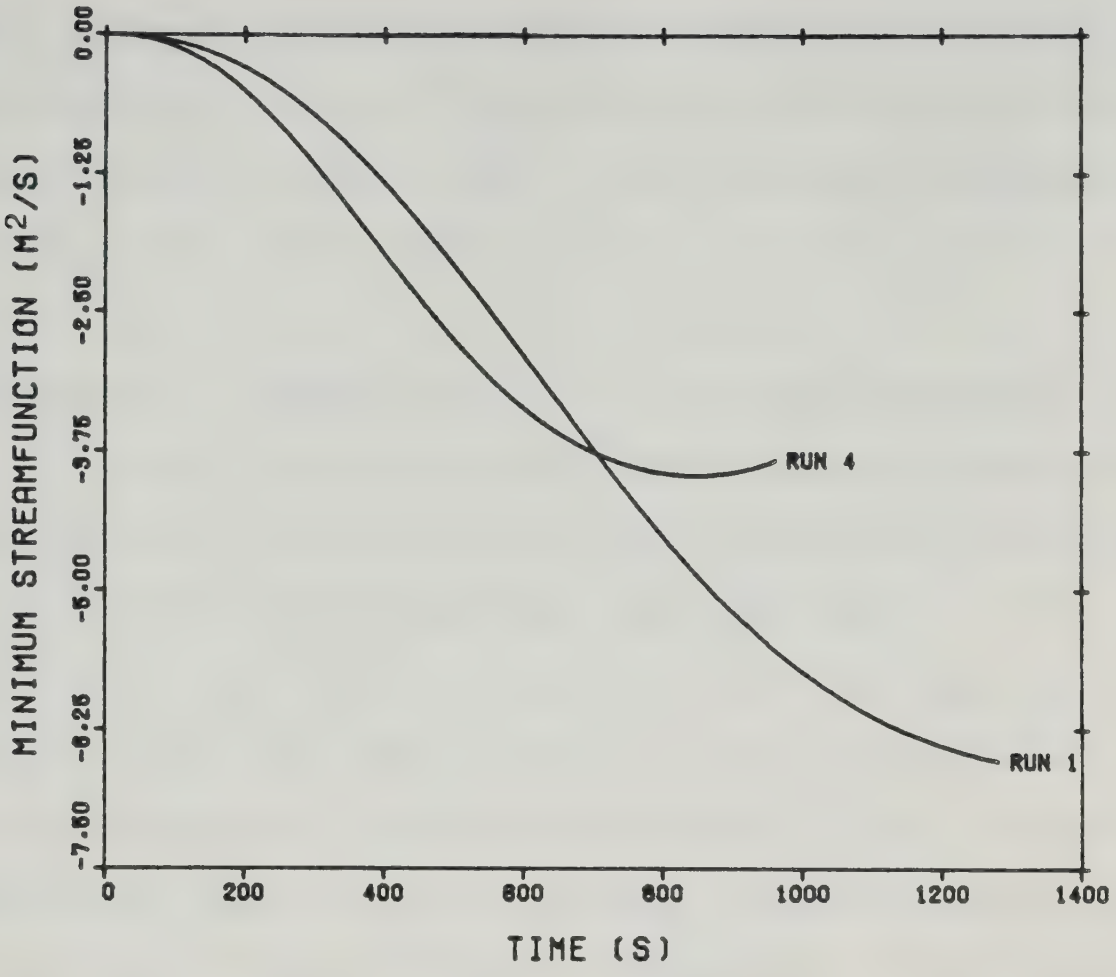


Figure 4.13a Minimum streamfunction versus time for the standard run (Run 1) and for Run 4

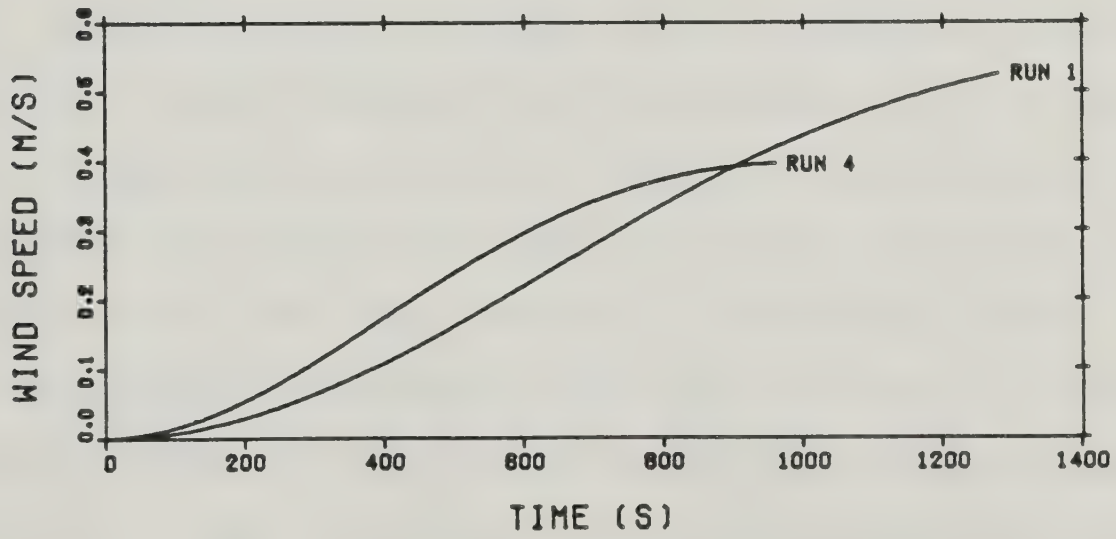


Figure 4.13b Maximum surface downslope wind speed versus time for the standard run (Run 1) and for Run 4

were expected to be 2 - 3 times larger than in Run 1. Since the downslope winds at a given time were only slightly larger in Run 4 than in Run 1, the mid-slope temperature profiles were quite similar.

4.6 Effect of Smaller Vertical Diffusion Coefficient - Run 5

In order to examine the circulation development when a much smaller vertical transfer rate through diffusion was used, a fifth integration was executed. With $K_z = 10^{-2}$ m^2 s^{-1} and $K_y = 1.0$ m^2 s^{-1}, time steps up to 400 seconds would, in theory, remain stable, according to criteria based on the diffusion terms (3.4.9). However, the horizontal advection term, (3.4.2), required a time step of 20 seconds or less. For this integration, a time step of 10 seconds was implemented. This meant that only 247 seconds of CPU time were needed in order to reach 2000 seconds of model time.

Through the much reduced vertical diffusion transfer, relative to the standard run, the streamline center was kept very close to the ground (4 - 8 m away). As well, the rate at which the extreme streamfunction value increased with time was much less than for Run 1. For example, after 1000 seconds, the streamfunction attained a value of -2.63 m^2 s^{-1} and was found about 8 m from the slope in Run 5 whereas Figures 4.1 and 4.4 indicate an extreme streamfunction value of -5.73 m^2 s^{-1} to exist about 29 m from the slope in Run 1 at that time. However, large downslope winds were the result

at the surface due to the large vertical streamfunction gradient formed close to the ground. Just above the ground itself, lower wind speeds than in Run 1 were found.

Table 4.5 indicates a quantitative comparison between the relative magnitudes of advection and diffusion just above the mid-slope region. Referring again to Table 4.3, which is appropriate to Run 1, provides an interesting comparison. Horizontal advection acted to cool the air above the surface, as in Run 1, but was larger in magnitude. The cool air at the surface could not be transferred up and away as quickly as in Run 1 because the vertical diffusion rates specified were much smaller. Vertical advection was positive (warm) and initially smaller than in Run 1 because the vertical velocities were smaller. After about 800 seconds, the vertical gradient in temperature was quite big, resulting in large positive vertical advective changes. The sum of these two components yielded an overall negative change in potential temperature, or cold advection, since the horizontal component dominated. This is in contrast to the standard run in which a layer of warm advection was produced near the surface which was able to counteract the cooling through diffusion. Horizontal diffusion was small and negative at this grid location, but was typically an order of magnitude larger than for the standard run. This was due to the slower transfer processes in the vertical which created large gradients in the temperature gradient close to the slope. Vertical diffusion was negative and approximately an order

Table 4.5 Contributions to $\partial\theta/\partial t$ from advection and diffusion just above mid-slope (J=8,K=7) for Run 5 at 200 second intervals

t	v	w	$-v\frac{\partial\theta}{\partial y}$	$-w\frac{\partial\theta}{\partial z}$	ADV.	$K_y\frac{\partial^2\theta}{\partial y^2}$	$K_z\frac{\partial^2\theta}{\partial z^2}$	DIF.	TOTAL
(s)	(m/s)	(m/s)	($^\circ$K/s)	($^\circ$K/s)	($^\circ$K/s)	($^\circ$K/s)	($^\circ$K/s)	($^\circ$K/s)	($^\circ$K/s)
0	0	0	0	0	0	0	0	0	0
200	-.010	-.001	-3×10^{-5}	$+2\times10^{-5}$	-1×10^{-5}	-6×10^{-7}	-1×10^{-4}	-1×10^{-4}	-1×10^{-4}
400	-.048	-.005	-2×10^{-4}	$+1\times10^{-4}$	-1×10^{-4}	-8×10^{-5}	-8×10^{-5}	-2×10^{-4}	-3×10^{-4}
600	-.116	-.012	-6×10^{-4}	$+4\times10^{-4}$	-2×10^{-4}	-8×10^{-5}	-8×10^{-5}	-2×10^{-4}	-4×10^{-4}
800	-.210	-.021	-1×10^{-3}	$+1\times10^{-3}$	-3×10^{-4}	-7×10^{-5}	-7×10^{-5}	-1×10^{-4}	-4×10^{-4}
1000	-.309	-.032	-2×10^{-3}	$+2\times10^{-3}$	-3×10^{-4}	-7×10^{-5}	-6×10^{-5}	-1×10^{-4}	-4×10^{-4}
1200	-.390	-.040	-3×10^{-3}	$+3\times10^{-3}$	-3×10^{-4}	-7×10^{-5}	-6×10^{-5}	-1×10^{-4}	-4×10^{-4}
1400	-.467	-.047	-4×10^{-3}	$+4\times10^{-3}$	-3×10^{-4}	-7×10^{-5}	-5×10^{-5}	-1×10^{-4}	-4×10^{-4}

of magnitude smaller in Run 5 than in the standard run. Overall, smaller cooling amounts occurred just above the ground than in Run 1 even though advection was a generally cooling influence.

4.7 Effect of Stability

4.7.1 General

Fleagle (1950) developed a very simple model to describe the motion of a compressible fluid due to cooling at the bottom by contact with a radiating surface of uniform slope and large extent. He showed that as the air accelerated down the slope, adiabatic heating resulted in a reversal in the pressure gradient, which retarded the flow. As the air decelerated, friction decreased, radiational cooling increased the pressure gradient and the cycle was repeated. The exact nature of the analytical solution depended on the form of the frictional term. If it was assumed proportional to the speed, the mean velocity in the layer close to the ground varied periodically at first and gradually became constant. The value of this unchanging downslope wind was found to be a.) proportional to the net outgoing radiation, b.) inversely proportional to the thickness of the layer to which cooling extends, and c.) inversely proportional to the slope of the ground.

Tyson (1968) described observations made in Pietiermaritzburg, S. Africa, from 1961 - 1965, in which

downvalley flows up to 6.5 m s^{-1} occurred soon after sunset. The wind then steadily weakened throughout the night as cool air of marked stability filled the entire valley up to the height of the ridge. This showed the variation in the strength of the flow under different stabilities.

Petkovsek and Hocevar (1971), in an analytical study, also included an ambient stratification and were able to demonstrate the importance of stratification in determining the strength of drainage flows. They found that the more the lapse rate in the atmosphere outside the cooled layer differed from isothermal and the closer it was to adiabatic, the larger was the downslope velocity.

McNider (1982) made a simple extension of Fleagle's work in order to examine the impact of various stratifications on the oscillatory nature of the resultant flow. These results showed that the period of the oscillation, as well as the strength of the flow, increased with decreasing stability. The periods he found varied from 20 - 90 minutes as the lapse rate decreased from 8 C° km^{-1} to 2 C° km^{-1}. These periods are somewhat larger than the model integration times of the valley model presented in this thesis and are not considered here. The mean downslope flow varied from 0.06 m s^{-1} to 0.29 m s^{-1} under the same variations in stability, above a slope of about 20 °.

4.7.2 Neutral Case Initially - Run 6

In order to simulate neutral stability conditions initially, a model integration was performed using a dry adiabatic lapse rate. As a result, the potential temperature field was constant everywhere initially. Accordingly, larger downslope velocities were expected since the effect of decreasing stratification is to accelerate the drainage flow. The stratification within a valley can range from near adiabatic at sunset, when drainage flows begin, to many degrees per kilometer as cool air pools within the valley. This neutral run required only 663 seconds of CPU time to reach 2000 seconds of model time.

In Run 6, uni-cellular flow was maintained out to 2000 seconds, but some indication was evident of the usual counterclockwise cell above the valley floor. The rate of intensification of the streamfunction center with time is plotted in Figure 4.14, along with the maximum downslope wind predicted. After about 1600 seconds, the extreme streamfunction value tended to decrease slightly. Downslope speeds of 0.9 m s^{-1} were obtained during this period. Up to about 800 seconds, the predicted maximum slope wind in this neutral case did not differ greatly from those of the standard run. By 1000 seconds, however, the winds for Run 6 were about 25 percent greater than for Run 1. The trajectory of the streamline center showed some tendency to move away from the slope at an earlier time than in the standard run. From 1000 to 2000 seconds, little movement of the center

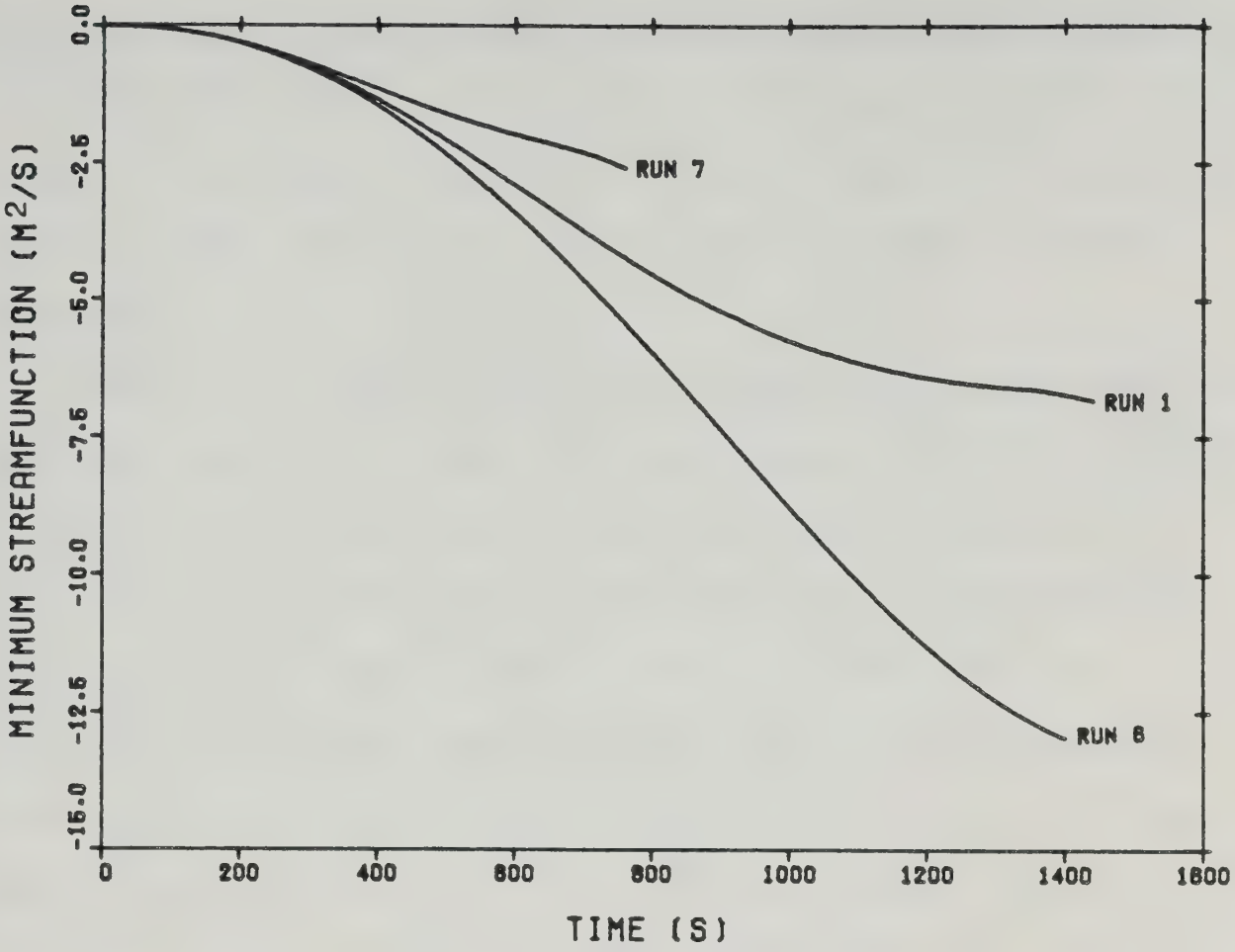


Figure 4.14a Minimum streamfunction versus time for the standard run (Run 1) and for Runs 6 and 7

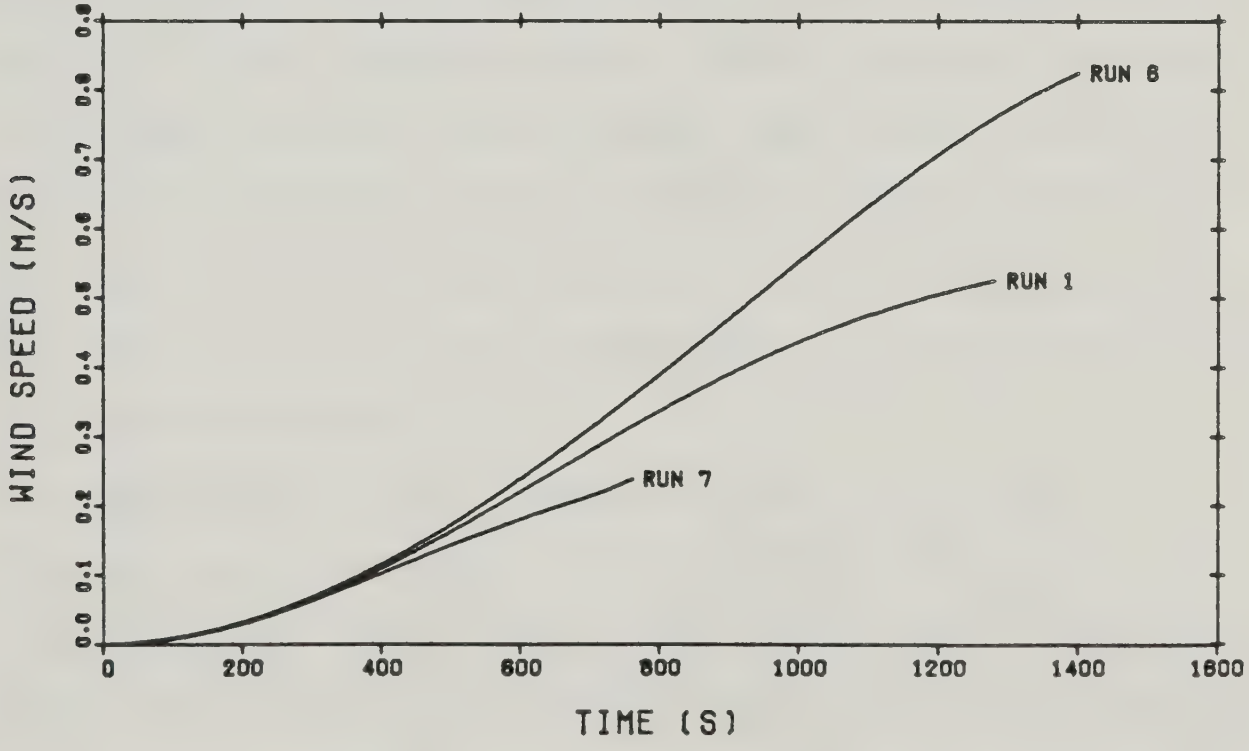


Figure 4.14b Maximum surface downslope wind speed versus time for the standard run (Run 1) and for Runs 6 and 7

occurred. Since, from Figure 4.14, the magnitude of the streamfunction center continued to increase, at least out to about 1600 seconds, increases in the vertical streamfunction gradient (and, therefore, the horizontal velocity) were substantial.

Table 4.6 gives the relative magnitudes of the various processes acting to alter the temperatures, valid at a grid point which is located 4 m above the slope (compare with Table 4.3 for Run 1). Horizontal advection of temperature was negative and approximately equalled that for Run 1 up to 700 seconds or so as the gradients and velocities involved were about the same just above the surface. Later, stronger velocities produced more cooling by horizontal advection, relative to Run 1. Vertical temperature advection was positive at this grid location in both cases, but was smaller in the neutral case due to the small temperature gradients. Total advection was a cooling process and acted in the same direction as diffusion. Due to the smaller temperature gradients in the horizontal and the vertical, both components of diffusion were smaller in the neutral case than in the initially stable one. Slightly faster cooling resulted overall.

Differences in the temperature profiles in the mid-slope region were small out to 800 seconds or so. Slightly larger cooling amounts were found near the ground. Aloft, less cooling was predicted in the neutral run as the temperature gradients there were quite small. Along the

Table 4.6 Contributions to $\partial\theta/\partial t$ from advection and diffusion just above mid-slope (J=8,K=7) for Run 6 at 200 second intervals

t	v	w	$-v\frac{\partial\theta}{\partial y}$	$-w\frac{\partial\theta}{\partial z}$	ADV.	$K_y\frac{\partial^2\theta}{\partial y^2}$	$K_z\frac{\partial^2\theta}{\partial z^2}$	DIF.	TOTAL
(s)	(m/s)	(m/s)	($^\circ$K/s)	($^\circ$K/s)	($^\circ$K/s)	($^\circ$K/s)	($^\circ$K/s)	($^\circ$K/s)	($^\circ$K/s)
0	0	0	0	0	0	0	0	0	0
200	-.023	-.002	-2×10^{-5}	$+1\times10^{-5}$	-1×10^{-5}	-4×10^{-6}	-5×10^{-4}	-5×10^{-4}	-5×10^{-4}
400	-.092	-.009	-1×10^{-4}	$+9\times10^{-5}$	-1×10^{-5}	-4×10^{-6}	-5×10^{-4}	-5×10^{-4}	-5×10^{-4}
600	-.198	-.020	-3×10^{-4}	$+2\times10^{-4}$	-1×10^{-4}	-5×10^{-6}	-5×10^{-4}	-5×10^{-4}	-6×10^{-4}
800	-.330	-.033	-6×10^{-4}	$+5\times10^{-4}$	-1×10^{-4}	-6×10^{-6}	-5×10^{-4}	-5×10^{-4}	-6×10^{-4}
1000	-.473	-.047	-9×10^{-4}	$+8\times10^{-4}$	-1×10^{-4}	-6×10^{-6}	-5×10^{-4}	-5×10^{-4}	-6×10^{-4}
1200	-.607	-.061	-1×10^{-3}	$+1\times10^{-3}$	-1×10^{-4}	-9×10^{-6}	-4×10^{-4}	-4×10^{-4}	-5×10^{-4}
1400	-.707	-.070	-2×10^{-3}	$+1\times10^{-3}$	-1×10^{-4}	-1×10^{-5}	-4×10^{-4}	-4×10^{-4}	-5×10^{-4}
1600	-.761	-.075	-2×10^{-3}	$+2\times10^{-3}$	-1×10^{-4}	-1×10^{-5}	-4×10^{-4}	-4×10^{-4}	-5×10^{-4}
1800	-.777	-.076	-2×10^{-3}	$+2\times10^{-3}$	-1×10^{-4}	-2×10^{-5}	-4×10^{-4}	-4×10^{-4}	-5×10^{-4}
2000	-.770	-.075	-2×10^{-3}	$+2\times10^{-3}$	-1×10^{-4}	-2×10^{-5}	-4×10^{-4}	-4×10^{-4}	-5×10^{-4}

trough boundary, much reduced cooling was found aloft, relative to the standard run, as well, even though the vertical wind speed was substantially larger.

4.7.3 More Stable Case Initially - Run 7

Another model integration, this time under extremely stable conditions, was performed. The lapse rate used initially was -0.04 C° m^{-1}, creating very large vertical potential temperature gradients of about 0.05 C° m^{-1}. In this run, however, a counterclockwise cell developed above the valley floor as in other runs after only 620 seconds, due to the large amounts of cooling there through vertical advection. Useful examination of the results can be made out as far as this time, at least. The evolution of the minimum streamfunction value, shown in Figure 4.14, shows clearly that the stability has acted to retard the development of the downslope flow (given that the streamline centers were located close together). After 600 seconds, for example, the maximum horizontal wind speed at the sloping surface was 0.24, 0.22, and 0.18 m s^{-1} for the runs with initial lapse rates of 0.01 C° m^{-1} (Run 6), -0.004 C° m^{-1} (Run 1), and -0.04 C° m^{-1} (Run 7), respectively.

Horizontal advection close to the ground was negative and slightly smaller than for the less stable run (Run 1) as a result of the somewhat lower wind speeds predicted in Run 7. Vertical advection, on the other hand, was much greater than for the less stable case and warm advection was the

overall effect. Changes through diffusion were negative and generally somewhat larger than in the standard run due to the larger gradients involved. Overall, cooling slightly above the surface was smaller in Run 7, mainly as a result of the higher rates of warm air advection.

The variation in vertical temperature gradient with time illustrates the differences in cooling amounts with height in different parts of the valley. Table 4.7 gives the vertical potential temperature gradient at three different valley locations (trough, mid-slope, and ridge) based on the temperatures at the ground and 32 m above. Results for each of the three initial stability regimes considered in this study are cited. In all cases, the inversion was strongest along the ridge boundary where warming by subsidence occurred aloft and cooling through diffusion near the ground were the dominant factors. Along the trough boundary, cooling occurred both near the surface and, to a lesser extent, further away. This caused some increase in the vertical temperature gradient with time, although it was not as large as that above the ridge.

4.8 Comparison with Observations - Run 8 and others

The results presented in this section are included in order to compare and contrast the predicted values and the observed. Various initial and boundary conditions were utilized, in accordance with the observations. Model verification was difficult since the total length of time of

Table 4.7 Vertical potential temperature gradients (based on surface temperatures and that 32 m above) under different lapse conditions for various locations in the valley

TROUGH				
Initial lapse rate (C^{o}/m)	t=0s	t=200s	t=400s	t=600s
+0.010 (Run 6)	0	+.0033	+.0061	+.0082
-0.004 (Run 1)	+.0140	+.0173	+.0198	+.0211
-0.040 (Run 7)	+.0508	+.0540	+.0558	+.0565
MID-SLOPE				
Initial lapse rate (C^{o}/m)	t=0s	t=200s	t=400s	t=600s
+0.010 (Run 6)	0	+.0033	+.0062	+.0085
-0.004 (Run 1)	+.0140	+.0173	+.0202	+.0225
-0.040 (Run 7)	+.0508	+.0541	+.0568	+.0587
RIDGE				
Initial lapse rate (C^{o}/m)	t=0s	t=200s	t=400s	t=600s
+0.010 (Run 6)	0	+.0033	+.0063	+.0090
-0.004 (Run 1)	+.0140	+.0174	+.0208	+.0243
-0.040 (Run 7)	+.0508	+.0544	+.0584	+.0628

integration was quite limited. As well, the data base was somewhat sparse, in terms of the location and numbers of observing stations (typically, three were available - both valley rims, plus profiles above some mid-slope region). However, some useful comments can be made.

The observed temperature and wind speed profile variations were used to determine the numerical values of the many constants involved in the model. For example, the evolution of the hourly mean temperatures observed at the Dawson Bridge site was used to extract surface cooling rates. These screen temperatures, obtained at 1.2 m above the ground at the rim and mid-slope regions, are shown in Figure 4.15 for three experimental days in 1978. The earlier onset of cooling along the slope, compared to the rim, is very evident. All seemed to indicate nearly constant cooling rates of 2 - 2.5 C° per hour.

During most observational evenings, the flux Richardson number quickly exceeded its critical limit. As discussed in Section 2 of Chapter 2, this brings about total suppression of turbulent exchange in the vertical. As a result, $(K_m)_z$ was set to zero throughout these final model integrations. Initially, while still under neutral conditions, such exchange could be significant just as the surface-based inversion is forming. In spite of this, a constant value was used during the whole period. The vertical exchange of heat through turbulence was effectively zero at most times as well. However, a non-zero K_T was used here in order to

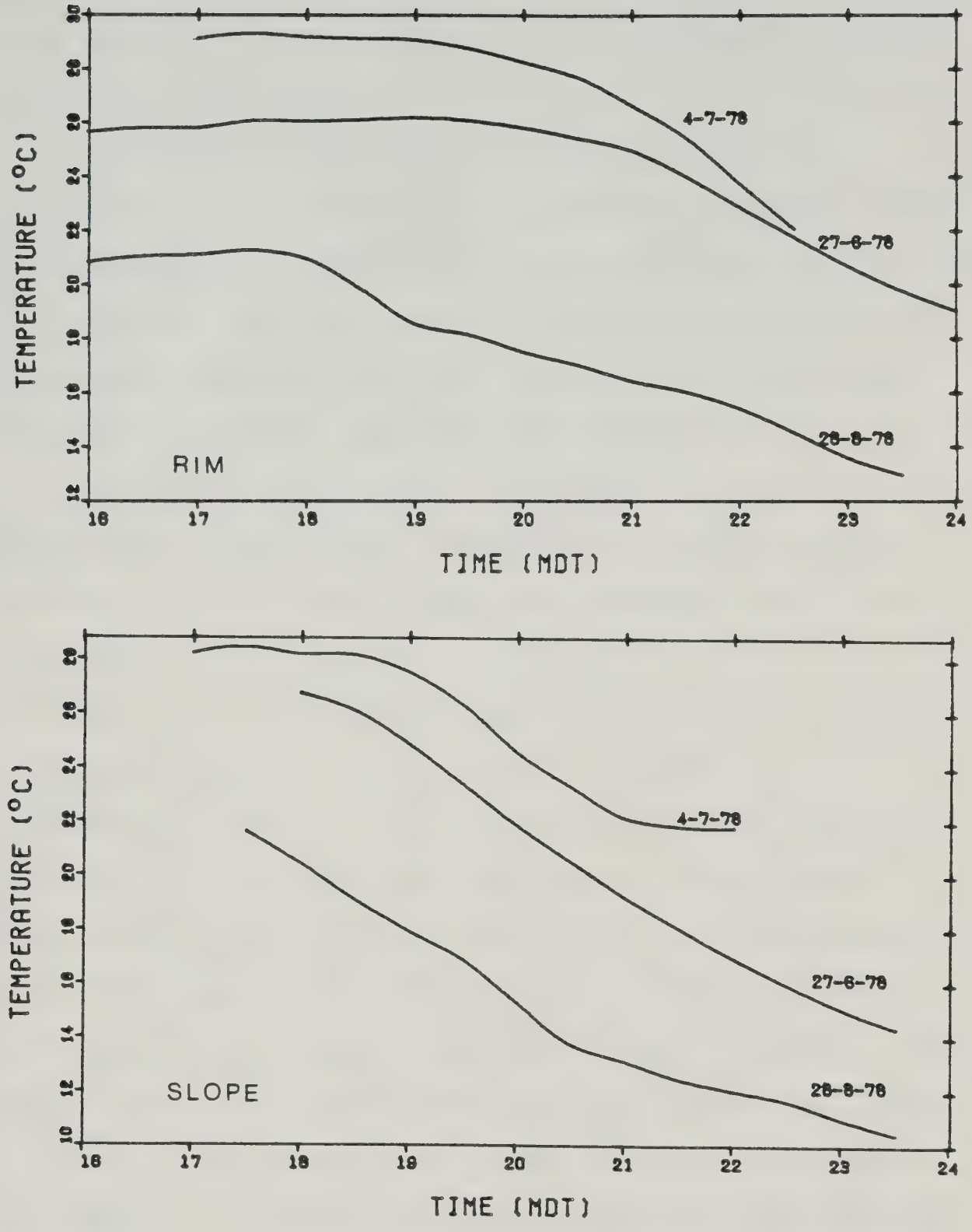


Figure 4.15 Observed evolution of screen temperatures (1.2 m above ground) for three experiments in 1978 at the Dawson Bridge site at (a.) east rim and (b.) east slope

simulate radiative exchange processes as outlined in Section 6 of Chapter 2. A value of 0.1 $m^2\ s^{-1}$, estimated by Brunt (1934), was used for K_R.

A preliminary investigation into the effect of eliminating vertical diffusion of momentum was made through a model integration having all parameters equal to those of Run 6, except that $(K_m)_z$ was zero. Relative differences in the minimum streamfunction and maximum surface downslope wind speed of about 10 per cent were found after 800 seconds of integration time. This was the hoped for result since reasonable wind speeds and temperature changes had been obtained in Run 6, using a vertical exchange coefficient of 1.0 $m^2\ s^{-1}$.

Finally, one integration was performed using the most appropriate values of $(K_m)_y = (K_T)_y = 1.0\ m^2\ s^{-1}$, $(K_m)_z = (K_T)_z = 0.0$, $K_R = 0.1\ m^2\ s^{-1}$ and a constant cooling rate of 2.5 C° per hour. This run was initiated under neutral stability conditions and a valley trough temperature of 297.6 °K, and is denoted as Run 8. A counterclockwise cell developed high above the valley floor after about 1450 seconds, as in the other runs. For this reason, the amount of cooling predicted after only 1200 seconds (20 minutes) was compared with that observed over similar time periods. The reduction in the vertical heat transfer coefficient, $((K_T)_z + K_R)$, resulted in small amounts of cooling away from the surface. At the location of the mid-slope station, a temperature profile was obtained on three dates in 1978 at

heights of up to 15 m, depending on the particular experiment. Based on the hourly mean temperatures, cooling amounts measured over the early evening hours from 1900 - 2100 MDT were computed. Assuming the cooling to be distributed uniformly over this period, one can derive the approximate amount of cooling in 1200 seconds for comparison with the model predictions. Figure 4.16 illustrates these observed mean cooling amounts at different heights along with that predicted in Run 8 above the mid-slope region. Clearly, the agreement is quite good.

At later times, after 2100 MDT, the amount of cooling was observed to decrease at higher levels, perhaps in rsponse to effective mixing by the downslope wind. This is evident in the valley model results when the cooling amount predicted at some height above the ground is examined as a function of time. For example, the temperature change predicted 8 m above the mid-slope region is 0.015, 0.047, 0.072, 0.090, 0.096, 0.083, 0.074 C° per 200 seconds based on total change over successive 200 second intervals. However, integration was not feasible much beyond 1200 seconds.

In accordance with the cooling being slowly transferred upwards, the downslope flow was confined to a relatively thin layer, compared to most other runs. However, due to the large horizontal temperature gradients close to the ground, considerably larger surface downslope wind speeds were predicted (with values up to about 0.9 m s^{-1} after 1200

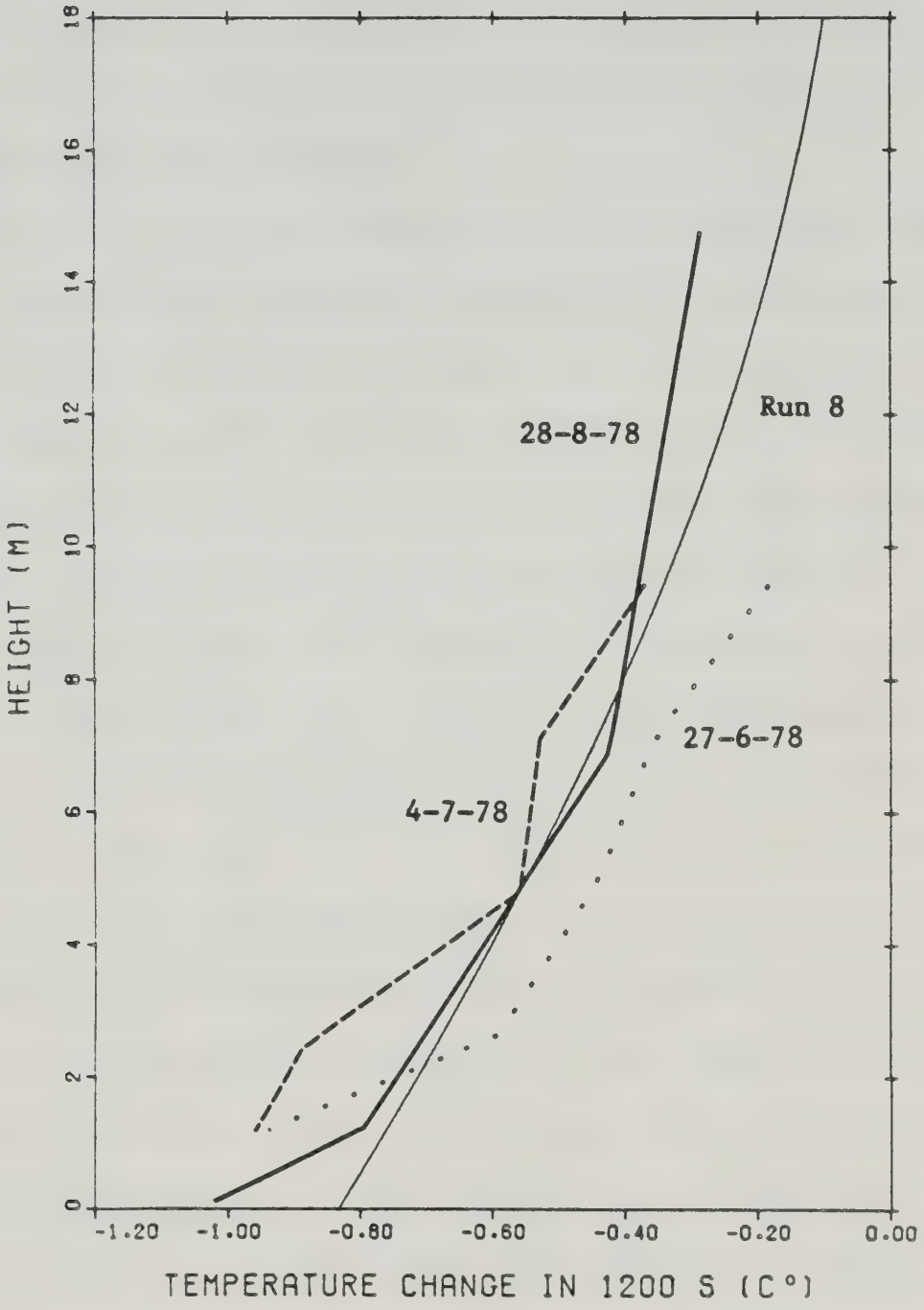


Figure 4.16 Observed cooling amounts versus height in 1200 seconds (mean values) and that predicted by the valley model in Run 8

seconds). It is believed that the earlier development of strong winds accounted for the existence of a counterclockwise cell above the trough through large amounts of adiabatic cooling there and the positive horizontal temperature gradient thus created.

The profile of the horizontal wind component predicted in Run 8 above the mid-slope region is illustrated in Figure 4.17 (negative values are plotted for flow directed from the valley ridge towards the trough). The depth of the downslope flow increased slightly as the wind speeds themselves developed. Maximum speeds were predicted to occur at the ground surface, under the 'free-slip' boundary conditions imposed in this model. As well, the flow developed rather quickly. Comparison with the mean observed wind shear from the valley experiments is provided in Figure 4.18. Periods during which R_f was supercritical were chosen since there would be little downward transfer of momentum from a prevailing wind aloft during such times. The slope wind was measured at a height of 0.8 m using a very sensitive Gill propeller anemometer. At heights of 1.7, 3.84, and 5.84 m, however, Rimco cup anemometers were used to measure the horizontal wind speed and these had a stall speed of about 0.25 m s^{-1}. For this reason, only 30 minute intervals with average wind speeds above this threshold were used. On the two evenings considered, June 27 and July 4, 1978, mean maximum speeds of 0.73 and 0.57 m s^{-1}, respectively, were found at the lowest level of measurement. The predicted

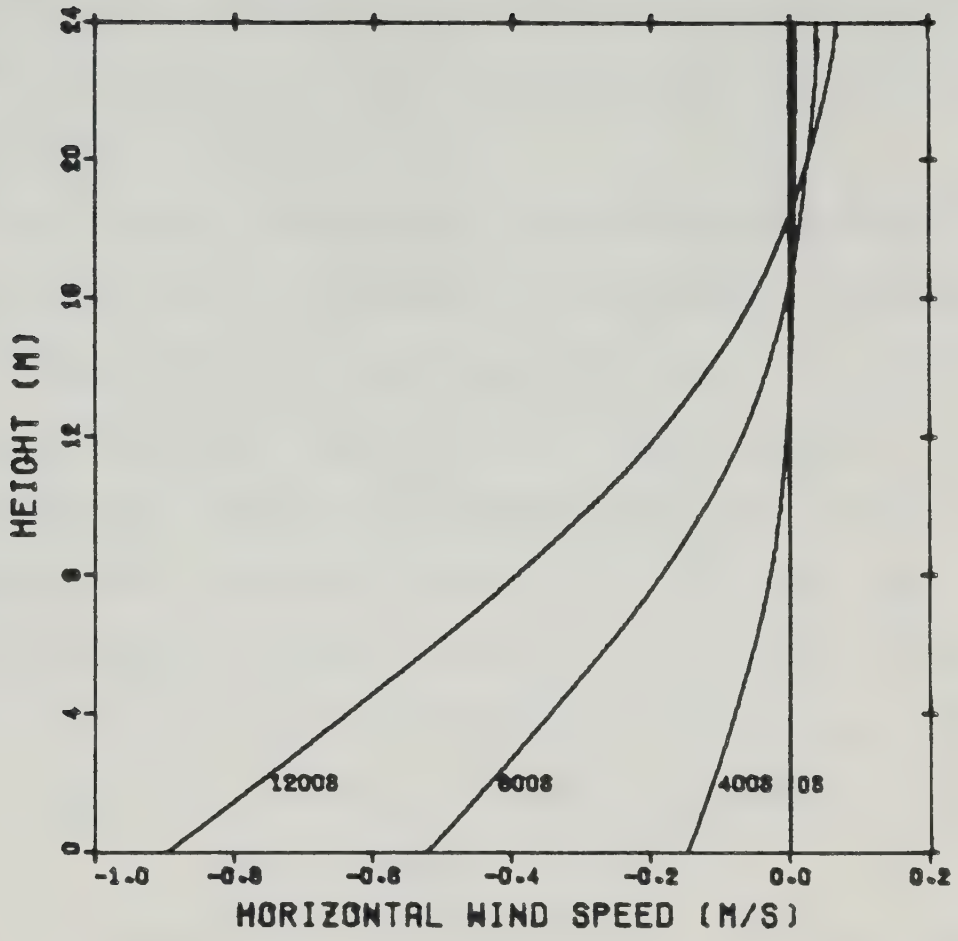


Figure 4.17 Horizontal velocity component versus height predicted by valley model in Run 8 out to 1200 seconds

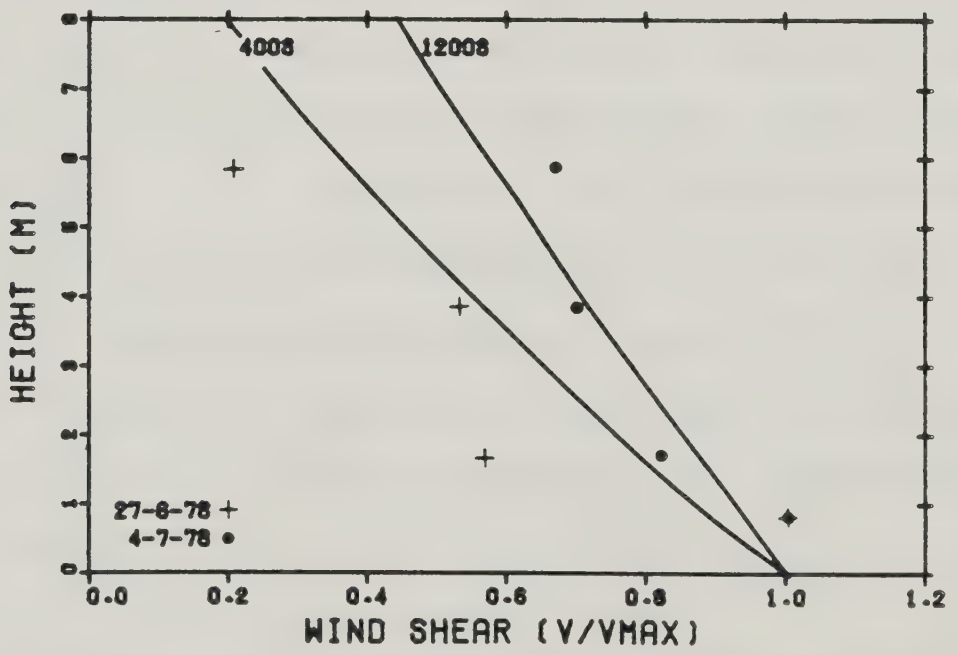


Figure 4.18 Observed wind shear and that predicted by valley model in Run 8 at 400 and 1200 seconds

shear above the slope region, which is very close to that predicted at the bottom of the slope where the observations were made, agrees quite well with the limited observations shown in Figure 4.18.

A final model integration was performed using (2.6.4), the surface cooling rate based on radiational losses. A net radiation loss per unit area per unit time, R_N, of 40 W m^{-2} was used. A vertical heat transfer coefficient of 1.0 m^2 s^{-1} was implemented in order to include some diffusional and some radiational exchange, with K_R = 0.3 m^2 s^{-1} as determined empirically by Anfossi et al. (1976). With these and other typical atmospheric values substituted into (2.6.4), the surface cooling rate was specified to be

$$T(0,t) = T(0,0) - 0.075\ t^{\frac{1}{2}}$$

where t is in seconds, and T(z,t) is in °C. This curve is plotted in Figure 4.19 out to 1200 seconds, along with the cooling produced with the constant cooling rate of 2.5 C° per hour specified in Run 8. Evidently, sizeable cooling is specified by (2.6.4) at early integration times although it falls off as $t^{0.5}$. In response to this large enforced cooling rate initially, rapid development of the circulation resulted in downslope wind speeds of about 1.5 m s^{-1} after only 600 seconds of integration time. Shortly after this, at about 760 seconds, a counterclockwise cell formed above the valley trough.

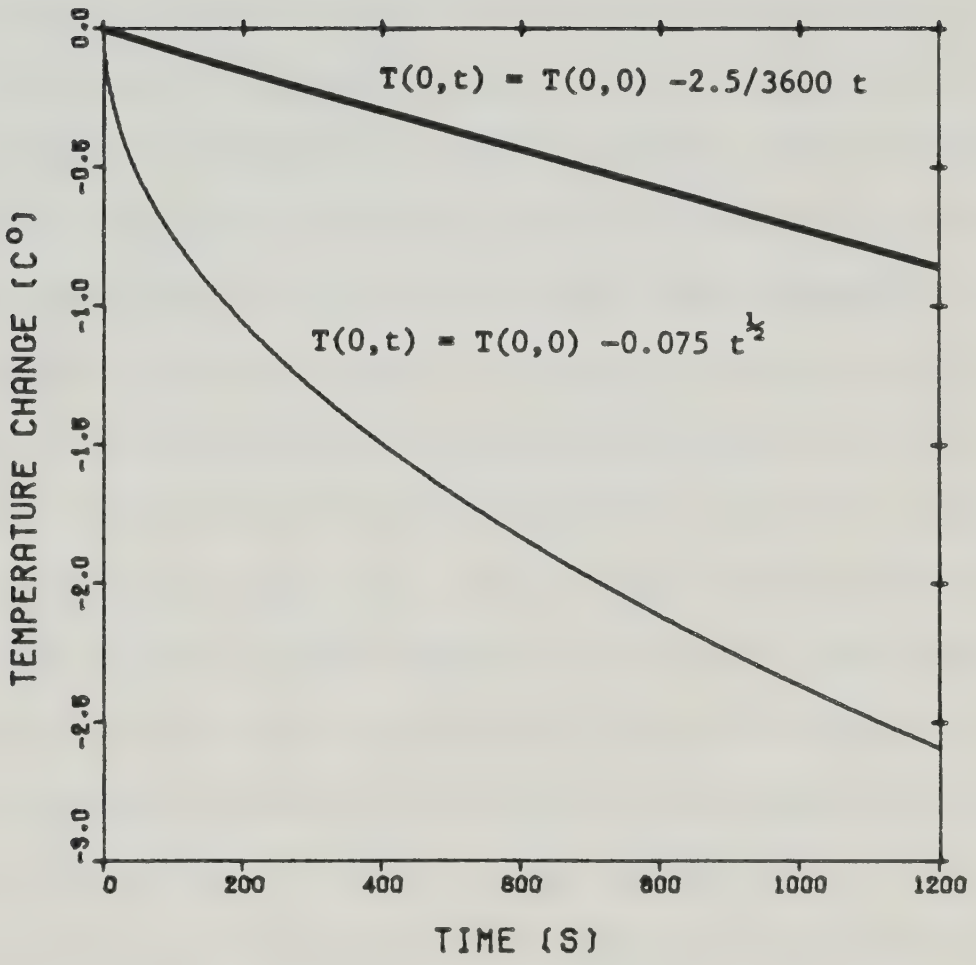


Figure 4.19 Two boundary conditions used to specify the surface temperature fields

Chapter 5

SUMMARY AND CONCLUSIONS

5.1 Summary

A two-dimensional finite-difference grid model has been developed in order to simulate the observed downslope circulation found to exist within the North Saskatchewan River valley. Some simplifications of the equations of motion were made, including neglect of Coriolis force, use of K-theory to describe turbulent motions, and two-dimensional flow in a vertical cross-section of the valley. The assumption of incompressible non-divergent flow permitted the use of streamfunction fields which are easily related to the valley components themselves. The thermodynamic equation, coupled with the vorticity equation, was solved numerically to predict the velocity and temperature at each grid point.

Downslope winds are produced in direct response to horizontal pressure gradients created through specified cooling rates at the ground. Radiative heat transfer was approximated in the thermodynamic equation as a diffusion process, with a radiative diffusivity, K_R. This followed considerations involving long-wave absorption and re-emission by water vapour and was introduced by Brunt in the 1930's. Two means of stipulating the surface boundary conditions were used. First, constant surface cooling rates were simply applied, as observed within the valley under consideration. Secondly, the radiative heat transfer equation

was solved analytically to predict an equivalent rate of temperature change at the ground. As this is the driving force for the development of the valley circulation, the exact nature of the temporal variation of the ground temperature is most significant.

Much of the model development in this study dealt with the numerical aspects of the finite-difference formulations of the terms in the governing equations. Due to problems inherent in the Dufort-Frankel scheme, when applied to diffusion terms in equations possessing several types of terms, its use was finally abondoned in favour of a forward-time, centered-space formulation. Advective terms were handled by a forward-time, upstream-space configuration. Solution of the elliptic partial differential equation relating streamfunction to vorticity was obtained using Liebmann sequential relaxation. This procedure consumed most of the CPU requirements.

Each integration was initiated with the atmosphere at rest. As a result, turbulent diffusion and radiation processes dominated in the early stages of each run. As the circulation developed, advection became increasingly important, depending upon the particular application. For example, one run with $(K_m)_z = (K_T)_z = 1.0$ m^2 s^{-1}predicted rates of change of temperature by advection and diffusion/radiation just above the slope of $+3 \times 10^{-4}$ and -8×10^{-4} C°/s, respectively, whereas another with $(K_m)_z = (K_T)_z = 0.01$ m^2 s^{-1} resulted in values of -3×10^{-4} and -1×10^{-4} C°/s at long

integration times (1200 seconds). This illustrated how advective and diffusive processes both strive to destroy any temperature anomalies present. When diffusive heat transfer is necessarily limited by the presence of marked stability, advective processes (whose magnitudes depend partially on gradients present) are proportionally increased.

The prediction of, or at least hint at the eventual development of, a counterclockwise flow high above the flat valley floor was evident in each integration. The timing of its appearance varied from run to run, however. This cell resulted from differences in vertical velocity (and thereby amounts of cooling through adiabatic expansion) at the same height across the valley, with a cooler area being produced close to the trough boundary. Through the solenoid term in the vorticity equation (which is proportional to the horizontal gradient in potential temperature), increasing vorticity was produced, and eventually positive vorticity values were attained in this region. A counterclockwise cell was the result. Under conditions of extreme stability, this phenomenom occurred quite early (after about 600 seconds), i.e. even very low vertical wind speeds combined with large vertical temperature gradients could produce a differential in cooling amounts at the same height at small integration times.

The sensitivity to the particular geometry of the valley cross-section being modelled was examined. In most runs, the upper boundary was located at a height of 108 m, close

to twice the valley depth. However, one integration with a lid at 144 m suggested that the evolution of the thermodynamic and flow fields was not very much affected, at least within the depth of the valley. As well, most integrations were performed within a cross-section which featured a flat valley bottom. When excluded, the flow was forced to rise sharply at the base of the slope and relatively higher vertical wind speeds resulted. In this case, the counterclockwise cell developed somewhat earlier. The conditions near the sloping surface and the rim were largely unaffected. One integration was executed with the sloping surface at an angle of 0.197 radians (compared with a usual value of 0.100 radians). In this case, downslope winds were up to 70 per cent higher, depending upon time of comparison. However, this difference was not maintained and, after 800 seconds, maximum surface slope winds of 0.37 m s^{-1} were predicted along the steeper slope whereas in the standard run, they were 0.34 m s^{-1}.

The magnitudes of the downslope wind speeds under a variety of initial stability regimes were investigated. As in other studies (both observational and modelling types), the development of the valley circulation was severely hindered in very stable situations. Detailed comparison with experimental data obtained within the North Saskatchewan River valley was difficult but generally good agreement was found in the low-level temperature profiles above the slope and in the magnitudes of the slope winds themselves. The exact time scale for the evolution of the valley wind and

temperature regimes is hard to ascertain. The observed wind reversal (decrease in speed with height) was predicted ; the model (under conditions of 'free-slip' at the lower boundary) produced maximum wind speeds coincident with the ground surface. Increased stability was brought about at the rim position, relative to the valley bottom, through subsidence.

5.2 Conclusions

The numerical model described some observed properties of the micrometeorology of the North Saskatchewan River valley. Although total integration times were only 10 - 20 minutes, useful conclusions regarding the development of the downslope flow can be made. Integrations were carried out by Thyer (1966) using a similar finite-difference representation of the equations over a simple 'V-shaped' region out to only 120 seconds. The advent of computational instability difficulties may have precluded longer integrations although this was not stated explicitly by the author. The inclusion of a flat valley bottom into the present model provides a more realistic simulation for applications to the North Saskatchewan River valley.

Investigations into the various possible numerical formulations of the terms in the governing equations led to the choice of forward-time, upstream-space for the advection terms and centered-time, centered-space for the solenoid

term in the vorticity equation. The appropriate selection of a scheme to approximate the diffusion terms was more difficult ; however, after applying several schemes to a simple one-dimensional diffusion equation, for which the analytical solution was derived, a two-level scheme in time proved desirable in this application. This resulted from the presence of other terms in the equations, which caused a disturbance in the computation of diffusive changes through altering the values at intermediate times.

Through variations in initial stabilities, surface cooling rates, and vertical transfer coefficients, the relative contributions of advection, diffusion, and radiation could be estimated under several regimes. Results from one integration, which was meant to simulate observed valley inversion conditions, clearly demonstrated the importance of radiative cooling processes close to the ground in the early stages of the slope wind development. At a location 4 m above the mid-slope region, for instance, radiational cooling was at least an order of magnitude larger than advectional cooling, at 200 seconds of integration time. Gradually, as the slope winds increased, changes in temperature due to advection increased. Horizontal advection acted to transport air away from the cooling surface, whereas vertical advection brought down warmer air from aloft. At all times, the net result was negative temperature advection although the differences in the magnitudes of these two terms were small. Eventually, after

1600 seconds of integration time, advective changes were about twice as large (-4×10^{-4} C° s^{-1}) as radiative or diffusive ones.

For comparison, the analytical solution to the one-dimensional vertical diffusion equation, using a diffusivity of 0.1 m^2 s^{-1} equal to that used in the above valley model integration, predicted a very similar low-level temperature profile. Therefore, when advection processes were not included, larger gradients resulted in increased radiative cooling and it seems evident that radiative heat transfer alone was effective in this application.

The model predicted quasi-steady-state conditions within about 20 minutes of integration time with development of downslope wind speeds of $\simeq$ 0.8 m s^{-1}. Both the predicted low-level temperature variations with height and the maximum slope winds agreed extremely well with the limited observations made within the North Saskathewan River valley in Edmonton.

5.3 Suggestions for Future Work

Due to the large amounts of computer run-time and storage costs, the number of model integrations was obviously restricted. Experimentation with various smaller and larger grid sizes was not feasible, and this may cast some uncertainty on the validity of the results. As the relaxation procedure appeared to consume the majority of the total cost for each integration, investigations into other

numerical or analytical methods of solving elliptic partial differential equations would prove extremely valuable. Even the Liebmann sequential relaxation technique used possesses various procedures by which the iteration process can be speeded up. For example, Haltiner (1971) indicated that convergence was more rapid over a N. Hemisphere grid when the sequence of points followed a pattern which began at the outer boundary and spiralled inwards. Similar strategies may have proven useful in this application. Also, the optimal over-relaxation coefficient may have varied from run to run.

The use of Fickian diffusion (i.e. constant in space and time) may be a major drawback in this study. The appropriate values of K_m and K_T are intimately related to the variations in the wind and temperature fields, and these continually evolve as the integration proceeds. Coefficients which depend on the local stability would be important in this application. In addition, transfer properties close to the lower surface are likely to be much different from those well above the ground. The incorporation of radiative transfer was initially considered to be beyond the scope of the study, but a simple approximation by a diffusion process permitted its ultimate inclusion.

Provision of an area of integration consisting of both slopes which define a given valley, using lower boundary conditions which simulate earlier shading on one slope than on the opposite one, would provide insight into the asymmetrical nature of the resultant flow. The

two-dimensional treatment of the problem may also be significant if the circulation predicted in this study were to be used as input into a pollutant transport model such as Rudolph (1980). In this case, a downvalley wind would create a helical trajectory with recirculation of pollutants possible if the source extended upvalley some distance.

REFERENCES

Ames, W. F., 1969: *Numerical Methods for Partial Differential Equations*, Barnes and Noble, Inc., New York, 291 pp.

Anfossi, D., P. Bacci, and A. Longhetto, 1976: Forecasting of Vertical Temperature Profiles in the Atmosphere during Nocturnal Radiation Inversions from Air Temperature Trend at Screen Height, *Quart. J. Roy. Meteor. Soc.*, 102, 173-180.

Batchelor, G. K., 1967: *An Introduction to Fluid Dynamics*, Cambridge University Press, Cambridge, 615 p.

Boyce, W. E. and R. C. di Prima, 1965: *Elementary Differential Equations and Boundary Value Problems*, John Wiley and Sons, Inc., New York, 533 p.

Brunt, D., 1934: *Physical and Dynamical Meteorology*, Cambridge University Press, Cambridge, 411 p.

Businger, J. A., 1973: Turbulent Transfer in the Atmospheric Boundary Layer, *Workshop on Micrometeorology*, D. A. Haugen, editor, American Meteorological Society, Boston, 101-149.

Defant, F., 1951: Local Winds, *Compendium of Meteorology*, T. M. Malone, editor, American Meteorological Society, Boston, 655-672.

di Cenzo, C. S., 1979: A Numerical Study of Temperature in an Urban Valley using a Radiative-Conductive Model, unpublished M. Sc. thesis, Department of Geography, U. of Alberta, Edmonton, Alberta, 159 p.

Estoque, M., 1963: A Numerical Model of the Atmospheric Boundary Layer, *J. Geophys. Res.*, 68, 1103-1113.

Fleagle, R. G., 1950: A Theory of Air Drainage, *J. Meteorol.*, 7, 3, 227-232.

Geiger, R., 1957: *The Climate near the Ground*, Oxford University Press, London, 611 p.

Hage, K. D., 1972: Nocturnal Temperatures in Edmonton, Alberta, *J. Appl. Met.*, 11, 2, 123-129.

Hage, K. D., 1979: *Air Pollution Study of the North Saskatchewan River Valley in Edmonton, Alberta*, Final Report under Research Proposal RS77-6 to the Research

Secretariat, Alberta Environment, Edmonton, 90 p.

Haltiner, G. J., 1971: *Numerical Weather Prediction*, John Wiley and Sons, Inc., Toronto, 317 p.

Haltiner, G. J. and R. T. Williams, 1980: *Numerical Prediction and Dynamic Meteorology*, John Wiley and Sons, Inc., Toronto, 477 p.

Klassen, W., 1962: *Micrometeorological Observations in the N. Saskatchewan River Valley*, Meteorological Branch, Canada Dept. of Transport, Cir - 3652, TEC - 408, 24 p.

Kozo, T. L., 1982: A Mathematical Model of Sea Breezes Along the Alaskan Beaufort Sea Coast : Part II, *J. Appl. Met.*, 21, 7, 906-924.

Malkus, J. S. and G. Witt, 1959: The Evolution of a Convective Element : A Numerical Calculation, *The Atmosphere and the Sea in Motion*, Rockefeller Institute Press, New York, 425-439.

McNider, R. T., 1982: A Note on Velocity Fluctuations in Drainage Flows, *J. Atmos. Sci.*, 39, 7, 1658-1660.

Mesinger, F. and A. Arakawa, 1976: *Numerical Methods used in Atmospheric Sciences*, WMO-ICSU Joint Organizing Committee, GARP Publication Series No. 17, V.1, 64 p.

Mitchell, A. R. and D. F. Griffiths, 1980: *The Finite-Difference Method in Partial Differential Equations*, John Wiley and Sons, Inc., Toronto, 272 p.

Molenkamp, C. R., 1968: Accuracy of Finite-Difference Methods Applied to the Advection Equation, *J. Appl. Met.*, 7, 160 -167.

Orszag, S. A., 1971: Notes and Correspondence - On the Elimination of Aliasing in Finite-Difference Schemes by Filtering High-Wavenumber Components, *J. Atmos. Sci.*, 28, 6, 1074.

Orville, H. D., 1964: On Mountain Upslope Winds, *J. Appl. Met.*, 21, 622-633.

Orville, H. D., 1965: A Numerical Study of the Initiation of Cumulus Clouds over Mountainous Terrain, *J. Atmos. Sci.*, 22, 684-699.

Orville, H. D., 1968: Ambient Wind Effects on the Initiation and Development of Cumulus Clouds over Mountains, *J. Atmos. Sci.*, 25, 385-403.

Paterson, R. D., 1978: A Micrometeorological Study of an

Urban Valley, unpublished M. Sc. thesis, Department of Geography, U. of Alberta, Edmonton, Alberta, 91 p.

Petkovsek, Z. and A. Hocevar, 1971: Night Drainage Winds, *Arch. Met. Geoph. Bioklim.*, Ser. A, **20**, 353-360.

Pielke, R. A., 1974: A Three-Dimensional Numerical Model of the Sea Breezes over S. Florida, *Mon. Wea. Rev.*, **102**, 2, 115-139.

Potter, D. E., 1973: *Computational Physics*, John Wiley and Sons, Inc., Toronto, 304 p.

Rao, K. S. and H. F. Snodgrass, 1981: A Non-stationary Nocturnal Drainage Flow Model, *Boundary-Layer Meteor.*, **20**, 309-320.

Richtmyer, R. D. and K. W. Morton, 1957: *Difference Methods for Initial-Value Problems*, Interscience Publishers, New York, 405 p.

Rudolph, R. C., 1980: A Numerical Model of Pollutant Transport in a Small Urban Valley, unpublished M. Sc. thesis, Department of Geography, U. of Alberta, Edmonton, Alberta, 126 p.

Tang, W., 1976: Theoretical Study of Cross-Valley Wind Circulation, *Arch. Met. Geoph. Bioklim.*, Ser. A, **25**, 1-18.

Thyer, N. H., 1966: A Theoretical Explanation of Mountain and Valley Winds by a Numerical Method, *Arch. Met. Geoph. Bioklim.*, Ser. A, **15**, 318-348.

Tyson, P. D., 1968: Velocity Fluctuations in the Mountain Wind, *J. Atmos. Sci.*, **25**, 381-384.

APPENDIX A : STABILITY ANALYSIS FOR ADVECTION EQUATION

The forward-time, upstream-space finite-difference scheme is examined for stability when applied to a one-dimensional linear advection equation such as

$$\frac{\partial S}{\partial t} = -v \frac{\partial S}{\partial y} \quad , \; v > 0 \quad . \tag{A.1}$$

The von Neumann or Fourier Series method is most often used, according to Mesinger and Arakawa (1976). Letting $S(y=J\Delta y, t=n\Delta t) = S(J,n)$, (A.1) can be written using finite-differences as

$$\frac{S(J,n+1) - S(J,n)}{\Delta t} = -v \left\{ \frac{S(J,n) - S(J-1,n)}{\Delta y} \right\} \quad , \; v > 0 \quad ,$$

or $$S(J,n+1) = (1-\mu)\, S(J,n) + \mu\, S(J-1,n) \quad , \; v > 0 \quad , \tag{A.2}$$

where $\mu = v\, \Delta t/\Delta y$.

Substituting a solution of the form

$$S(J,n) = S(0,n) \exp(i\beta J \Delta y) \quad , \tag{A.3}$$

one obtains $$S(0,n+1) = (1-\mu)\, S(0,n) + \mu\, S(0,n) \exp(-i\beta\Delta y) \quad . \tag{A.4}$$

An amplification factor, λ, is defined such that

$$S(0,n+1) = |\lambda|\, S(0,n) \quad . \tag{A.5}$$

The von Neumann criterion for stability can be stated as

$$|\lambda| \leq 1 \quad . \tag{A.6}$$

Substitution of (A.5) into (A.4), and simplification, yields

$$\lambda = 1 - \mu + \mu \exp(-i\beta\Delta y)$$

$$|\lambda|^2 = (1 - \mu + \mu \cos(\beta\Delta y))^2 + (-\mu \sin(\beta\Delta y))^2$$

$$|\lambda|^2 = 1 - 2\mu(1 - \mu)\ (1 - \cos(\beta\Delta y)) \quad . \qquad (A.7)$$

Thus, von Neumann's criterion for stability becomes, from (A.6),

$$1 - 2\mu(1 - \mu)\ (1 - \cos(\beta\Delta y)) \leq 1 \quad . \qquad (A.8)$$

Since $\mu > 0$ and $1-\cos(\beta\Delta y) > 0$, (A.8) becomes simply

$$\mu = v \frac{\Delta t}{\Delta y} \leq 1 \quad . \qquad (A.9)$$

This is the well-known Courant-Friedrichs-Lewy (C.F.L.) criterion.

The von Neumann method of examining stability based on Fourier Series, is valid only if the coefficient of the difference equation (v in (A.1)) is constant. The method can be applied locally if the difference equation has a variable coefficient. Mitchell and Griffiths (1980) cite that there is much numerical evidence to support the contention that a method will be stable if the von Neumann condition is satisfied at every point of the field, even if derived as though the coefficients were constant.

To obtain further information on the behavior of the numerical solution, (A.8) can be examined in more detail. A sketch of $|\lambda|^2$ versus μ for various wave numbers is given in Figure A.1. Within the stable region ($|\lambda|^2 \leq 1$), this scheme

is damping for all values of $\mu < 1$ and the amount of damping depends on the wavelength. In this derivation, however, the true solution has a constant amplitude - this indicates some type of error due to the finite-difference representation. These problems should be kept in mind when the results in Chapter 4 are considered.

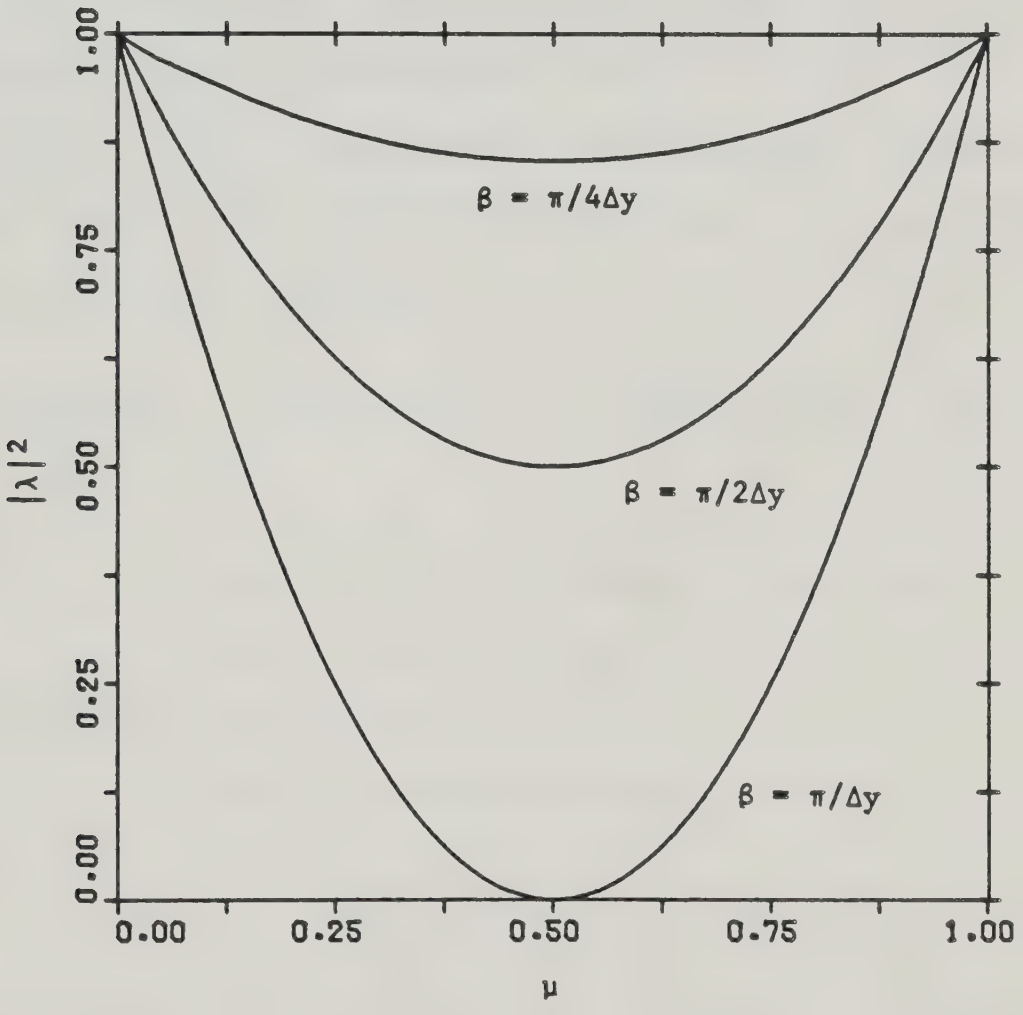


Figure A.1 Amplification factor versus μ using forward-time, upstream-space scheme applied to advection equation

APPENDIX B - STABILITY ANALYSIS FOR DIFFUSION EQUATION

The Dufort-Frankel finite-difference scheme is first examined for stability when applied to a one-dimensional linear diffusion equation such as

$$\frac{\partial S}{\partial t} = K \frac{\partial^2 S}{\partial y^2} \quad . \tag{B.1}$$

The von Neumann method of stability analysis is applied, using the same notation as in Appendix A, as given in an exercise in Mitchell and Griffiths (1980). (B.1) can be written in finite-difference form as

$$S(J,n+1)\ (1 + 2r) = 2r\ \{S(J+1,n) + S(J-1,n)\} + (1 - 2r)\ S(J,n-1) \tag{B.2}$$

where $r = K\ \Delta t/\Delta y^2$. Rewriting this as a two-level system, in vector form, one obtains

$$\begin{bmatrix} S(J,n+1) \\ T(J,n+1) \end{bmatrix} = \begin{bmatrix} (2r/(1+2r))\ D & (1-2r)/(1+2r) \\ 1 & 0 \end{bmatrix} \begin{bmatrix} S(J,n) \\ T(J,n) \end{bmatrix} \tag{B.3}$$

where D = centered difference operator such that

$$D\ S(J,n) = S(J+1,n) - S(J-1,n) \quad .$$

Substituting a solution of the form

$$U(J,n) = U(0,n)\ \exp(i\beta J\Delta y) \quad , \tag{B.4}$$

where

$$U = \begin{bmatrix} S \\ T \end{bmatrix}$$

and rewriting the result gives

$$U(0,n+1) = \underbrace{\begin{bmatrix} (4r/(1+2r))\ \cos(\beta\Delta y) & (1-2r)/(1+2r) \\ 1 & 0 \end{bmatrix}}_{\text{amplification matrix}} U(0,n) \tag{B.5}$$

The eigenvalues, λ_i, of the amplification matrix above satisfy $|A - \lambda I| = 0$ and are found to be such that

$$\lambda_i^2 - \frac{4r \cos(\beta\Delta y)\, \lambda_i}{1+2r} - \frac{(1-2r)}{1+2r} = 0 \quad .$$

Solving this quadratic in λ_i, one obtains

$$\lambda_{1,2} = \frac{2r \cos(\beta\Delta y) \pm (-4r^2 \sin(\beta\Delta y) + 1)^{\frac{1}{2}}}{1+2r} \quad . \tag{B.6}$$

The von Neumann necessary condition for stability of a two-level system is

$$\max |\lambda_i| \leq 1 \tag{B.7}$$

From (B.6), the maximum value of λ_1 or λ_2 is seen, by inspection, to satisfy (B.7) for all values of $r = K\,\Delta t/\Delta y^2$. Thus, the Dufort-Frankel scheme is unconditionally stable.

The forward-time, centered-space scheme will be examined in terms of stability also using the von Neumann method. This scheme, applied to (B.1), can be expressed as

$$S(J,n+1) = (1-2r)\, S(J,n) + r\{S(J-1,n) + S(J+1,n)\} \tag{B.8}$$

where $r = K\,\Delta t/\Delta y^2$ as before. Substitution of a solution of the form

$$S(J,n) = S(0,n) \exp(i\beta J\Delta y) \tag{A.3}$$

results in, after simplification,

$$S(0,n+1) = S(0,n)\, \{(1-2r) + r \exp(-i\beta\Delta y) + \exp(i\beta\Delta y)\} \tag{A.4}$$

Using the definition of an amplification factor given by (A.5), yields $\lambda = 1 - 2r + r\{\exp(-i\beta\Delta y) + \exp(i\beta\Delta y)\}$

According to (A.6), numerical stability results in

$$|\lambda| = |1 - 4r \sin^2(\beta\Delta y/2)| \leq 1 \quad .$$

By inspection, this occurs with $0 \leq r \leq 1/(2 \sin^2(\beta \Delta y))$ which leads to the stability condition

$$r = \frac{K \Delta t}{\Delta y^2} \leq \frac{1}{2} \tag{B.9}$$

APPENDIX C - ANALYTICAL SOLUTION TO ONE-DIMENSIONAL DIFFUSION EQUATION

In this appendix, an analytical solution to the one-dimensional heat diffusion equation defined by

$$\frac{\partial \theta}{\partial t} = K \frac{\partial^2 \theta}{\partial z^2}, \quad 0 \leq z \leq H, \; t > 0 \quad , \tag{3.5.1}$$

is derived, subject to the following boundary conditions.

$$\theta(H,t) = T, \; t > 0 \quad , \tag{3.5.2}$$

$$\theta(0,t) = \theta(0,0) - \alpha t, \; t > 0 \quad , \tag{3.5.3}$$

and initial conditions

$$\theta(z,0) = (T - \theta(0,0))\, z/H + \theta(0,0), \; 0 \leq z \leq H \quad . \tag{3.5.5}$$

Following the methods for solving partial differential equations with non-homogeneous boundary conditions suggested in Boyce and di Prima (1965), the following transformation is made :

$$A(z,t) = \theta(z,t) - B(z,t) \tag{C.1}$$

The differential equation, (3.5.1), in terms of A and B is now

$$\frac{\partial A}{\partial t} + \frac{\partial B}{\partial t} - K \frac{\partial^2 A}{\partial z^2} - K \frac{\partial^2 B}{\partial z^2} = 0, \; 0 \leq z \leq H, \; t > 0 \quad , \tag{C.2}$$

and the boundary conditions, (3.5.2) and (3.5.3), are now

$$A(H,t) + B(H,t) = T, \; t > 0 \quad , \tag{C.3}$$

$$A(0,t) + B(0,t) = \theta(0,0) - \alpha t, \; t > 0 \quad . \tag{C.4}$$

The initial conditions, (3.5.5), become under this transformation

$$A(z,0) + B(z,0) = (T - \theta(0,0))z/H + \theta(0,0), \; 0 \leq z \leq H \quad . \tag{C.5}$$

It is now required to find some $B(z,t)$ such that $B(H,t) = T$ and $B(0,t) = \theta(0,0) - \alpha t$ in order that the boundary conditions, (C.3) and (C.4), become homogeneous. By inspection, this can be accomplished if we set

$$B(z,t) = (\theta(0,0) - \alpha t)\,(1 - z/H) + zT/H \quad . \tag{C.6}$$

With this choice of $B(z,t)$,

$$\frac{\partial B}{\partial t} = -\alpha(1 - z/H) \quad ,$$

$$K\frac{\partial^2 B}{\partial z^2} = 0 \quad ,$$

and so (C.2) becomes

$$\frac{\partial A}{\partial t} - K\frac{\partial^2 A}{\partial z^2} = \alpha(1 - z/H) = q(z),\ 0 \leq z \leq H,\ t > 0 \quad , \tag{C.7}$$

and as well, the boundary and initial conditions ((C.3), (C.4), and (C.5), respectively) become

$$A(H,t) = 0,\ t > 0 \quad , \tag{C.8}$$

$$A(0,t) = 0,\ t > 0 \quad , \tag{C.9}$$

$$A(z,0) = 0,\ 0 \leq z \leq H \quad . \tag{C.10}$$

Note that the above boundary conditions are now homogeneous as desired. However, the differential equation, (C.7), has become non-homogeneous. A second transformation is therefore required :

$$C(z,t) = A(z,t) - D(z) \tag{C.11}$$

The differential equation, (C.2), can now be written as

$$\frac{\partial C}{\partial t} - K\frac{\partial^2 C}{\partial z^2} - K\frac{\partial^2 D}{\partial z^2} = q(z) \quad . \tag{C.12}$$

By setting

$$-K\frac{\partial^2 D}{\partial z^2} = q(z),\ 0 \leq z \leq H,\ t > 0 \quad , \tag{C.13}$$

equation (C.12) becomes homogeneous as required, with the corresponding boundary conditions

$$D(H) = 0 \quad , \tag{C.14}$$

$$D(0) = 0 \quad . \tag{C.15}$$

From (C.7), $q(z) = \alpha\ (1 - z/H)$, so (C.13) becomes

$$\frac{\partial^2 D}{\partial z^2} = \frac{\alpha}{K}\ (z/H - 1)\ ,\ 0 \leq z \leq H \quad . \tag{C.16}$$

The general solution to this, subject to (C.14) and (C.15), is

$$D(z) = \frac{\alpha}{K}\ \{z^3/6H - z^2/2 + Hz/3\} \quad . \tag{C.17}$$

found by integrating (C.16) and evaluating the constants of integration using the boundary conditions. Substituting this back into (C.12) results in a homogeneous equation in C(z,t) alone :

$$\frac{\partial C}{\partial t} - K\frac{\partial^2 C}{\partial z^2} = 0\ ,\ 0 \leq z \leq H,\ t > 0 \quad , \tag{C.18}$$

with boundary conditions of

$$C(H,t) = 0\ ,\ t > 0 \quad , \tag{C.19}$$

$$C(0,t) = 0\ ,\ t > 0 \quad , \tag{C.20}$$

and initial conditions of

$$C(z,0) = A(z,0) - D(z) = -\frac{\alpha}{K}\ \{z^3/6H - z^2/2 + zH/3\} = p(z) \tag{C.21}$$

$$0 \leq z \leq H \quad .$$

The general solution using separation of variables technique is found in any partial differential equations textbook, to be

$$C(z,t) = \sum_{n=1}^{\infty} b_n \exp(-n^2\pi^2 Kt/H^2) \sin(n\pi z/H) \ , \ 0 \leq z \leq H, \ t > 0 \quad (C.22)$$

where $$b_n = 2/H \int_0^H p(z) \sin(n\pi z/H) \, dz$$

$$= 2/H \int_0^H -\frac{\alpha}{K} \{z^3/6H - z^2/2 - zH/3\} \, dz$$

$$= - 2H^2\alpha/(n\pi)^3 K$$

Backtransforming twice to return to the original variable, $\theta(z,t)$, using (C.22), (C.17), (C.11), (C.6), and (C.1) gives the general solution to (3.5.1) to be

$$\theta(z,t) = \sum_{n=1}^{\infty} \{(-2H^2\alpha/(n\pi)^3 K) \exp(-n^2\pi^2 Kt/H^2) \sin(n\pi z/H)\}$$

$$+ \frac{\alpha}{K} (z^3/6H - z^2/2 - zH/3) + (\theta(0,0) - \alpha t) (1 - z/H) \quad (3.5.6)$$

$$+ zT/H, \qquad 0 \leq z \leq H, \ t > 0 \ .$$

APPENDIX D - SOURCE CODE FOR COMPUTER PROGRAM

The following source code was developed by the author for execution on the University of Alberta's AMDAHL 580/5860 computer, which operates under the Michigan Terminal System.

```
      IMPLICIT REAL*8(A - H,O - Z)
      DIMENSION THO(16,28), ZO(16,28), VO(16,28), WO(16,28), TH1(16,28),
     1          ,Z1(16,28), V1(16,28), W1(16,28), PHI(16,28), A1(16,28),
     2           A2(16,28), T(28), ZKM(16), TKM(16), A3(16,28),
     3           A4(16,28), A5(16,28), A6(16,28), FOR1(10), FOR2(10),
     4           ZKM2(16), TKM2(16)
      INTEGER TEND
      REAL*8 MAGNV, KHZ, KVZ, KHT, KVT
      COMMON TTOT, FOR1, FOR2, KL, JEND, JCOR, KEND, KMID, JJB
      COMMON /A/ KHZ, KVZ, KHT, KVT
C
C      THE FOLLOWING ARRAYS ARE DEFINED OVER THE VALLEY CROSS-SECTION
C      THO - POTENTIAL TEMPERATURE AT PREVIOUS TIME STEP
C      TH1 - POTENTIAL TMPERATURE AT PRESENT TIME STEP
C      ZO - VORTICITY AT PREVIOUS TIME STEP
C      Z1 - VORTICITY AT PRESENT TIME STEP
C      PHI - STREAMFUNCTION AT PRESENT TIME STEP
C      VO - CROSS-VALLEY WIND SPEED AT PREVIOUS TIME STEP
C      V1 - CROSS-VALLEY WIND SPEED AT PRESENT TIME STEP
C      WO - VERTICAL WIND SPEED AT PREVIOUS TIME STEP
C      W1 - VERTICAL WIND SPEED AT PRESENT TIME STEP
C      A1 - ADVECTIVE CHANGES TO POTENTIAL TEMPERATURE
C      A2 - DIFFUSIVE CHANGES TO POTENTIAL TEMPERATURE
C      A4 - ADVECTIVE CHANGES TO VORTICITY
C      A5 - DIFFUSIVE CHANGES TO VORTICITY
C      A6 - SOLENOID TERM
C      LOGICAL UNIT 5 : INPUT
C      LOGICAL UNIT 6 : POTENTIAL TEMPERATURE, A1,A2
C      LOGICAL UNIT 7 : STORES LAST TWO TIME STEPS FOR CONTINUATION OF
C                       RUN AT A LATER TIME
C      LOGICAL UNIT 8 : VORTICITY, A4,A5,A6
C      LOGICAL UNIT 9 : STREAMFUNCTION
C      LOGICAL UNIT 10 : CROSS-VALLEY WIND SPEED
C      LOGICAL UNIT 11 : VERTICAL WIND SPEED
C      LOGICAL UNIT 12 : DATA FOR LAST TWO TIME STEPS WHEN RUN BEING
C                        CONTINUED AT A LATER TIME
C
      CALL FREAD(5, 'I,4R*8,2I:', TEND, EPS, RALPHA, T(1), DELTAT, KEND,
     1     MAXITR)
C
C      TEND - FINAL INTEGRATION TIME DESIRED
C      EPS - CRITERION USED TO STOP RELAXATION PROCESSS
C      RALPHA - OVER-RELAXATION COEFFICIENT
C      T(1) - INITIAL SURFACE TEMPERATURE
C      DELTAT - LENGTH OF TIME STEP
C      KEND - HEIGHT OF UPPER BOUNDARY (GRID UNITS)
C      MAXITR - MAXIMUM NUMBER OF RELAXATION PASSES ALLOWED
C
      CALL FREAD(5, '3R*8:', DZ1, DZ2, DY)
C
C      DZ1 - VERTICAL GRID SIZE IN LOWER PART OF VALLEY CROSS-SECTION
C      DZ2 - VERTICAL GRID SIZE IN UPPER PART OF VALLEY CROSS-SECTION
C      DY - HORIZONTAL GRID SIZE EVERYWHERE
C
```

```
      RATIO = DZ2 / DZ1
      IRATIO = RATIO
      KVLY = (52. + DZ1) / DZ1
      KVLYM1 = KVLY - 1
      KMID = (72. + DZ1) / DZ1
      JEND = (600. + DY) / DY
      KENDMI = KEND - IRATIO
      JCOR = (80 + DY) / DY
C
C     KVLY - HEIGHT OF RIDGE (GRID UNITS)
C     KMID - HEIGHT AT WHICH VERTICAL GRID SIZE IS REDUCED (GRID UNITS)
C     JEND - LENGTH OF HALF VALLEY CROSS-SECTION (GRID UNITS)
C     JCOR - LENGTH OF FLAT VALLEY FLOOR (GRID UNITS)
C
      DATA G /9.806D0/, CP /1012.0D0/, RHO /1.2D0/, R /287.0D0/
      ALPHA = DATAN(0.1D0)
      CALL FREAD(5, '2R:', GAMMA, COOLR)
C
C     THE FOLLOWING ARE PHYSICAL CONSTANTS
C     G - ACCELERATION DUE TO GRAVITY (M/S/S)
C     CP - SPECIFIC HEAT OF AIR AT CONSTANT PRESSURE (J/KG/DEG C)
C     RHO - DENSITY OF AIR (KG/M/M/M)
C     R - GAS CONSTANT FOR DRY AIR (J/KG/DEG C)
C     ALPHA - ANGLE OF SLOPING GROUND SURFACE (RADIANS)
C     GAMMA - LAPSE RATE OF TEMPERATURE (C DEG/M)
C     COOLR - RATE OF COOLING AT SURFACE (C DEG/S)
C
      CALL FREAD(5, '2I:', KL, JJB)
      READ (5,790) (FOR1(I),I=1,10)
      READ (5,790) (FOR2(I),I=1,10)
      CALL FREAD(5, 'I,2R*8:', KOPT, TPR, COPT)
      ITPR = TPR
C
C       KL, JJB - DETERMINE PORTION OF GRID TO BE PRINTED OUT BY S/R
C OUTPUT
C     KOPT - IF 0 : DIFFUSIVITIES ARE CONSTANT EVERYWHERE
C            IF 1 : DIFFUSIVITIES CAN BE DEFINED
C                   USING S/R SUBK(JEND,KEND,JCOR,KVLY)
C     TPR - TIME INTERVAL AT WHICH MATRICES ARE PRINTED OUT
C     COPT - IF 0 : INTEGRATION BEGINS AT T = 0 SECONDS
C            IF 1 : INTEGRATION CONTINUES ACCORDING TO LOGICAL UNIT 12
C
      CALL FREAD(5, '4R*8:', KHZ, KVZ, KHT, KVT)
C
C     KHZ - HORIZONTAL MOMENTUM DIFFUSIVITY
C     KVZ - VERTICAL MOMENTUM DIFFUSIVITY
C     KHT - HORIZONTAL THERMAL DIFFUSIVITY
C     KVT - VERTICAL THERMAL DIFFUSIVITY
C
      DO 10 K = 1, KEND
        DO 10 J = 1, JEND
          VO(J,K) = 0.D0
          WO(J,K) = 0.D0
          ZO(J,K) = 0.D0
          PHI(J,K) = 0.D0
          V1(J,K) = 0.D0
          W1(J,K) = 0.D0
          Z1(J,K) = 0.D0
   10 CONTINUE
      DO 20 J = 1, JEND
   20 ZKM(J) = 0.D0
      IF (KOPT .EQ. 1) GO TO 30
      ITC = 0
      IP1 = 0
      TTOT = 0.D0
      GO TO 40
   30 CALL SUBK(JEND, KEND, JCOR, KVLY)
```

```
C
C     TEMPERATURE ABOVE TROUGH (INITIALLY)
C
  40 IF (COPT .EQ. 1) GO TO 130
     DO 70 K = 2, KEND
       IF (K .GT. KMID .AND. (K - 1)/RATIO - (K - 1)/IRATIO .NE. 0.0)
    1     GO TO 70
       IF (K .GT. KMID) GO TO 50
       INC = 1
       GO TO 60
  50   INC = IRATIO
  60   T(K) = T(K - INC) - GAMMA * DZ1 * INC
  70 CONTINUE
C
C     POTENTIAL TEMPERATURE ABOVE TROUGH - INITIALLY
C
     C1 = G / CP - GAMMA
     THO(1,1) = T(1) * (1000./930.) ** (R/CP)
     Z = 0.D0
     P = 1000. * (T(1)/THO(1,1)) ** (CP/R)
     THO(1,2) = DEXP(DLOG(THO(1,1)) + C1*DZ1/((T(1) + T(2))/2.))
     Z = DZ1
     P = 1000. * (T(2)/THO(1,2)) ** (CP/R)
     DO 100 K = 3, KEND
       IF (K .GT. KMID .AND. (K - 1)/RATIO - (K - 1)/IRATIO .NE. 0.0)
    1     GO TO 100
       IF (K .GT. KMID) GO TO 80
       INC = 1
       DZ = DZ1
       GO TO 90
  80   INC = IRATIO
       DZ = DZ2
  90   THO(1,K) = DEXP(DLOG(THO(1,K - INC*2)) + C1*DZ*2./T(K - INC))
       Z = (K*DZ1) - DZ1
       P = 1000. * (T(K)/THO(1,K)) ** (CP/R)
 100 CONTINUE
C
C     POTENTIAL TEMPERATURE WITHIN VALLEY CROSS-SECTION
C
     DO 120 K = 1, KEND
       JFINAL = K - 1 + JCOR
       IF (JFINAL .GE. JEND) JFINAL = JEND
       DO 110 J = 2, JFINAL
         IF (K .GT. KMID .AND. (K - 1)/RATIO - (K - 1)/IRATIO .NE. 0.0)
    1       GO TO 120
         THO(J,K) = THO(J - 1,K)
 110   CONTINUE
 120 CONTINUE
     IUNIT = 6
     WRITE (IUNIT,690) TTOT
     CALL OUTPUT(IUNIT, THO)
     IUNIT = 8
     WRITE (IUNIT,730) TTOT
     CALL OUTPUT(IUNIT, ZO)
     GO TO 160
 130 IUNIT = 12
     READ (IUNIT,850) ITC, TTOT, DELTAT
     IF (ITC .EQ. 1) GO TO 150
     READ (IUNIT,140) IDUM
 140 FORMAT (I1)
     CALL UNSAVE(IUNIT, THO)
     READ (IUNIT,140) IDUM
     CALL UNSAVE(IUNIT, ZO)
     READ (IUNIT,140) IDUM
     CALL UNSAVE(IUNIT, PHI)
     READ (IUNIT,140) IDUM
     CALL UNSAVE(IUNIT, VO)
     READ (IUNIT,140) IDUM
     CALL UNSAVE(IUNIT, WO)
     GO TO 160
```

```
 150 READ (IUNIT,140) IDUM
     CALL UNSAVE(IUNIT, THO)
     READ (IUNIT,140) IDUM
     CALL UNSAVE(IUNIT, TH1)
     READ (IUNIT,140) IDUM
     CALL UNSAVE(IUNIT, ZO)
     READ (IUNIT,140) IDUM
     CALL UNSAVE(IUNIT, Z1)
     READ (IUNIT,140) IDUM
     CALL UNSAVE(IUNIT, PHI)
     READ (IUNIT,140) IDUM
     CALL UNSAVE(IUNIT, VO)
     READ (IUNIT,140) IDUM
     CALL UNSAVE(IUNIT, V1)
     READ (IUNIT,140) IDUM
     CALL UNSAVE(IUNIT, WO)
     READ (IUNIT,140) IDUM
     CALL UNSAVE(IUNIT, W1)
C
C      CHANGES IN POTENTIAL TEMPERATURE AND VORTICITY
C
 160 TTOT = TTOT + DELTAT
     ITTOT = TTOT
     DO 320 K = 1, KEND
       IF (K .GT. KMID .AND. (K - 1)/RATIO - (K - 1)/IRATIO .NE. 0.0)
    1     GO TO 320
       JFINAL = K + JCOR - 1
       IF (JFINAL .GT. JEND) JFINAL = JEND
       IF (K .GE. KMID) GO TO 170
       DZ = DZ1
       INC = 1
       GO TO 180
 170   DZ = DZ2
       INC = IRATIO
 180   DO 310 J = 1, JFINAL
         IF (K .EQ. KMID) ZKM(J) = ZKM2(J)
         IF (K .EQ. KMID) TKM(J) = TKM2(J)
         IF (K .EQ. 1 .OR. K .EQ. J - JCOR + 1) GO TO 200
         IF (K .EQ. KEND) GO TO 220
         IF (J .EQ. 1 .OR. J .EQ. JEND) GO TO 230
C
C      INTERIOR OF REGION AWAY FROM BOUNDARIES - INITIALLY
C
         IF (ITC .EQ. 1) GO TO 190
         DTHDY = (THO(J + 1,K) - THO(J - 1,K)) / DY / 2.DO
         CALL ADVEC(ZO(J + 1,K), ZO(J,K), ZO(J - 1,K), DY, VO(J,K),
    1         HADV)
         CALL ADVEC(ZO(J,K + INC), ZO(J,K), ZO(J,K - INC), DZ, WO(J,K),
    1         VADV)
         A4(J,K) = -(HADV + VADV)
         DIFY = (ZO(J - 1,K) - 2.DO*ZO(J,K) + ZO(J + 1,K)) / DY / DY *
    1    KHZ
         DIFZ = (ZO(J,K + INC) - 2.DO*ZO(J,K) + ZO(J,K - INC)) / DZ /
    1    DZ * KVZ
         A5(J,K) = DIFY + DIFZ
         A6(J,K) = G / THO(J,K) * DTHDY
         Z1(J,K) = ZO(J,K) + DELTAT * (A4(J,K) + A5(J,K) + A6(J,K))
         ZKM(J) = ZO(J,K)
         IF (K .EQ. KMID - IRATIO) ZKM2(J) = ZO(J,K)
         CALL ADVEC(THO(J + 1,K), THO(J,K), THO(J - 1,K), DY, VO(J,K),
    1         HADV)
         CALL ADVEC(THO(J,K + INC), THO(J,K), THO(J,K - INC), DZ,
    1         WO(J,K), VADV)
         A1(J,K) = -(HADV + VADV)
         DIFY = (THO(J - 1,K) - 2.DO*THO(J,K) + THO(J + 1,K)) / DY /
    1    DY * KHT
         DIFZ = (THO(J,K - INC) - 2.DO*THO(J,K) + THO(J,K + INC)) / DZ
    1    / DZ * KVT
         A2(J,K) = DIFY + DIFZ
         TH1(J,K) = THO(J,K) + DELTAT * (A1(J,K) + A2(J,K))
         TKM(J) = THO(J,K)
         IF (K .EQ. KMID - IRATIO) TKM2(J) = THO(J,K)
         GO TO 310
```

```
C
C     INTERIOR OF REGION AWAY FROM BOUNDARIES - SUBSEQUENT TIMES
C
 190     DTHDY = (TH1(J + 1,K) - THO(J - 1,K)) / DY / 2.DO
         CALL DIFFOR(ZO(J + 1,K), ZO(J,K), ZTEMP, DY, KHZ, DIFY)
         CALL DIFFOR(ZO(J,K + INC), ZO(J,K), ZKM(J), DZ, KVZ, DIFZ)
         A5(J,K) = DIFY + DIFZ
         A6(J,K) = G / TH1(J,K) * DTHDY
         CALL ADVEC(ZO(J + 1,K), ZO(J,K), ZTEMP, DY, VO(J,K), HADV)
         CALL ADVEC(ZO(J,K + INC), ZO(J,K), ZKM(J), DZ, WO(J,K), VADV)
         A4(J,K) = -(HADV + VADV)
         ZTEMP = ZO(J,K)
         ZO(J,K) = Z1(J,K)
         Z1(J,K) = ZTEMP + 2.DO * DELTAT * (A4(J,K) + A5(J,K) + A6(J,K)
     1   )
         ZKM(J) = ZTEMP
         IF (K .EQ. KMID - IRATIO) ZKM2(J) = ZTEMP
         CALL ADVEC(THO(J + 1,K), THO(J,K), THTEMP, DY, VO(J,K), HADV)
         CALL ADVEC(THO(J,K + INC), THO(J,K), TKM(J), DZ, WO(J,K),
     1        VADV)
         A1(J,K) = -(HADV + VADV)
         CALL DIFFOR(THO(J + 1,K), THO(J,K), THTEMP, DY, KHT, DIFY)
         CALL DIFFOR(THO(J,K + INC), THO(J,K), TKM(J), DZ, KVT, DIFZ)
         A2(J,K) = DIFY + DIFZ
         THTEMP = THO(J,K)
         THO(J,K) = TH1(J,K)
         TH1(J,K) = THTEMP + 2.DO * DELTAT * (A1(J,K) + A2(J,K))
         TKM(J) = THTEMP
         IF (K .EQ. KMID - IRATIO) TKM2(J) = THTEMP
         GO TO 310
C
C     AT GROUND SURFACE - INITIALLY
C
 200     IF (ITC .EQ. 1) GO TO 210
         ZKM(J) = ZO(J,K)
         A4(J,K) = -9.999DO
         A5(J,K) = -9.999DO
         A6(J,K) = -9.999DO
         TH1(J,K) = THO(J,K) + DELTAT * COOLR
         TKM(J) = THO(J,K)
         A1(J,K) = -9.999DO
         A2(J,K) = -9.999DO
         GO TO 310
C
C     AT GROUND SURFACE - SUBSEQUENT TIMES
C
 210     ZKM(J) = ZO(J,K)
         A4(J,K) = -9.999DO
         A5(J,K) = -9.999DO
         A6(J,K) = -9.999DO
         THTEMP = THO(J,K)
         THO(J,K) = TH1(J,K)
         TH1(J,K) = THTEMP + 2.DO * DELTAT * COOLR
         TKM(J) = THTEMP
         A1(J,K) = -9.999DO
         A2(J,K) = -9.999DO
         GO TO 310
C
C     TOP BOUNDARY OF REGION
C
 220     A1(J,K) = 0.DO
         A2(J,K) = 0.DO
         A4(J,K) = 0.DO
         A5(J,K) = 0.DO
         A6(J,K) = 0.DO
         Z1(J,K) = 0.DO
         TH1(J,K) = THO(J,K)
         GO TO 310
```

```
C
C     ABOVE TROUGH OR RIDGE - INITIALLY
C
 230      IF (ITC .EQ. 1) GO TO 260
          CALL ADVEC(ZO(J,K + INC), ZO(J,K), ZKM(J), DZ, WO(J,K), VADV)
          A4(J,K) = -VADV
          DIFZ = (ZO(J,K - INC) - 2.DO*ZO(J,K) + ZO(J,K + INC)) / DZ /
     1    DZ * KVZ
          DIFY = -2.DO * ZO(J,K) * KHZ / DY / DY
          A5(J,K) = DIFY + DIFZ
          A6(J,K) = 0.DO
          Z1(J,K) = ZO(J,K) + DELTAT * (A4(J,K) + A5(J,K))
          ZKM(J) = ZO(J,K)
          IF (K .EQ. KMID - IRATIO) ZKM2(J) = ZO(J,K)
          CALL ADVEC(THO(J,K + INC), THO(J,K), TKM(J), DZ, WO(J,K),
     1         VADV)
          DIFZ = (THO(J,K - INC) - 2.DO*THO(J,K) + THO(J,K + INC)) / DZ
     1    / DZ * KVT
          IF (J .GT. 1) GO TO 240
          DIFY = 2.DO * (THO(J + 1,K) - THO(J,K)) / DY / DY * KHT
          GO TO 250
 240      DIFY = 2.DO * (THO(J - 1,K) - THO(J,K)) / DY / DY * KHT
 250      A1(J,K) = -VADV
          A2(J,K) = DIFY + DIFZ
          TH1(J,K) = THO(J,K) + DELTAT * (A1(J,K) + A2(J,K))
          TKM(J) = THO(J,K)
          IF (K .EQ. KMID - IRATIO) TKM2(J) = THO(J,K)
          GO TO 310
C
C     ABOVE TROUGH OR RIDGE - SUBSEQUENT TIMES
C
 260      CALL ADVEC(ZO(J,K + INC), ZO(J,K), ZKM(J), DZ, WO(J,K), VADV)
          A4(J,K) = -VADV
          CALL DIFFOR(ZO(J,K + INC), ZO(J,K), ZKM(J), DZ, KVZ, DIFZ)
          IF (J .GT. 1) GO TO 270
          CALL DIFFOR(ZO(J + 1,K), ZO(J,K), -ZO(J + 1,K), DY, KHZ, DIFY)
          GO TO 280
 270      CALL DIFFOR(-ZTEMP, ZO(J,K), ZTEMP, DY, KHZ, DIFY)
 280      ZTEMP = ZO(J,K)
          A5(J,K) = DIFY + DIFZ
          A6(J,K) = 0.DO
          ZO(J,K) = Z1(J,K)
          Z1(J,K) = ZTEMP + 2.DO * DELTAT * (A4(J,K) + A5(J,K))
          ZKM(J) = ZTEMP
          IF (K .EQ. KMID - IRATIO) ZKM2(J) = ZTEMP
          CALL ADVEC(THO(J,K + INC), THO(J,K), TKM(J), DZ, WO(J,K),
     1         VADV)
          A1(J,K) = -VADV
          CALL DIFFOR(THO(J,K + INC), THO(J,K), TKM(J), DZ, KVT, DIFZ)
          IF (J .GT. 1) GO TO 290
          CALL DIFFOR(THO(J + 1,K), THO(J,K), THO(J + 1,K), DY, KHT,
     1         DIFY)
          GO TO 300
 290      CALL DIFFOR(THTEMP, THO(J,K), THTEMP, DY, KHT, DIFY)
 300      A2(J,K) = DIFY + DIFZ
          THTEMP = THO(J,K)
          THO(J,K) = TH1(J,K)
          TH1(J,K) = THTEMP + 2.DO * DELTAT * (A1(J,K) + A2(J,K))
          TKM(J) = THTEMP
          IF (K .EQ. KMID - IRATIO) TKM2(J) = THTEMP
 310    CONTINUE
 320  CONTINUE
      IF (ITTOT/TPR - ITTOT/ITPR .NE. 0.0) GO TO 330
      IUNIT = 6
      WRITE (IUNIT,800)
      WRITE (IUNIT,700) TTOT
      CALL OUTPUT(IUNIT, A1)
      WRITE (IUNIT,710) TTOT
      CALL OUTPUT(IUNIT, A2)
      WRITE (IUNIT,690) TTOT
      CALL OUTPUT(IUNIT, TH1)
```

```
      IUNIT = 8
      WRITE (IUNIT,800)
      WRITE (IUNIT,770) TTOT
      CALL OUTPUT(IUNIT, A4)
      WRITE (IUNIT,780) TTOT
      CALL OUTPUT(IUNIT, A5)
      WRITE (IUNIT,800)
      WRITE (IUNIT,720) TTOT
      CALL OUTPUT(IUNIT, A6)
C
C     RELAX TO OBTAIN STREAMFUNCTIONS
C
 330  DO 380 I = 1, MAXITR
        ERROR = 0.D0
        DO 370 K = 2, KENDMI
          IF (K .GT. KMID .AND. (K - 1)/RATIO - (K - 1)/IRATIO .NE. 0.0)
     1       GO TO 370
          JFINAL = K + JCOR - 2
          IF (JFINAL .GT. JEND - 1) JFINAL = JEND - 1
          DO 360 J = 2, JFINAL
            IF (K .GE. KMID) GO TO 340
            DZ = DZ1
            INC = 1
            GO TO 350
 340        DZ = DZ2
            INC = IRATIO
 350        PHIOLD = PHI(J,K)
            RES = Z1(J,K) + (PHI(J + 1,K) - 2.D0*PHI(J,K) + PHI(J - 1,K)
     1      ) / DY / DY
            RES = RES + (PHI(J,K + INC) - 2.D0*PHI(J,K) + PHI(J,K - INC)
     1      ) / DZ / DZ
            PHI(J,K) = PHIOLD + RES * RALPHA / (2.D0/DY/DY + 2.D0/DZ/DZ)
            PH = DABS(PHIOLD - PHI(J,K))
            IF (PH .LT. ERROR) GO TO 360
            ERROR = PH
            JM = J
            KM = K
 360      CONTINUE
 370    CONTINUE
        ITER = I
        IF (ERROR .LT. EPS) GO TO 390
 380  CONTINUE
 390  IF (ITTOT/TPR - ITTOT/ITPR .NE. 0.0) GO TO 400
      IUNIT = 9
      IF (IP1 .EQ. 0) WRITE (IUNIT,810) TTOT, ITER, ERROR
      IF (IP1 .EQ. 1) WRITE (IUNIT,800)
      IF (IP1 .EQ. 1) WRITE (IUNIT,740) TTOT, ITER, ERROR
      CALL OUTPUT(IUNIT, PHI)
C
C     VELOCITY FIELDS ARE DERIVED FROM STREAMLINES
C
 400  DO 410 K = 1, KEND
        DO 410 J = 1, JEND
          VO(J,K) = V1(J,K)
          WO(J,K) = W1(J,K)
 410  CONTINUE
      VM = 0.D0
      WM = 0.D0
      DO 510 K = 1, KEND
        IF (K .GT. KMID .AND. (K - 1)/RATIO - (K - 1)/IRATIO .NE. 0.0)
     1     GO TO 510
        JFINAL = K + JCOR - 1
        IF (JFINAL .GE. JEND) JFINAL = JEND
        DO 500 J = 1, JFINAL
          IF (K .EQ. KEND) GO TO 460
          IF (K .EQ. 1) GO TO 470
          IF (K .EQ. J - JCOR + 1) GO TO 480
          IF (J .EQ. 1 .OR. J .EQ. JEND) GO TO 440
          IF (K .GE. KMID) GO TO 420
```

```
            DZ = DZ1
            INC = 1
            GO TO 430
  420       DZ = DZ2
            INC = IRATIO
  430       V1(J,K) = (PHI(J,K + INC) - PHI(J,K - INC)) / 2.DO / DZ
            W1(J,K) = -(PHI(J + 1,K) - PHI(J - 1,K)) / 2.DO / DY
            GO TO 490
  440       V1(J,K) = O.DO
            IF (J .EQ. JEND) GO TO 450
            W1(J,K) = -PHI(J + 1,K) / DY
            GO TO 490
  450       W1(J,K) = PHI(J - 1,K) / DY
            GO TO 490
  460       V1(J,K) = O.DO
            W1(J,K) = O.DO
            GO TO 500
  470       V1(J,K) = (2.DO*PHI(J,K + 1) - O.5DO*PHI(J,K + 2)) / DZ1
            IF (J .EQ. 1) V1(J,K) = O.DO
            W1(J,K) = O.DO
            GO TO 490
  480       DPHIDY = (2.DO*PHI(J - 1,K) - O.5DO*PHI(J - 2,K)) / DY
            DPHIDZ = (2.DO*PHI(J,K + 1) - O.5DO*PHI(J,K + 2)) / DZ1
            MAGNV = DSQRT(DPHIDY*DPHIDY + DPHIDZ*DPHIDZ)
            V1(J,K) = -MAGNV * DCOS(ALPHA)
            IF (J .EQ. JEND) V1(J,K) = O.DO
            W1(J,K) = -MAGNV * DSIN(ALPHA)
            IF (J .EQ. JEND) W1(J,K) = PHI(J - 1,K) / DY
            GO TO 490
  490       IF (DABS(V1(J,K)) .GT. VM) VM = DABS(V1(J,K))
            IF (DABS(W1(J,K)) .GT. WM) WM = DABS(W1(J,K))
  500     CONTINUE
  510   CONTINUE
        IF (ITTOT/TPR - ITTOT/ITPR .NE. O.O) GO TO 520
        IUNIT = 10
        IF (IP1 .EQ. O) WRITE (IUNIT,820) TTOT
        IF (IP1 .EQ. 1) WRITE (IUNIT,800)
        IF (IP1 .EQ. 1) WRITE (IUNIT,750) TTOT
        CALL OUTPUT(IUNIT, V1)
        IUNIT = 11
        IF (IP1 .EQ. O) WRITE (IUNIT,830) TTOT
        IF (IP1 .EQ. 1) WRITE (IUNIT,800)
        IF (IP1 .EQ. 1) WRITE (IUNIT,760) TTOT
        CALL OUTPUT(IUNIT, W1)
C
C       VORTICITY AT SURFACE
C
  520   Z1(1,1) = O.DO
        Z1(JEND,KVLY) = O.DO
        DO 560 K = 1, KVLYM1
          JBEGIN = 2
          IF (K .GE. 2) JBEGIN = K - 1 + JCOR
          JFINAL = K - 1 + JCOR
          DO 550 J = JBEGIN, JFINAL
            IF (J .LT. JFINAL) GO TO 530
            DWDY = (-1.5DO*W1(J,K) + 2.DO*W1(J - 1,K) - O.5DO*W1(J - 2,K))
       1     / DY
            GO TO 540
  530       DWDY = O.DO
  540       DVDZ = (-1.5DO*V1(J,K) + 2.DO*V1(J,K + 1) - O.5DO*V1(J,K + 2))
       1     / DZ1
            ZO(J,K) = Z1(J,K)
            Z1(J,K) = DWDY - DVDZ
  550     CONTINUE
  560   CONTINUE
        IF (ITTOT/TPR - ITTOT/ITPR .NE. O.O) GO TO 570
        IUNIT = 8
        WRITE (IUNIT,730) TTOT
        CALL OUTPUT(IUNIT, Z1)
```

```
C
C     IS CFL CRITERION SATISFIED ?
C
 570 IF (IP1 .EQ. 1) GO TO 580
     IP1 = 1
     GO TO 590
 580 IP1 = 0
 590 IF (VM .EQ. 0.0 .OR. WM .EQ. 0.0) GO TO 640
     IF (VM .GT. 4.0 .OR. WM .GT. 4.0) GO TO 840
     DELTY = DY / VM / 2.D0 * 0.8D0
     DELTZ = DZ1 / WM / 2.D0 * 0.8D0
     DTOLD = DELTAT
 600 IF (DELTAT .LT. DELTY .AND. DELTAT .LT. DELTZ) GO TO 620
     DELTAT = DELTAT / 2.D0
     WRITE (6,610) DELTAT, TTOT
 610 FORMAT (' ', 'DELTA T REDUCED TO', F6.2, 'AT TIME =', F10.2)
     IF (DELTAT .LT. 1.D0) GO TO 840
     GO TO 600
 620 IF (DELTAT .EQ. DTOLD) GO TO 640
     ITC = 0
     DO 630 K = 1, KEND
       DO 630 J = 1, JEND
         THO(J,K) = TH1(J,K)
         ZO(J,K) = Z1(J,K)
         VO(J,K) = V1(J,K)
         WO(J,K) = W1(J,K)
 630 CONTINUE
     IF (TTOT .GE. TEND) GO TO 840
     GO TO 160
 640 ITC = 1
     IF (TTOT .GE. TEND) GO TO 840
     GO TO 160
 650 FORMAT (' ', 'HEIGHT(M.)    PRES(MB.)    TEMP(DEG K)    POT TEMP(D
    1EG K)')
 660 FORMAT (2X, F5.1, 10X, F5.1, 2(6X,F11.7))
 670 FORMAT (' ', 'AFTER', I3, 'ITER., MAX. ERROR = ', F12.10,
    1       ' AND OCCURS AT (J,K) = (', I3, ',', I3, ')')
 680 FORMAT ('1')
 690 FORMAT ('1', 'POTENTIAL TEMPERATURE (THETA) AT TIME = ', F7.2)
 700 FORMAT (' ', 'ADVECTION TERMS (THETA) AT TIME = ', F7.2)
 710 FORMAT ('1', 'DIFFUSION TERMS (THETA) AT TIME = ', F7.2)
 720 FORMAT (' ', 'BUOYANCY TERM (Z) AT TIME = ', F7.2)
 730 FORMAT ('1', 'VORTICITY (Z) AT TIME = ', F7.2)
 740 FORMAT (' ', 'STREAMFUNCTION (PHI) AT TIME = ', F7.2, ' (AFTER ',
    1       I3, ' ITERATIONS,ERROR = ', F12.10, ')')
 750 FORMAT (' ', 'CROSS-VALLEY WIND SPEED (V) AT TIME = ', F7.2)
 760 FORMAT (' ', 'VERTICAL WIND SPEED (W) AT TIME = ', F7.2)
 770 FORMAT (' ', 'ADVECTION TERMS (Z) AT TIME = ', F7.2)
 780 FORMAT ('1', 'DIFFUSION TERMS (Z) AT TIME = ', F7.2)
 790 FORMAT (10A8)
 800 FORMAT (/)
 810 FORMAT ('1', 'STREAMFUNCTION (PHI) AT TIME = ', F7.2, ' (AFTER ',
    1       I3, ' ITERATIONS,ERROR = ', F12.10, ')')
 820 FORMAT ('1', 'CROSS-VALLEY WIND SPEED (V) AT TIME = ', F7.2)
 830 FORMAT ('1', 'VERTICAL WIND SPEED (W) AT TIME = ', F7.2)
 840 IUNIT = 7
     WRITE (IUNIT,850) ITC, TTOT, DELTAT
 850 FORMAT (I1, 2F7.2)
     IF (ITC .EQ. 1) GO TO 860
     WRITE (IUNIT,690) TTOT
     CALL SAVE(IUNIT, THO)
     WRITE (IUNIT,730) TTOT
     CALL SAVE(IUNIT, ZO)
     WRITE (IUNIT,810) TTOT, ITER, ERROR
     CALL SAVE(IUNIT, PHI)
     WRITE (IUNIT,820) TTOT
     CALL SAVE(IUNIT, VO)
     WRITE (IUNIT,830) TTOT
     CALL SAVE(IUNIT, WO)
     GO TO 870
```

```
 860 TM = TTOT - DTOLD
     WRITE (IUNIT,690) TM
     CALL SAVE(IUNIT, TH0)
     WRITE (IUNIT,690) TTOT
     CALL SAVE(IUNIT, TH1)
     WRITE (IUNIT,730) TM
     CALL SAVE(IUNIT, Z0)
     WRITE (IUNIT,730) TTOT
     CALL SAVE(IUNIT, Z1)
     WRITE (IUNIT,810) TTOT, ITER, ERROR
     CALL SAVE(IUNIT, PHI)
     WRITE (IUNIT,820) TM
     CALL SAVE(IUNIT, V0)
     WRITE (IUNIT,820) TTOT
     CALL SAVE(IUNIT, V1)
     WRITE (IUNIT,830) TM
     CALL SAVE(IUNIT, W0)
     WRITE (IUNIT,830) TTOT
     CALL SAVE(IUNIT, W1)
 870 STOP
     END
     SUBROUTINE ADVEC(AB0, AMID, ABEL, D, VEL, RES)
C
C      FORWARD-TIME, UPSTREAM-SPACE FORMULATION OF ADVECTION TERMS
C
     IMPLICIT REAL*8(A - H,0 - Z)
     IF (VEL .GT. 0.D0) GO TO 10
     RES = VEL * (AB0 - AMID) / D
     RETURN
  10 RES = VEL * (AMID - ABEL) / D
     RETURN
     END
     SUBROUTINE DIFFOR(AB0, AMID, ABEL, D, AK, RES)
C
C      FORWARD-TIME, CENTERED-SPACE FORMULATION OF DIFFUSION TERMS
C
     IMPLICIT REAL*8(A - H,0 - Z)
     R = AK / D / D
     RES = R * (ABEL - 2.D0*AMID + AB0)
     RETURN
     END
     SUBROUTINE OUTPUT(IUNIT, A)
C
C      DATA IS WRITTEN ONTO VARIOUS LOGICAL UNITS
C
     IMPLICIT REAL*8(A - H,0 - Z)
     DIMENSION A(16,28), FOR1(10), FOR2(10)
     COMMON TT0T, FOR1, FOR2, KL, JEND, JCOR, KEND, KMID, JJB
     KK = KEND + 1 - KL
     J1 = -JJB
  10 J1 = J1 + JJB + 1
     J3 = J1 + JJB
     J2 = J3
     IF (J2 .GT. JEND) J2 = JEND
     IF (J1 .NE. 1) WRITE (IUNIT,20)
  20 FORMAT ('1')
     DO 70 K = KK, KEND
       KBACK = KEND + 1 - K
       IF (J1 .GT. (KBACK - 1 + JCOR)) GO TO 70
       IF (J2 .GT. (KBACK - 1 + JCOR)) J2 = KBACK - 1 + JCOR
       IF (IUNIT .EQ. 6) GO TO 30
       WRITE (IUNIT,FOR1) (A(J,KBACK),J=J1,J2)
       GO TO 50
  30   IF (A(1,1) .GT. 250.0) GO TO 40
       WRITE (IUNIT,FOR1) (A(J,KBACK),J=J1,J2)
       GO TO 50
  40   WRITE (IUNIT,FOR2) (A(J,KBACK),J=J1,J2)
  50   IF (KBACK .GT. KMID) K = K + 2
       IF (KBACK .GT. KMID) WRITE (IUNIT,60)
  60   FORMAT (' ', /)
  70 CONTINUE
     IF (J3 .LT. JEND) GO TO 10
     RETURN
     END
```

```
      SUBROUTINE SAVE(IUNIT, A)
C
C      DATA IS WRITTEN ONTO LOGICAL UNIT 7 FOR CONTINUATION OF RUN
C      AT A LATER TIME
C
      IMPLICIT REAL*8(A - H,O - Z)
      DIMENSION A(16,28), FOR1(10), FOR2(10)
      COMMON TTOT, FOR1, FOR2, KL, JEND, JCOR, KEND, KMID, JJB
      KK = KEND + 1 - KL
      J1 = 1
      DO 20 K = KK, KEND
        KBACK = KEND + 1 - K
        J2 = KBACK - 1 + JCOR
        IF (J2 .GT. JEND) J2 = JEND
        WRITE (IUNIT,10) (A(J,KBACK),J=J1,J2)
   10   FORMAT (1X, 16D23.15)
        IF (KBACK .GT. KMID) K = K + 2
   20 CONTINUE
      RETURN
      END
      SUBROUTINE UNSAVE(IUNIT, A)
C
C      DATA IS READ FROM LOGICAL UNIT 12 FOR CONTINUATION OF RUN
C      AT A LATER TIME
C
      IMPLICIT REAL*8(A - H,O - Z)
      DIMENSION A(16,28), FOR1(10), FOR2(10)
      COMMON TTOT, FOR1, FOR2, KL, JEND, JCOR, KEND, KMID, JJB
      KK = KEND + 1 - KL
      J1 = 1
      DO 20 K = KK, KEND
        KBACK = KEND + 1 - K
        J2 = KBACK - 1 + JCOR
        IF (J2 .GT. JEND) J2 = JEND
        READ (IUNIT,10) (A(J,KBACK),J=J1,J2)
   10   FORMAT (1X, 16D23.15)
        IF (KBACK .GT. KMID) K = K + 2
   20 CONTINUE
      RETURN
      END
      SUBROUTINE SUBK(JEND, KEND, JCOR, KVLY)
C
C      DEFINES DIFFUSIVITIES (ALTER AS DESIRED)
C      IF K = K(Z), HOWEVER, GOVERNING EQUATIONS MAY CHANGE
C
      IMPLICIT REAL*8(A - H,O - Z)
      REAL*8 KHZ, KVZ, KHT, KVT
      COMMON /A/ KHZ, KVZ, KHT, KVT
      KHZ = 1.DO
      KHT = 1.DO
      KVZ = O.DO
      KVT = O.DO
      RETURN
      END
```

B30369